Title

L-type Ca2+ channels as therapeutic targets for Early afterdepolarization-related arrhythmias

Author

Madhvani, Roshni Vyas

Publication Date

2014

Peer reviewed|Thesis/dissertation

UNIVERSITY OF CALIFORNIA
Los Angeles

L-type Ca^{2+} channels as therapeutic targets for Early afterdepolarization-related arrhythmias

A dissertation submitted in satisfaction of the requirements for the degree Doctor of Philosophy in Molecular, Cellular and Integrative Physiology

By

Roshni Vyas Madhvani

2014

ABSTRACT OF THE DISSERTATION

By

Roshni Vyas Madhvani

Doctor of Philosophy in Molecular, Cellular & Integrative Physiology

University of California, Los Angeles, 2012

Professor Riccardo Olcese, Chair

Early afterdepolarizations (EADs) are highly arrhythmogenic transient depolarizations occurring during phase 2 or 3 of the cardiac action potential (AP). Using the dynamic clamp technique, I combined mathematical modeling and electrophysiology in real-time to introduce a virtual L-type Ca^{2+} current ($I_{Ca,L}$) in dissociated rabbit ventricular myocytes. I sought to i) understand the etiology of EAD development and their dependence on $I_{Ca,L}$ and ii) identify therapeutic strategies to suppress EADs by shaping a new L-type Ca^{2+} current. To investigate the therapeutic potential of $I_{Ca,L}$ modifications in suppressing EADs, I first induced a robust EAD regime by exposing cardiomyocytes either to hypokalemia or oxidative stress. EADs were completely abolished by blocking the endogenous $I_{Ca,L}$ with nifedipine, a specific Ca^{2+} channel blocker, but promptly restored under dynamic clamp by a virtual Ca^{2+} current modeled as modified by H_2O_2. Using this experimental paradigm, my results in Chapter 2 demonstrate that EADs are highly sensitive to minimal changes (1-5 mV) in the half activation/inactivation potentials ($V_{1/2}$) of $I_{Ca,L}$, such that $V_{1/2}$ modifications which reduce the window current voltage range were highly effective at suppressing EADs. In Chapter 3, I expand upon these findings and systematically explore the relevance of other biophysical parameters of $I_{Ca,L}$. The results highlight the importance of a third biophysical parameter, the non-inactivating component of $I_{Ca,L}$, in EAD suppression. As such, dynamic clamp experiments identified three steady-state

biophysical properties of $I_{Ca,L}$ as ideal therapeutic targets to suppress EADs and resulting cardiac arrhythmias while maintaining contractility. Chapter 4 builds upon these results by employing a biological approach to achieve the modifications to $I_{Ca,L}$ biophysical properties by altering the subunit composition of L-type Ca^{2+} channels (LTCCs) in cardiac myocytes. The striking results demonstrate that the larger $I_{Ca,L}$ window current produced by overexpressing the β_{2a} subunit contributes to increased EAD susceptibility while the overexpressing β_3 subunit may have a protective effect regardless of the increase in overall current density. Based on these findings, I propose that knock-down of the pro-arrhythmic β_{2a} subunit may represent a more appealing strategy to control the occurrence of EADs in cardiac myocytes. These results support the hypothesis that EAD occurrence can be controlled by fine-tuning the biophysical properties of the L-type Ca^{2+} current. Therefore, with the innovative combination of electrophysiology and mathematical modeling, this project brings forward a biological solution to suppress EAD under otherwise arrhythmogenic conditions and is of great cardiovascular relevance, as it is centered on finding a solution to a lethal cardiac arrhythmias by characterizing and manipulating the operation of cardiac ion channels.

The dissertation of Roshni Vyas Madhvani is approved by

Zhillin Qu

James N. Weiss

Ligia G. Toro de Stefani

Mansoureh Eghbali

Riccardo Olcese, Chair

To my husband and my family, I am grateful for all your love and support.

TABLE OF CONTENTS

List of Figures

CHAPTER 1 :

CHAPTER 2 :

List of Tables

Symbols & Abbreviations

AP: action potential

APD: action potential duration

EADs: early afterdepolarizations

LTCC: L-type Ca^{2+} Channels

$I_{Ca,L}$: L-type Ca^{2+} current

RTXI: real-time experimental interface

SR: sarcoplasmic reticulum

VDI: voltage-depedent inactivation

CDI: calcium-dependent inactivation

CaM: calmodulin

CaMKII: Ca^{2+}/calmodulin-dependent protein kinase II

NCX: Na^{+}/Ca^{2+} exchanger

SERCA: sarco-endoplasmic reticulum Ca^{2+}-ATPase

V_m: membrane potential

VF: ventricular fibrillation

VT: ventricular tachycardia

SCD: sudden cardiac death

Acknowledgements

The work described in this dissertation was a collaborative effort with support and assistance from many people in our laboratory as well other laboratories.

All the research described here has been performed under the direction of Dr. Riccardo Olcese, Dr. James N. Weiss, Dr. Zhilin Qu, Dr. Alan Garfinkel, and Dr. Hrayr Karaguezian.

First and foremost, I would like to thank my advisor, Dr. Riccardo Olcese for his patience and guidance from the moment I joined the lab as a technician, through the application process for graduate school and during my dissertation project. Without his confidence in my talents, I could not have gained confidence in myself. Thanks to the training I have received under his supervision, I am well-qualified to pursue a scientific career that I can be proud of.

I would also like to recognize the remarkable effort put forth by Dr. Antonios Pantazis in helping me fully grasp the conceptual design of the dynamic clamp technique as well as ongoing technical help and troubleshooting the operation of my dynamic patch clamp setup. Furthermore, Dr. Pantazis adapted and implemented the BK_{Ca} channel model in RTXI described in Chapter 5.

Additionally, I would like to show my appreciation and gratitude to all the members of the Olcese laboratory, past and present, who have helped me and guided me in any way shape or form. I thank: Azadeh Kohanteb for her contribution to experiments in *Xenopus* oocytes described in Chapter 4; Silvie Suriany and Marina Angelini for their ongoing help with the project, Nicoletta Savalli, Taleh Yusifov and Saemi Park for constructive discussions and guidance.

Dr. James N. Weiss and the members of his team, Thao Nguyen and Christopher Ko, have helped advanced my understanding of cardiovascular physiology and the cellular mechanisms for cardiac arrhythmias immensely. I would also like to thank Nicole Petrochuk, Rahil Patel, and Pauline Morand for their expertise with and dedication to cardiac myocyte isolations on a regular basis.

Dr. Zhilin Qu and his team, Yuanfang Xie, have contributed to the mathematical model of the cardiac action potential that has been implemented in the dynamic clamp. Without their help, much of this project could not have been done. Moreover, I have learned a great deal from them about computational modeling and how powerful it can be to describe biological phenomena.

Dr. Alan Garfinkel and his student, Nils P. Borgstrom, have contributed computer simulations of the ventricular cell-types from the heart (epi, M, and endocardial myocytes) in Chapter 3. These simulations helped validate my findings from dynamic clamp experiments to all cell types found the in the ventricles.

The real-time PCR and immunocytochemistry experiments described in Chapter 4 have been performed with expert guidance from Dr. Mansoureh Eghbali and her student Andrea Iorga. I am very grateful for their help with the design of these experiments as well as many reagents and tools.

I would also like to thank Dr. James Tidball for his leadership of the Molecular, Cellular and Integrative Physiology PhD program. Thanks to his dedication to excellence, I am fortunate enough to graduate from one of the most prestigious Physiology programs in the country.

Finally, I would like to thank my dissertation committee for ongoing constructive discussions and support.

BIOGRAPHICAL SKETCH

NAME	POSITION TITLE
ROSHNI VYAS MADHVANI	GRADUATE STUDENT RESEARCHER
eRA COMMONS USER NAME (credential, e.g., agency login)	

EDUCATION/TRAINING *(Begin with baccalaureate or other initial professional education, such as nursing, and include postdoctoral training.)*

INSTITUTION AND LOCATION	DEGREE *(if applicable)*	YEAR(s)	FIELD OF STUDY
University of California, Los Angeles, Los Angeles, CA	B.S.	2006	Neuroscience
Stanford University, Palo Alto, CA	M.S.	2008	Biology

5.6.1 POSITIONS AND EMPLOYMENT

07/2009 – Present **Graduate Student Researcher**, Dept. of Anesthesiology, Division of Molecular Medicine, UCLA
01/2008 – 03/2008 **Teaching Assistant,** Department of Bioengineering, Stanford University
09/2007 – 12/2007 **Teaching Assistant,** Department of Biochemistry, Stanford University
07/2006 – 05/2007 **Research Assistant,** Department of Biochemistry, Drexel University
09/2004 – 12/2005 **Lab Assistant**, Department of Anesthesiology, Division of Molecular Medicine, UCLA
08/2003 – 08/2004 **Lab Assistant**, Department of Physiology, UCLA

Other Experience and Professional Memberships

2005-2013 Member, Biophysical Society
2008-Present Member, Stanford Professional Women
2010-2012 Member, Biological Sciences Council (MCIP Representative)
2012-2013 Member, Cardiac Muscle Society

HONORS:

02/11/2012 – Molecular, Cellular, and Integrative Physiology (MCIP) Annual Retreat, **Best Poster Presentation**
07/2010 – 06/2012 American Heart Association, Western States Affiliate, **Harold & Lillian Kraus Pre-doctoral Fellowship**
02/2011 – Gordon Research Conference: Cardiac Arrhythmias Mechanisms, **Invited speaker**
02/27/2010 – Molecular, Cellular, and Integrative Physiology (MCIP) Annual Retreat, **Best Poster Presentation**
2009 – 2010 UCLA, Dept. of Anesthesiology, Div. of Molecular Medicine, **Pre-doctoral Fellowship**
09/2008 – 12/2009 UCLA, **Graduate Division University Fellowship**

B. PEER-REVIEWED PUBLICATIONS

1. Ermolova N., **Madhvani R.V.**, Kaback H.R. (2006) Site-directed alkylation of cysteine replacements in the lactose permease of Escherichia coli: helices I, III, VI, and XI. **Biochemistry.** 45(13):4182-9.

2. Gudzenko V.,Shiferaw Y., Savalli N., **Vyas R.**, Weiss JN and Olcese R. (2007) Influence of Channel Subunit Composition on L-Type Ca^{2+} current Kinetics: Implications for Novel Approaches in Controlling Cardiac Wave Stability. ***Am J Physiol Heart Circ Physiol*.** 293(3):H1805-15.

3. **Madhvani R.V.**, Xie, Y., Pantazis, A., Garfinkel A., Qu, Z., Weiss J.N. and Olcese R. (2011) Shaping a New Ca^{2+} Conductance to Suppress Early Afterdepolarizations in Cardiac Myocytes. ***J Physiol.*** 589 (24) 6081-6092.

4. **Madhvani R.V.,** Xie, Y., Pantazis, A., Suriany, S., Borgstrom, N.P., Garfinkel A., Qu, Z., Weiss J.N. and Olcese R. The Late Component of the L-type Ca Current is a Critical Target To Suppress Cardiac Early Afterdepolarizations. *Submitted to Cardiovasc Res.*

C. SELECTED POSTER PRESENTATIONS

1. **R.V. Madhvani**, A. Kohanteb, Y. Xie, A. Pantazis, S. John, A. Garfinkel, Z. Qu, J.N. Weiss and Riccardo Olcese. Fighting Cardiac Arrhythmias by Shaping A New L-Type Ca2+ Current, **American Society of Anesthesiologists Annual Meeting**, 2010

2. **R.V. Madhvani**, A. Kohanteb, Y. Xie, A. Pantazis, S. John, A. Garfinkel, Z. Qu, J.N. Weiss and Riccardo Olcese. Suppressing Early Afterdepolarizations by Modifying the Ca2+ Window Current, **Gordon Research Conference: Cardiac Arrhythmia Mechanisms**, 2011

3. **R.V. Madhvani**, A. Kohanteb, Y. Xie, A. Pantazis, S. John, A. Garfinkel, Z. Qu, J.N. Weiss and Riccardo Olcese. Suppressing Early Afterdepolarizations in Cardiac Myocytes by Shaping a Modified Ca2+ Conductance under Dynamic Clamp, **Biophysical Society Annual Meeting**, 2011

4. **R.V. Madhvani**, A. Kohanteb, Y. Xie, A. Pantazis, S. John, A. Garfinkel, Z. Qu, J.N. Weiss and Riccardo Olcese. Suppressing Early Afterdepolarizations by Modifying the Ca2+ Window Current, **American Society of Anesthesiologists Annual Meeting**, 2011

5. **R.V. Madhvani**, Y.Xie, A. Pantazis, A. Garfinkel, Z. Qu, J.N. Weiss and R. Olcese. How Do L-type Ca^{2+} Current Kinetics Contribute to Early Afterdepolarizations in Cardiac Myocytes?, **Biophysical Society Annual Meeting**, 2012

6. **R.V. Madhvani**, Y.Xie, A. Pantazis, A. Garfinkel, Z. Qu, J.N. Weiss and R. Olcese. Relevance of L-type Ca^{2+} Current Kinetics to Early Afterdepolarizations in Cardiac Myocytes, **American Society of Anesthesiologiests Annual Meeting**, 2012

7. **R.V. Madhvani**, Y.Xie, A. Pantazis, A. Garfinkel, Z. Qu, J.N. Weiss and R. Olcese. Tuning L-Type Ca2+ Current Properties To Suppress Early Afterdepolarizations, **Biophysical Society Annual Meeting**, 2013

Chapter 1:

Introduction

1.1 Electro-mechanical activity of the heart.

Normal electrical activity within the heart consists of a wave of depolarization initiated by the sinoatrial nodal cells, known as the pacemaker cells[1]. The depolarizing wave, the cardiac action potential, travels synchronously through the cardiac syncytium from the atria, to the atrio-ventricular node, through the his-bundle and finally through the ventricular tissue (Fig. 1.1). Compared to neuronal action potentials (APs), cardiac APs are markedly prolonged due to the presence of a plateau. The plateau phase is critical for the proper functioning of the cardiac tissue since it allows enough time for Ca^{2+} to enter the cell, induce Ca^{2+} release from the sarcoplasmic reticulum (SR), which binds to actin and myosin filaments, and initiates contraction of the cardiac muscle, an event which ultimately pumps blood and nutrients to all other tissues in the body. Once blood is pumped out of the ventricles, the muscle fibers must relax to allow refilling for the next beat; therefore, Ca^{2+} must be recycled back into the SR or extruded back into the extracellular medium, and the tissue must repolarize before the next oncoming AP, when the process begins again. This cycle of excitation, contraction and relaxation occurs billions of times in an average human lifespan.

1.2 The cardiac action potential.

At the cellular level, the AP is a result of the perfectly coordinated activity of a number of ion channels, which facilitate the flux of Na^+, Ca^{2+} and K^+, and various other ions across the plasma membrane. Na^+ influx drives the membrane potential (V_m) towards its electro-chemical equilibrium potential to form the sharp upstroke of the AP upto ~40 mV (phase 0) (Fig 1.2). The positive V_m activates both the transient outward K^+ current $(I_{to})^2$ and, with a slight delay, the L-type Ca^{2+} current $(I_{Ca,L})^3$. Thus, a lag in activation of $I_{Ca,L}$ results in a transient repolarization phase (phase 1) which is followed by the plateau (phase 2) upon activation of the inward Ca^{2+} current which is balanced by the delayed rectifier K^+ currents such as I_{Kr} and I_{Ks}[4]. During this time, the Ca^{2+} entering the cell through the L-type Ca^{2+} channels (LTCCs) has widespread

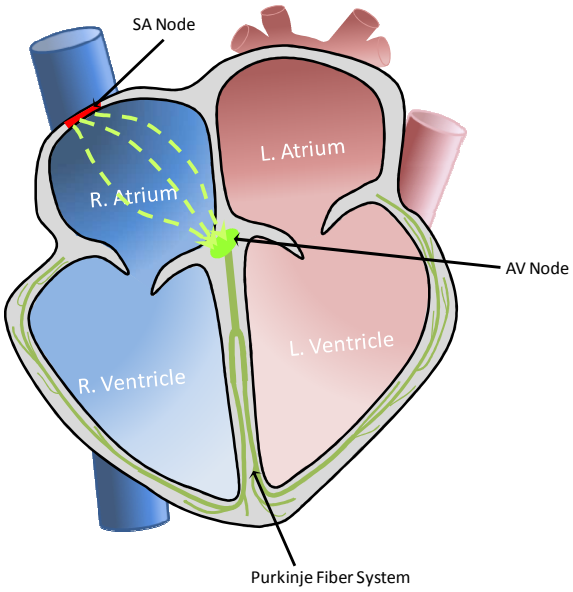

Figure 1.1 The Conduction System of the Heart. The natural rhythm of the heart is dictated by the pacemaker cells within the Sino-atrial (SA) node. The electrical impulse travels from the SA node, through the atrial tissue to the atrio-ventricular (AV) node, and via the His-Purkinje fibers to the ventricular tissue.

consequences within the cell. First, Ca^{2+} binds to calmodulin (CaM), which is directly associated with the L-type Ca^{2+} channel, and initiates Ca^{2+}-dependent inactivation (CDI). The Ca^{2+} within the dyadic space also induces Ca^{2+} release from the SR by activating ryanodine receptors (RyRs), a phenomenon known as Ca-Induced Ca-Release (CICR). This massive increase in Ca^{2+} concentration in the myocyte (from 0.1 µM up to 1µM), engages the contraction machinery as the actin and myosin filaments transduce chemical energy into mechanical force[5]. Eventually, a decay in the Ca^{2+} current due to CDI and voltage-dependent inactivation (VDI) of the LTCCs allows K^+ conductances to dominate, and hence repolarize the V_m towards the equilibrium potential for K^+ (phase 3). During this phase, the surplus intracellular Ca^{2+} is pumped back to either the extracellular medium or the SR via the Na-Ca^{2+}-exchanger (NCX) or the sarco-endoplasmic reticulum Ca^{2+}-ATPase (SERCA), respectively. This resets the cell to a diastolic state (phase 4), during which the myocyte relaxes and is ready for the next oncoming beat.

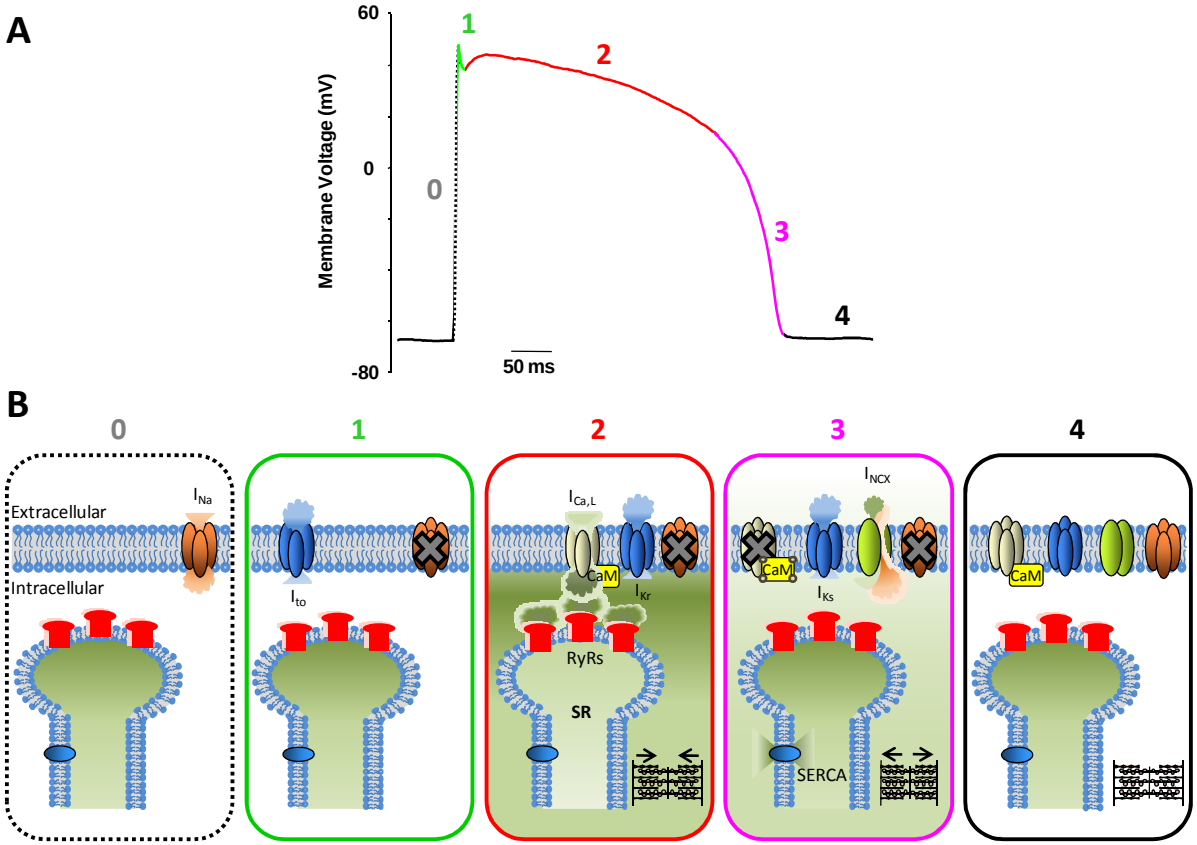

Figure 1.2 The Cardiac Action Potential. A) Phases of a typical cardiac action potential (AP), phases 0-4, are shown in a representative recording from an isolated rabbit ventricular myocyte. B) During phase 0 (grey dashed box) Na^+ channels activate and depolarize the membrane potential (V_m) resulting in a sharp upstroke. During phase 1 (green box) Na^+ channels quickly inactivate and activation of a transient outward current (I_{to}) of K^+ ions causes a brief dip in the V_m. During phase 2 (red box), the outward current of K^+ channels is balanced by the influx of Ca^{2+} from L-type Ca^{2+} channels resulting in a plateau phase during which the membrane potential does not change much. Furthermore, Ca^{2+} influx causes Ca^{2+} release from the SR via RyR channels, therefore the overall $[Ca^{2+}]$ is high (indicated by the green shading), leading to the contraction of the actin and myosin filaments. During phase 3 (pink box) Ca^{2+} channels begin to inactivate and K^+ currents dominate causing the membrane potential to repolarize. During this time, The Ca^{2+} that entered the cell is extruded by the NCX and the Ca^{2+} release by the SR is re-uptaken by the SERCA pump leading to the overall decline in $[Ca^{2+}]$ and a relaxation of the actin and myosin filaments. Phase 4 is the diastolic interval during which all channels recover from inactivation and are ready to undergo the excitation-contraction cycle once again.

1.3 Early afterdepolarizations as triggers for cardiac arrhythmias.

The natural rhythm of the heart can be disrupted due to a number of genetic or acquired conditions. The type of abnormal rhythm (i.e. tachycardia vs. bradycardia) and the origin of the disturbance (i.e. atrial or ventricular) can vary and thus indicate the severity of the disorder and risk of mortality. The most dangerous cardiac arrhythmias often arise in ventricular tissue and include ventricular tachycardia (VT) and ventricular fibrillation (VF)[6]. VT is characterized by a

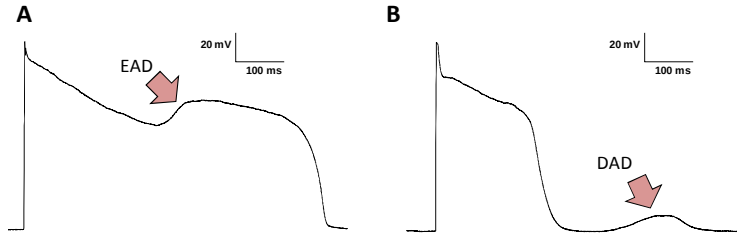

Figure 1.3 Early Afterdepolarizations & Delayed Afterdepolarizations. A) An early afterdepolarzation (EAD) is shown during phase 2 of the cardiac action potential. Note the reversal of repolarization and the prolongation of the APD. B) A delayed afterdepolarization (DAD) occurs after repolarization of the AP is complete. Since Ca^{2+} channels cannot be activated at hyperpolarized membrane potentials during diastole, the cellular mechanisms for DADs are considered separate from those of EADs.

rapid heartbeat, which is a result of ectopic beats (i.e. the heart rate is set outside of the pacemaker sites) in the ventricles brought on by cellular triggers. Such triggers, whether they occur during systole or diastole, can cause premature excitability and lead to spiral waves which can then degenerate to wave break, a hallmark of ventricular fibrillation. Cellular triggers of VT and VF are called early afterdepolarizations (EADs) if they occur during systole or delayed afterdepolarizations (DADs) if they occur during diastole (Fig. 1.3). Although both EADs and DADs are considered highly arrhythmogenic, the underlying mechanism for each is still an open area of investigation. In this dissertation, I will focus on the cellular mechanisms for EADs.

1.4 Cellular Mechanisms for EADs and the "Window" current

What defines an EAD? An EAD is a transient depolarization during phase 2 or phase 3 of the cardiac AP that tends to emerge at low pacing frequencies[7] and hence is associated with bradycardic arrhythmias[8, 9]. EADs were first described in canine purkinje fibers in the 1970s[10]. At the time, it was unknown which ionic currents were responsible for EAD occurrence, although it was proposed that a net increase of inward currents over outward currents is required. Inward currents such as the Na^+ current (I_{Na}), or the Ca^{2+} current ($I_{Ca,L}$)[11] were subsequently suggested as potential conductances involved in EAD formation.

Direct evidence for sarcolemmal Ca^{2+} entry (as opposed to Ca^{2+} release from intracellular stores) playing a key role in EAD occurrence came from Marban *et. al.* who demonstrated, in ferret ventricular tissue, that an increase in extracellular Ca^{2+} augmented EAD occurrence, while blocking SR Ca^{2+} release with ryanodine or chelating intracellular Ca^{2+} maintained EADs[12]. Furthermore, they also showed that opening of Ca^{2+} channels directly resulted in the appearance of EADs by applying Bay K8644, a Ca^{2+} channel agonist, and that EADs were subsequently eliminated using a Ca^{2+} channel blocker, nitrendipine. January *et. al.* also obtained similar results, and suggested that APD prolongation and flattening of the AP plateau within a range of potentials was crucial and a prerequisite for the appearance of EADs[13]. These findings implied that EAD induction was dependent on both time and voltage-dependent mechanisms. January and colleagues observed that the voltages where EADs were induced overlapped with the voltages where recovery from inactivation of the LTCCs occurs[14]. Using sophisticated voltage-clamp protocols, January and Riddle subsequently tested their hypothesis that reactivation of LTCCs contributes to EAD formation by demonstrating that the voltage-dependence of EADs mirrors the voltage-dependence and time-dependent recovery of LTCCs[15], however they did not rule out the possibility that other inward currents such the electrogenic current carried by the Na-Ca exchanger[16] may also play a role. Their experiments provided the first indication that L-type Ca^{2+} channel reopening during steady-state may allow the flux of an inward current due to the overlap of the activation and inactivation curves of LTCCs[17]. This steady-state current, called the Ca^{2+} "window" current, was further shown to be sizable in neonatal rat cardiomyocytes[18], strengthening the case for reactivation of LTCCs as a direct cause of EADs.

Most investigators accept two broad classification of EADs based on whether they occur during the plateau (phase 2) or during repolarization (phase 3). Depending on this classification, the proposed mechanism for EAD occurrence varies. Since phase 3 EADs tend to arise at more

hyperpolarized membrane potentials (below -40 mV) compared to phase 2 EADs, which occur at the plateau potential (between -10 mV and +20 mV), a number of laboratories have proposed that either the Na^+ window current or reverse-mode action of the Na-Ca exchanger[16, 19] could play a major role in phase 3 EADs. The reasoning behind this idea is due to the fact that Ca^{2+} channels are not active below - 40mV, and therefore unlikely to contribute to EAD formation. Modeling studies also corroborated the possibility of Na-Ca exchange current contributing to phase 3 EADs ($I_{Na\text{-}Ca}$)[20, 21].

In a majority of the studies described above, EADs were induced either by the presence of Cs^+ to block K^+ currents and delay repolarization or by directly altering the gating properties of LTCCs using an agonist such as Bay K8644. These experimental models of EAD induction are highly relevant for patients with long QT syndromes caused by channelopathies[22-24]. However, in patients with ventricular arrhythmias the underlying mechanism of arrhythmogenesis may vary depending on the clinical context. For example, pathophysiological conditions induced by stress, ischemia-reperfusion injury, heart failure etc. may alter the mechanism by which EAD-mediated triggered activity arises.

An important pathophysiological condition that is highly relevant both locally, in the cardiac tissue, and systemically is oxidative stress[25-27]. Blood carries nutrients, most importantly oxygen, which is required as the terminal electron acceptor in a series of redox reactions in the electron transport chain for the production of ATP on the inner membrane of mitochondria. A constant supply of ATP is critical during the cardiac excitation-contraction cycle for many membrane proteins such as the Na^+-K^+ pump, the Na^+-Ca^{2+} exchanger and many others, which utilize the chemical energy of ATP to drive the transport of ions against their electro-chemical gradients and hence maintain ionic balances across cell membranes. Therefore, a disruption in blood flow (ischemia) causes a reduced supply of oxygen leading to an altered metabolic state which

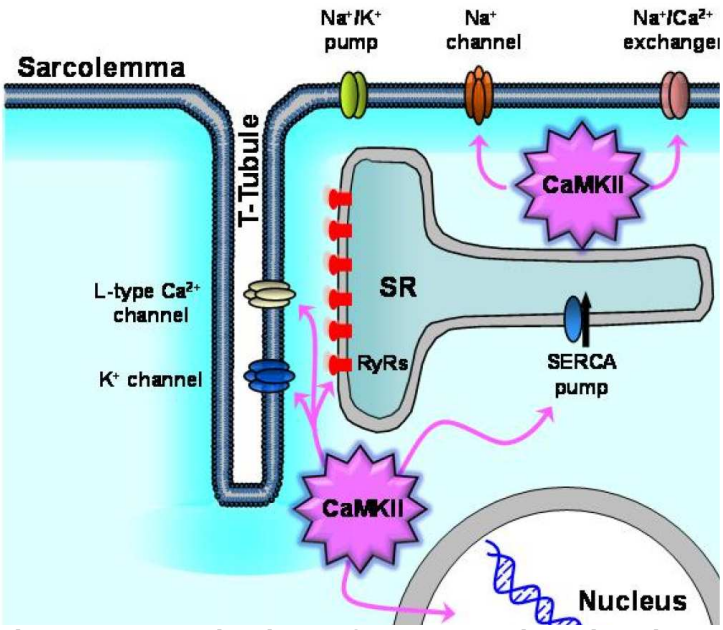

Figure 1.4 Activation of CaMKII Phosphorylates Multiple Targets Within Cardiac Myocytes. Reactive oxygen species can activate CaMKII and induce phosphorylation of Na^+ channels, LTCCs, K+ channels, NCX, RyRs, and the SERCA pump. All these alterations lead to an altered state in which Ca^{2+} handling and cellular excitability are drastically different.

activates inflammatory signaling pathways and the production of reactive oxygen species (ROS). Thus, electrical remodeling due to oxidative stress may cause widespread consequences for cellular excitability and Ca^{2+} homeostasis. To complicate matters further, increased intracellular Ca^{2+} levels and activation of ROS compounds both independently activate Ca/calmodulin-dependent protein kinase II (CaMKII), a second messenger which phosphorylates multiple targets within the cell including Na^+ and Ca^{2+} channels, RyRs, as well as transporters like SERCA, among others[28, 29] (Fig. 1.4).

Several groups have demonstrated the EAD-genic effects of ROS and/or CaMKII [30-34]. Hydrogen peroxide (H_2O_2), a potent biologically reactive ROS which can easily cross the plasma membrane, is directly produced in cardiac tissue upon reperfusion following ischemic injury[35-37]. The time-course of the effects of H_2O_2 on the cardiac AP were first described by Beresewicz *et. al.* in rat and guinea pig myocytes[38]. Upon the addition of 30 μM H_2O_2 in the superfusate, they observed a flattening of the plateau and prolongation of AP duration (APD) followed by the appearance of one or more EADs within approximately 10 minutes. Ward *et. al.* subsequently demonstrated that the effects of 100 μM H_2O_2, namely APD prolongation, EAD formation, and slowing of I_{Na} inactivation, could be inhibited using 8 μM tetrodotoxin (TTX), a

Na^+ channel blocker. Based on their observations that H_2O_2 slowed I_{Na} inactivation kinetics, and that application of Anthopleurin A (a compound well-known for slowing the rate of I_{Na} inactivation) mimicked the effects of H_2O_2 in terms of APD prolongation and EAD induction, they concluded that Na^+ channels likely play a major role in the pro-arrhythmic effects of H_2O_2. More recently, it was demonstrated that a 10 μM dose of a novel compound, Ranolazine, which selectively blocks the persistent inward Na^+ current was effective at attenuating APD prolongation, suppressing EADs and blocking late I_{Na}[34]. The proposed underlying mechanism of H_20_2-induced remodeling of the AP is not limited to I_{Na} however. Many laboratories have provided evidence which suggests that H_2O_2 modifies many different ionic conductances involved in shaping the AP such as $I_{Ca,L}$, $I_{K,ATP}$, I_{Kr}, I_{NCX}, and the Ca^{2+} transient (produced by RyRs), among others[30, 38-43]. Whether there is a single ionic conductance responsible for the pro-arrhythmic effects of H_2O_2 or simply that each of the observed changes in currents contribute remains to be fully understood.

1.5 L-type Ca^{2+} Channels

Calcium channels are critical for the proper function of diverse cell types such as neurons, smooth muscle cells and cardiomyocytes, and are found in organisms ranging from invertebrates to mammals[44, 45]. By regulating the influx of Ca^{2+}, these channels influence a variety of downstream physiological processes such as synaptic transmission, transcription, gene expression, and muscle contraction[46, 47]. Their profound importance in sustaining life is reinforced by the observation that mice lacking the gene encoding LTCCs die during early embryonic development[48]. In cardiac tissue, two types of Ca^{2+} channels exist: L-type and T-type[49]. Although both types of channels are activated in response to depolarized membrane potentials, each are classified based on their threshold for activation and time-course of inactivation. L-type Ca^{2+} channels are activated by high voltages and the resulting inward current is longer in duration than T-type Ca^{2+} channels which are activated by low voltages and

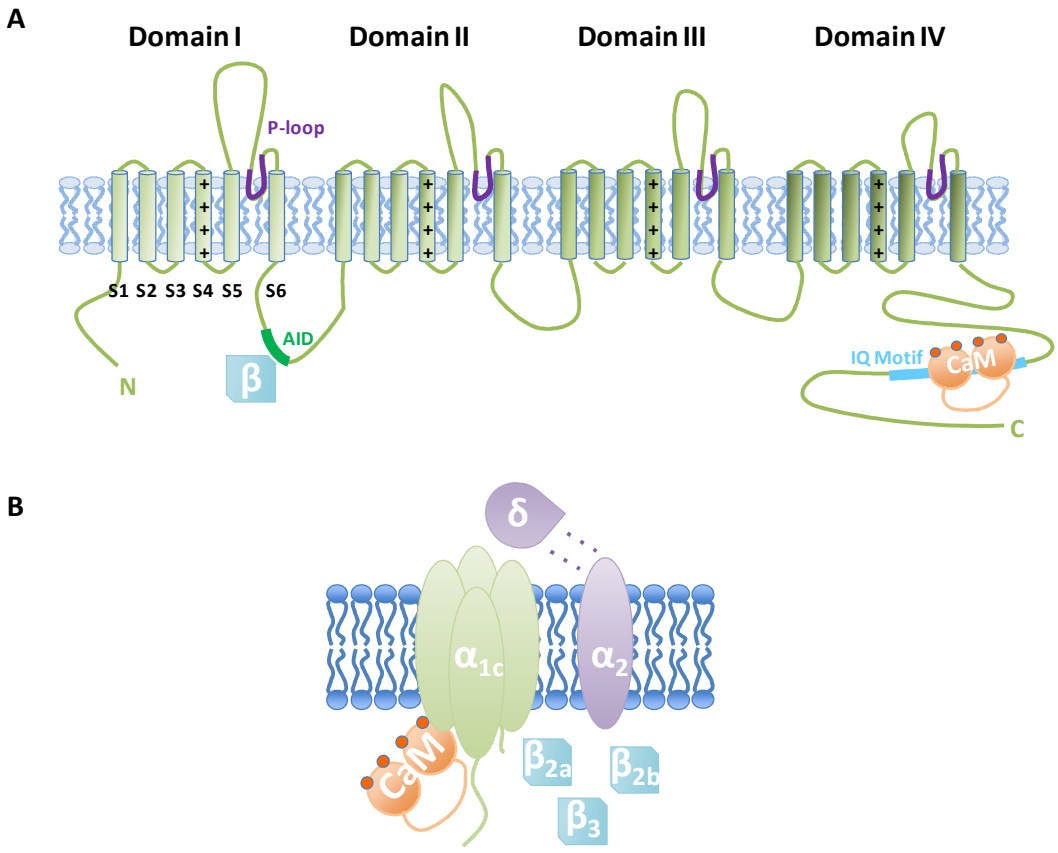

Figure 1.5 Topology & Orgnaization of L-type Ca^{2+} Channel Complexes. The L-type Ca^{2+} channel polypeptide consists of four tandem repeats (Domains I-IV), each crossing the membrane six times (S1-S6). Helix S4 contains positively charged residues, which together with S1-S3, make up the voltage-sensing domain, whereas the loop between S5-S6 from each repeat contribute to the ion-selective pore. The intracellular loop between domains I and II contains the α-interaction domain (AID) which binds β subunits, while the C-terminal tail contains the calmodulin (CaM) binding IQ-motif. (B) A cartoon of the multimeric composition of LTCC complexes: the α_{1C} pore-forming subunit is shown coassembled with intracellular β subunits, CaM and an extracelluar $\alpha_2\delta$ subunit.

produce a transient current. Additionally, the Ca^{2+} current carried by LTCCs decays with time, in both, a voltage and calcium-dependent manner. In the ventricular myocytes, L-type channels predominate and are localized primarily in the T-tubules[50].

Although the inward current carried by LTCCs was characterized in the 1960s[51], the molecular identitiy of the cardiac L-type Ca^{2+} channel was established by Mikami and colleagues from rabbit hearts in the late 1980s[52]. Also called dihydropyridine receptors (DHPRs) due to their sensitivity to dihydropyridines, L-type Ca^{2+} channels are multimeric protein complexes, made up

of a pore forming α_1 subunit, a transmembrane $\alpha_2\delta$ subunit, and multiple intracellular β subunits (Fig.1.5B). Association of the $\alpha_2\delta$ and β subunits with the α_1 subunit not only alters channel gating, but also promotes channel trafficking and increases their membrane expression[53]. The α subunit is encoded by a single gene (CACNA1) and has multiple splice variants (α_{1A}-α_{1E} or $Ca_V1.2$-$Ca_V1.4$). Similarly, the $\alpha_2\delta$ subunit is also encoded by a single gene, however, unlike α_1, it is post-translationally cleaved into two separate proteins, which are trafficked to the plasma membrane, where α_2 is exported to the extracellular milieu where it is linked to the δ subunit via disulfide bonds[54]. In contrast, four β subunits (β1-β4) are encoded by separate genes, each of which have multiple splice variants which localize intracellularly and are involved in diverse cellular signaling pathways[55]. Topology of the α subunit is, in some respects, similar to that of Na^+ channels in that the entire channel is assembled from a single polypeptide chain consisting of four distinct domains (non-identical repeats) made up of six transmembrane α-helical segments each (Fig. 1.5). The four domains are linked by intracellular loops which have residues that interact with β subunits via the α-interaction domain (AID), while the intracellular C-terminal tail contains the IQ motif which confers sensitivity to the associated Ca^{2+}-sensor, CaM[56], which in turn drives Ca^{2+}-dependent responses such as inactivation and facilitation[57, 58]. The voltage sensing particles are made up by S4 transmembrane segments which have positively charged residues that are displaced upon membrane depolarization. The pore of the channel is formed by a loop (P-loop) between the S5 and S6 transmembrane segments and includes a selectivity filter, which allows the conduction of Ca^{2+} ions. Therefore, the essential machinery of the channel, in terms of the voltage sensors, the conduction pore and other gating modules are all found within the α subunit, while the auxiliary $\alpha_2\delta$ and β subunits are mainly modulatory. Co-expression with $\alpha_2\delta$ and β subunits profoundly modifies LTCC biophysical properties, increasing surface membrane expression, open probability, and modulating voltage dependence and kinetics[3, 59-61].

A defining regulatory feature of LTCCs is their dual mechanisms of inactivation by both voltage and intracellular Ca^{2+}, which serve to limit the level of Ca^{2+} influx during prolonged depolarization and as a result, regulate the toxic downstream effects of elevated intracellular Ca^{2+}. The existence of these two inactivation mechanisms in cardiac preparations were first described in the mid-1980s by multiple laboratories[62, 63], however the molecular determinants of these processes were not known. Voltage-dependent inactivation (called VDI) is an intrinsic feature of the α_1 subunit as demonstrated by experiments in *Xenopus* oocytes with Ca^{2+} channel chimeras[64]. In this study, Zhang and colleagues constructed chimeras of multiple voltage-gated Ca^{2+} channels with different inactivation kinetics. Using this strategy, they were able to pinpoint the S6 segment of domain I as a key molecular determinant of the fast inactivation of Ca channels leading them to hypothesize that the mechanism underlying voltage-dependent inactivation occurs by a collapse in the pore of the channel, similar to C-type inactivation in K^+ channels[65, 66].

Subsequent studies proposed a “hinged lid” mechanism, similar in principle to the ball-and-chain inactivation mechanism of Na^+ channels[67], in which the I-II linker region was thought to dock to the S6 segments of domain II and III[68]. This mechanism was based on evidence from chimeras between α_{1c} (slow inactivation kinetics) and α_{1E} (rapid inactivation kinetics) which demonstrated that substituting the I-II linker or the S6 segments of domain II or III of α_{1E} could confer fast inactivation to α_{1C} channels, but all three of those regions of the α_{1C} sequence were necessary to confer slow inactivation to α_{1E} channels. Meanwhile, others demonstrated the importance of a methionine residue in the S6 segment of domain IV of neuronal α_{1A}[69]. Collectively, these studies implicate all four domains as key regulators of VDI in voltage-gated Ca^{2+} channels.

Notably, mutations in α_1 (G406R) have been identified which eliminate VDI, resulting in a multisystemic disorder called Timothy Syndrome, in which patients present with autism, heart

defects and lethal arrhythmias [22, 23, 70, 71]. A different mutation in α_{1C}, V2014I, results in a shift of the steady-state voltage-dependent inactivation curve to more negative potentials, and was found in patients suffering from Brugada Syndrome, which exhibit arrhythmia and sudden cardiac death[72]. These life-threatening channelopathies reveal the importance of a shift to a non-conductive state in a timely manner during prolonged depolarization in voltage-gated Ca^{2+} channels in excitable tissues. However, understanding of the VDI mechanism is further complicated by the presence of both fast and slow components. The fast component occurs on a time-scale of milliseconds while the slow component occurs within seconds. Furthermore, the contribution of ancillary subunits such as $\alpha_2\delta$ and β to VDI adds to the functional diversity of LTCCs. Given that $\alpha_2\delta$ and most β subunits (except β_{2a}) shift the voltage dependence of inactivation towards more hyperpolarized potentials, despite the fact that they share no structural similarity and bind to different parts of α_1, emphasizes the notion that the molecular determinants of VDI are not localized within a single region of the α_1 subunit, but rather that VDI is a decentralized process which requires cumulative changes in protein structure. Therefore, it is not surprising that a unified theory of the molecular mechanism of VDI is still poorly understood.

Calcium-dependent inactivation (CDI) of LTCCs, on the other hand, has been studied extensively[73-77]. An early study by Hadley and Lederer, demonstrated that while step-wise increases in $[Ca^{2+}]$ using photo-sensitive caged Ca^{2+} compounds such as DM-nitrophen or nitr-5 inactivated $I_{Ca,L}$, the gating currents were unchanged suggesting that the mechanism for CDI was unrelated to voltage-dependent conformational changes in the channel[73]. Moreover, they provided evidence that was in opposition to a prevalent hypothesis at the time, that a rise in $[Ca^{2+}]$ leads to dephosphorylation of LTCCs, rendering them inactive[78]. In particular, they noted that the time course of CDI following a flash of Ca^{2+} release was too fast to be accounted for by

an enzymatic reaction and proposed that perhaps a more accurate scenario involves the enzymatic regulation of an inhibitory Ca^{2+}-binding site within the channel.

Single-channel experiments, further teased apart the kinetic mechanisms underlying CDI without the confounding factor of Ca^{2+} domains[74]. Imredy *et al.* demonstrated that upon an increase in Ca^{2+}, channel gating shifts from a regime characterized by intense bursts of activity to one with sporadic openings due to a 100-fold reduction in opening rate. This provided a distinct mechanism from that of VDI, which is characterized by a reduction in channel availability[79]. Furthermore, in the same study, they provided concrete evidence against the phosphatase hypothesis using whole-cell patch clamp in cardiomyocytes. They elegantly, isolated the effects of CDI by subtracting Ca^{2+} and Ba^{2+} currents in patches with ryanodine to block SR Ca^{2+} release. Using this experimental design, they found that even in the presence of phosphatase inhibitors, CDI was evident and perhaps even slightly more pronounced. As a result, they concluded that the biochemical mechanism responsible for initiating CDI is independent of the phosphorylation state of the channel. Subsequent studies, identified potential Ca^{2+} binding[80] and calmodulin (CaM) binding motifs[81] within the channel, yet the precise biophysical basis of CDI remained elusive until 1999. During this time, two different laboratories independently arrived at the same conclusion: namely, that CaM is essential for imparting Ca^{2+} sensitivity to LTCCs and for regulating both CDI and Ca^{2+}-dependent facilitation[82, 83]. Most notably, Alseikhan *et al.* unequivocally demonstrated the physiological importance of CaM as a Ca^{2+}-sensor mediating CDI in LTCCs of cardiac myocytes using engineerined CaM[75]. This approach, in which the CaM was mutated at all four Ca^{2+}-binding sites[84] to abolish its Ca^{2+}-sensitivity and heterogously expressed in adult rat cardiomyocytes, allowed the investigators to probe the physiological role of Ca^{2+}-dependent regulation of LTCCs associated with CaM. Their intriguing results show that in cells expressing the recombinant

CaM, CDI was eliminated and only a monotonic decay (due to VDI) remained resulting in very long APDs.

Thus, biochemical and structural characterization of proteins can provide important clues about their function and physiological roles. Despite the intense efforts put forth by biophysicists, physiologists, biochemists, and others towards understanding the relationship between structure and function of LTCCs, a high-resolution structure of the α subunit remains elusive. Crystallographic studies of the β subunits, on the other hand, have proved to be more fruitful, with the structures of the core regions of β_{2a}, β_3 and β_4 subunits revealing their modular nature[85-87]. The results, from various laboratories, are in agreement and specify the existence of a Src Homology 3 domain (SH3) and a guanylate kinase (GK) domain linked by a HOOK region. Thus, such a description makes β subunits a part of the family of membrane-associated guanylate kinases (MAGUKs), a diverse set of intracellular proteins, which assemble as multimeric protein complexes.

An important feature of β subunits is their direct association with and modulation of the α subunit (although not their sole function[88, 89]). Therefore, thorough consideration of the molecular structures involved in the α-β interaction is essential to unravel the mechanism by which β subunits alter the gating of the channel. To this end, various biochemical and electrophysiological investigations have proposed an 18 residue region within the I-II loop of the α subunit, called the α interaction domain (AID), as being required for the interaction with β subunits[90-92]. Analogously, β subunits contain a region known as the β interaction domain (BID), which associates with the AID[93]. With regards to the $\alpha_2\delta$ subunit, a structural motif known as a Von Willebrand factor-A (VWA) domain, known for binding extracellular matrix proteins has been identified within the transmembrane α_2 subunit. While the importance of this domain lies within its metal-ion-dependent adhesion site (MIDAS), which is required for channel trafficking[94],

elegant chimeric studies have described the role of the δ subunit predominantly on channel gating[95].

How does the interaction between α_1 and its auxiliary subunits influence channel properties? As mentioned above, numerous studies have demonstrated the ability of LTCC auxiliary subunits to act as chaperones to increase membrane expression and current density[94, 96-99]. The mechanism for this function, particularly with respect to β subunits, has been studied extensively[97-99]. Abundant structural and biochemical evidence suggests that the α-β interaction forms early during post-translation processing and masks an endoplasmic reticulum (ER) retention signal on the I-II loop of the α subunit[97, 100]. Moreover, removing the I-II loop from LTCCs promotes expression even in the absence of auxiliary subunits[100]. A recent study, however, proposed an alternative explanation for the mechanism of β-mediated upregulation of LTCCs[101]. More specifically, Altier *et. al.* observed that in the absence of β, LTCCs were robustly ubiquitinated by the RFP2 ubiquitin ligase and targeted for degradation within the ER. Therefore, rather than merely chaperoning the trafficking of channels to the plasma membrane, β subunits may play a protective role and prevent targeted degradation of LTCCs.

Characterization of the effects of β subunit interaction on the gating properties of LTCCs demonstrated a significant shift of the conductance-voltage (G-V) relationship toward more negative potentials in the presence of β_{2a} in heterologously expressed channels, while the voltage dependence of the charge movements (gating currents) remained unchanged[102]. Hence, although β subunits facilitate channel opening at more negative potentials, gating current measurements (movement of the voltage sensors) revealed that the effects of β subunits on gating occurs only after voltage sensor relaxation has occurred. Furthermore, in addition to the steady-state voltage-dependence, it is well established that both the activation and inactivation kinetics are significantly altered in the presence of β subunits[103, 104]. Colecraft

and colleagues examined the contribution of different β subunits on LTCC gating by measuring single-channel currents in cell-attached patches of rat ventricular cells expressing each β subunit (β_{1b}, β_{2a}, and β_3)[60]. Notably, their results demonstrate that each subunit endows the channel with distinctive kinetic profiles, with cells expressing β_{2a} displaying bursts of activity without undergoing inactivation. Furthermore, in an effort to pinpoint the identity of the endogenous β subunit in cardiac cells, they heterogously-expressed each β subunit in HEK293 cells to recapitulate the kinetic profile of endogenous LTCCs in cardiac cells. They found that the expression of β_{2b} most closely resembled both the macroscopic and single-channel currents found in cardiac cells, in agreement with the commonly held position in the field that β_2 predominates in ventricular cells[105-108].

Therefore, collectively, the extensive biophysical characterization of LTCCs and their auxiliary subunits reveal that the extent of Ca^{2+} influx during the action potential is determined by both their time-dependent and steady-state biophysical properties. These include the kinetics of channel opening, the kinetics of CDI and VDI, the kinetics of recovery from inactivation and by the membrane potential, which determines the driving force for Ca^{2+} entry as well as the fraction of channels in various conductive and non-conductive states.

Collectively, the findings from the studies reviewed above emphasize that although the molecular mechanisms of β-induced changes in structural and functional properties of LTCCs is relatively well-understood, the dynamic changes in subunit composition and the subcellular localization *in vivo* modulate the physiological functions and roles that LTCCs play. Of particular importance are the changes in physiological function of LTCCs during pathophysiological conditions in cardiac tissue. For example, in the failing heart the combination of a number of molecular and cellular changes such as disorganized T-tubules[109], altered gating of LTCCs[110, 111], and expression of auxiliary subunits[112] collectively render the heart more susceptible to arrhythmias[113-115]. Although many of these changes are compensatory, and etiologically developed to maintain cardiac output to ensure that all organs receive adequate blood flow,

often with a chronic increase in load, electrophysiological disturbances eventually overtake and lead to sudden cardiac death. Therefore, therapeutic interventions aimed towards ameliorating electrophysiological disturbances may be important for many patients in the early stages of heart failure.

1.6 The Dynamic Patch Clamp

The patch clamp technique, first developed by Neher and Sakmann[116], revolutionized the field of physiology and biophysics by allowing electrophysiologists to directly study ion channel function. The technique is based on the idea that a finely pulled glass tube (pipette) with an electrode inside can form a tight seal (called a "gigaseal") with the lipid bilayer of cell membranes upon applying light negative pressure, forming the "cell-attached" configuration (Fig. 1.6). Once a high-resistance seal on the order of gigaohms is made, various physical disturbances can be applied to render the cell membrane into different configurations. The cell-attached configuration allows one to record membrane currents from intact cells where only the extracellular solutions can be altered. After achieving a gigaseal, one can rupture the membrane with additional negative pressure to be in whole-cell mode, where the pipette solution is continuous with the cytoplasmic mileu. In this mode, the cell can be dialyzed with a desired solution or compound and the extracellular solution can also be changed. Alternatively, one can swiftly retract the pipette from the cell body after gigaseal to achieve the inside-out excised patch mode in which one has access to the cytoplasmic face of the channels. If such a maneuver is made in whole-cell mode, the cell membrane will reseal upon itself to form a small vesicle at the pipette tip, called outside-out excised patch, in which the extracellular side of the channels can be manipulated. Therefore, depending on the question at hand all these configurations of patch clamp can yield useful information about the behavior of ion channels and other membrane proteins.

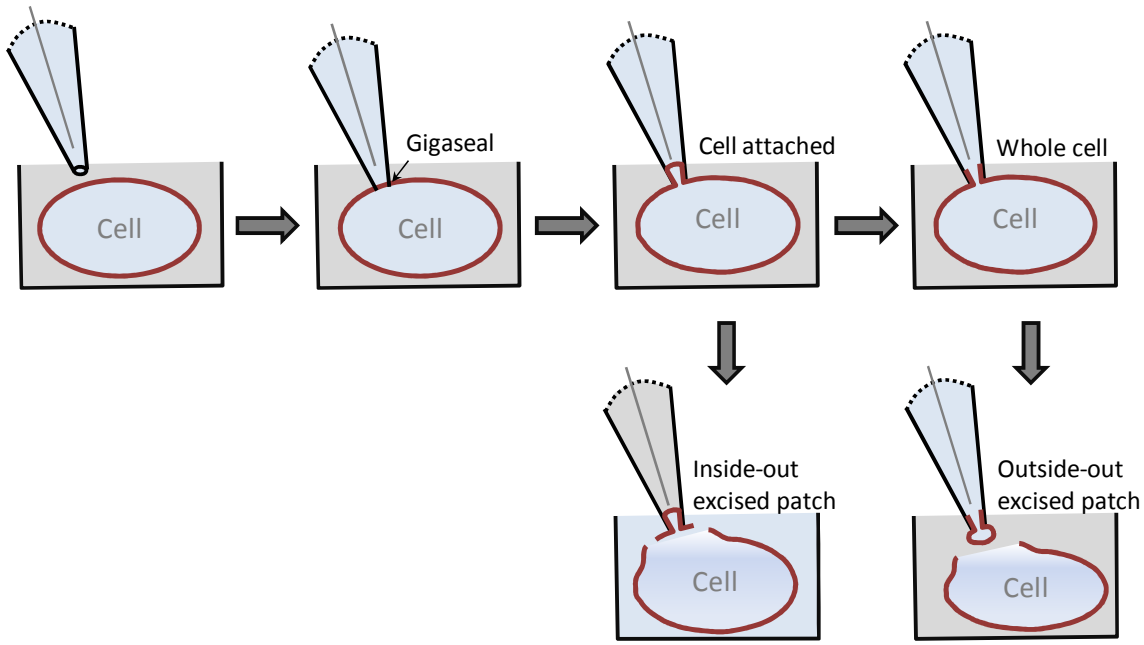

Figure 1.6 The Patch Clamp Technique & Its Configurations. A high resistance seal called a "gigaseal" is formed when negative pressure is applied after the pipette is in contact with the cell membrane. Recordings made in this configuration, measure single channel currents from the extracellular side of the cell membrane. In whole-cell mode, the cell membrane is ruptured by applying additional negative pressure thereby allowing one access to the interior of the cell and record a sum of all currents crossing the entire cell membrane. From cell-attached mode, one can retract the pipette to detach a portion of the membrane from the rest of the cell to enter the "inside-out" excised patch mode. In this way, one can record single channel currents from the extracellular side while altering the solution on the intracellular side. Alternatively, from whole-cell mode, one can retract the pipette to form a vesicle at the tip of the pipette, called the "outside-out" excised patch. In this configuration, single channel currents can be recorded from the intracellular side while altering the solution on the extracellular side.

The patch clamp recordings made in my experiments are all in the whole-cell configuration, where, after the formation of a gigaseal, applying additional negative pressure ruptures the membrane to allow access to the cytoplasm. In this configuration, the recorded signal reflects the sum of all electrical activity across the entire cell membrane rather than through a single ion channel or through a population channels. In this manner, depending on the mode of the amplifier, one can record voltage deflections such as action potentials (current clamp), or ionic fluxes through specific ion channels such as Ca^{2+} currents (voltage clamp). In the current clamp mode, a current pulse injected via the electrode raises the membrane potential sufficiently to a

threshold at which activation of Na^+ channels initiates an action potential in excitable cells. In voltage clamp mode, the membrane potential is held constant by a negative feedback loop, which continuously samples membrane potential and passes current to “clamp” the voltage at a desired value. Since a change in membrane potential activates ion channels resulting in ionic fluxes which, in turn, change the membrane potential, the current injected by the electrode the maintain the command potential is equal in magnitude but opposite in charge to the ionic fluxes through ion channels.

Both current clamp and voltage clamp techniques have been widely used and refined since the development of the patch clamp in the early 1980’s to better understand the role of ion channels, transporters and pumps in various physiological settings as well as to characterize their structural and functional properties. Thus, the understanding of the behavior of excitable cells *in vitro* and *in vivo* has progressed greatly with the use of these techniques. Furthermore, it has facilitated the development of mathematical models of complex electrophysiological phenomena. Nevertheless, each method has its own set of limitations. While action potential recordings in current clamp mode can provide clues about physiologically relevant changes in the electrical activity of the cell, it cannot reveal the source of such alterations. On the other hand, recordings of ionic currents can provide information on the changes in functional properties of ion channels, but fails to convey how such changes may impact electrical signals *in vivo*. To overcome these limitations, researchers have long used mathematical models to provide a finer understanding of complex cellular behavior[117, 118]. One can incorporate data from both current clamp and voltage clamp studies to build detailed computational models which can recapitulate phenomena ranging from single channel behavior[119, 120] to full organ systems, such as the heart[121, 122]. Although the quantitative descriptions provided by many of these models are based on compilations of experimental data acquired over many years and hence, are highly sophisticated, often, assumptions must be made to account for gaps in knowledge and therefore have limitations of their own.

To overcome many of these limitations (although not all), a powerful new technique was developed independently, and in parallel, by cardiac physiologists and neurophysiologists [123, 124]. Tan and Joyner initially used the dynamic clamp technique to understand the contribution of intercellular coupling via gap junctions to AP morphology in rabbit ventricular cells in the whole-cell current clamp mode[123]. In this early implementation of the dynamic clamp, Tan and Joyner electrically coupled two individual myocytes that were not in direct contact by introducing and external circuit that was capable of altering the resistance between the two cells to any given value; in essence, they computationally introduced gap junctional currents. Thereby, they could measure the individual APs of both myocytes in real-time while varying the junctional resistance and therefore could maintain the electrophysiological integrity of each cell and tease apart the contribution of cell-cell coupling in a discrete manner. Based on their results, they were able to conclude that small currents introduced by cell-cell coupling can have a major impact on AP duration in ventricular tissue. Similarly, citing an inability to vary the strength of synaptic connections in neuronal networks, Sharp *et al.* introduced a computationally derived synaptic current between two oscillatory neurons to study the consequences on their firing properties[124]. In addition to a purely electrical synapse (analogous to the gap junctional current in Tan and Joyner's study), Sharp et al. could initiate a chemical synapse between the two cells upon a rise in the membrane potential of the presynaptic cell by using an iontophoretic release of the neurotransmitter γ-aminobutyric acid (GABA) onto the post-synaptic cell. Using this system, they probed how synaptic inputs can alter electrical signals and their frequencies in neuronal networks. Since the neurons need not even be in the same environment (i.e. same culture dish) to be coupled, the dynamic clamp setup allows one to dissect relative significance of a number of variables, which are difficult to isolate in conventional patch clamp setups. For example, in the work of Sharp et al. described above, they could now selectively apply pharmacological agents such as the K^+ channel blocker tetraethylammonium (TEA) to one cell or both to further

understand to what extent the intrinsic properties of either pre- or post-synaptic cells play a role in regulating the frequency of oscillations.

Subsequent to the seminal work on the development of the dynamic clamp described above, neurophysiologists in particular embraced the utility of the dynamic clamp technique. This led to numerous insights on the behavior of neuronal systems at both the cellular and network levels[125]. During the course of these studies, the technique was repeatedly adapted and refined to address the issue at hand, resulting in a variety of configurations and applications. For example, the first implementations of the dynamic clamp allowed the investigators to electrically couple two individual cells, however others have used dynamic clamp to introduce one or more computationally derived conductances into cells, both voltage-independent as well as voltage-dependent. In order to introduce a voltage-dependent conductance into an excitable cell, bidirectional communication must be established between the computational model of the conductance and the cell (Fig. 1.7). Once the cell is patch clamped (whole-cell) in the current clamp mode, the cell membrane potential is acquired and serves as an input for the computed conductance, which activates based on its voltage-dependence properties. Activation (and thereby injection) of the computed current alters the membrane voltage of the cell, which is again sampled by the "virtual" computational conductance, therefore the cycle of current injection and voltage sampling continues in real-time until the membrane potential reaches a level where the conductance no longer activates or until the inactivation mechanisms incorporated in the computational model reduce or shut-off current injection. On the other hand, voltage-independent conductaces can be programmed to be injected into the cell at a desired time of the recording or continuously. Therefore, the power of the dynamic clamp lies in its ability to introduce novel, tunable conductances into live cells in real-time. Furthermore, it serves as an invaluable tool for making predictions about how targeting the biophysical properties of individual ion channels can affect the initiation, propagation, and morphology of electrical signals in excitable cells.

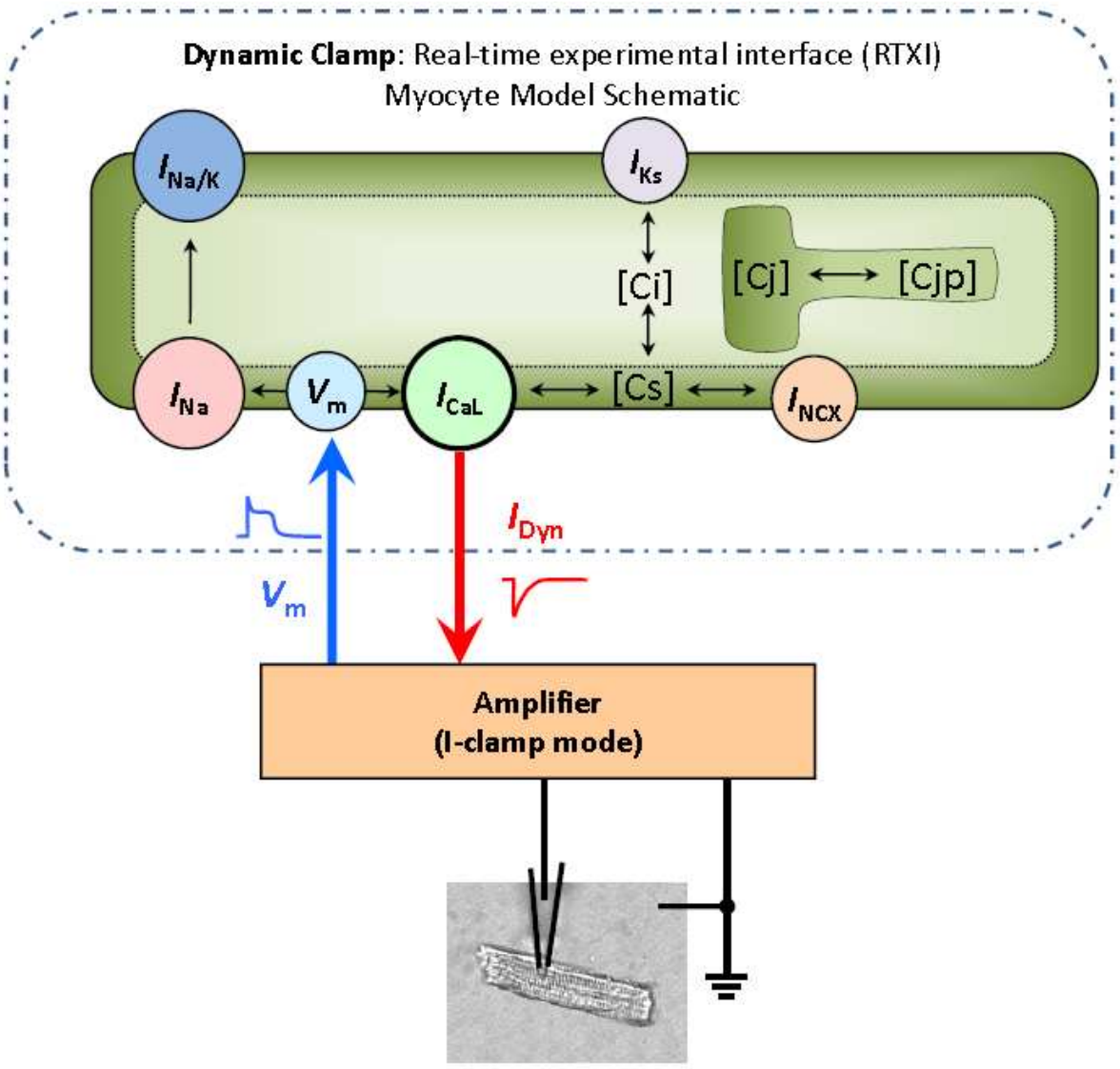

Figure 1.7 The Dynamic Clamp Technique. A diagram of our Dynamic Clamp set-up, which allows us to introduce a "virtual" conductance into a myocyte in real-time. A rabbit ventricular myocyte is whole-cell patch-clamped with an amplifier in current-clamp mode. The myocyte's V_m signal is digitized and input to a computer (blue arrow) running a ventricular action potential model. This model includes macroscopic Hodgin-Huxley (HH) - type formulations for four conductances ($I_{Ca,L}$; the fast Na channel I_{Na}; the Na/K pump I_{NaK}; the Na/Ca exchanger I_{NCX}) and a sophisticated Ca^{2+} cycling algorithm that calculates [Ca^{2+}] for discrete cellular compartments, as well as Na and K cycling (not shown). The calculated ionic conductances can be output in any combination to produce I_{Dyn}. In this case, $I_{Dyn} = I_{Ca,L}$ (red arrow). I_{Dyn} is converted to analog before being input to the amplifier as the current command and injected into the clamped myocyte. This alters its V_m, which is in turn sampled for the next computation. Thus there is a dynamic, bidirectional relationship between V_m and model conductance output, at a sampling/computation frequency of 10kHz.

1.7 Quantitative models of cardiac action potentials.

Beginning with the seminal quantitative description of the relationship of ionic currents and membrane voltage in the squid axon put forth by Hodgkin and Huxley during the 1950's[117], mathematical modeling has played a critical role in providing mechanistic insight of the behavior of ion channels and their emergent properties. It was then widely accepted that the general properties of cellular excitability could be applied to cardiac tissue, paving the way for the first computation model of the cardiac AP, established by Denis Noble[126, 127]. Unlike nerve APs however, Noble found that two different potassium conductances were required to explain both the instantaneous rectification following depolarization (phase 1) and the delayed rectification to the resting membrane potential (phase 3). Although, the equations presented by Noble were meant to apply to purkinje and pacemaker cells, the formulations of sodium and potassium conductances were shown to be sufficient to elicit the long-lasting APs characteristic of all cardiac cells, completely devoid of other inward conductances such as Ca^{2+} (which we now know is essential). It wasn't until the late 1970s that a quantitative model for the ventricular action potential was developed by Beeler and Reuter, by integrating experimental evidence from voltage-clamp recordings from a variety of cardiac preparations[128]. In their discussion of the major ionic conductances that shape the ventricular AP, they stressed the contribution of the "slow inward current mainly carried by Ca^{2+} ions" on the AP plateau.

During the 1980s and 1990s, with the increase in computing power, quantitative descriptions and models of the cardiac ionic fluxes which make up the AP became progressively more sophisticated. Moreover, due to the technical advances in voltage-clamp methods (i.e patch-clamp)[129], which allowed one to record ionic currents from single channels and to achieve a fast clamp in isolated cells, the fields of ion channel biophysics and cardiac physiology became vastly more prolific. As a result, subsequent computational models such as the Luo-Rudy model, could recapitulate experimental data largely from single-channel recordings of ionic

currents from isolated ventricular myocytes[20]. The Luo-Rudy model incorporated six ionic currents such as the fast inward sodium current (I_{Na}), the slow inward Ca^{2+} current (whose formulation was unchanged from the Beeler-Reuter model), a time-dependent delayed rectifier potassium current (I_K), a time-independent inward rectifier potassium current (I_{K1}), a plateau potassium current (I_{Kp}) and a background potassium current (I_b). Using this model, Luo *et. al.* examined the origin of known aberrations of the cardiac action potential; for example, APD prolongation and supernormal excitability, namely early afterdepolarizations.

Recently, the collaborative efforts of both theoreticians and experimentalists have enabled the development of highly detailed AP models capable of providing insight on the mechanisms of cardiac arrhythmias from cellular to organ levels [130-132]. These AP models are devised to recapitulate various aspects of cardiac physiology and represent a theoretical framework of experimental and clinical findings such as wavebreak in cardiac tissue, APD restitution, susceptibility to triggered activity, etc. The cardiac AP duration is extremely dependent on the rate at which the heart is paced. Depending on whether a subsequent beat appears too soon or after an appropriate time interval, the AP can fail to capture (refractory period), be too short in duration, or recover completely. The APD restitution curve describes this relationship between the AP duration and the preceding diastolic interval and, notably, its slope has been linked to electrical stability of the cardiac tissue[133, 134]. It is well-established that the refractory period of the cardiac AP is directly dependent on recovery from an inactivated state of LTCCs. To account for these properties of the APD restitution, Mahajan and colleagues replaced the Hodgkin-Huxley formulation of $I_{Ca,L}$ from the Shannon *et. al.* model with a seven-state Markovian formulation in order to develop a rabbit AP model which could replicate experimentally observed APD restitution curves and Ca_i dynamics at rapid heart rates. Therefore using this AP model, they could more accurately describe interactions between voltage and Ca_i dynamics. This model was adapted for the dynamic clamp experiments used in this dissertation project.

Specifically, the formulation of $I_{Ca,L}$ was changed back to the original Hodgkin-Huxley-type formulation to allow us to modify specific parameters of $I_{Ca,L}$ in a discrete manner, rather than changing the gating behavior of the channel, which can be more difficult to interpret.

1.8 Therapeutic Strategies for Controlling Cardiac Arrhythmias

Thus far, I have presented evidence from basic science studies over the last three decades demonstrating the importance of inward conductances, specifically the L-type Ca^{2+} channels and its unique biophysical properties, in promoting EAD formation in mammalian cardiomyocytes. Based on these findings, many scientists and clinicians have proposed the use of Na^{+} and Ca^{2+} channel blockers as therapeutic targets to control the occurrence of arrnythmogenic triggers such as EADs[135-139]. Of these, dihydropyridines, Ca^{2+} channel blockers (classified as class IV anti-arrhythmics), have received considerable attention over the years[140], ranging from studies in isolated myocytes[12] to whole heart studies[141] to clinical trials[142]. Unfortunately, despite the promising results from preliminary studies in animal models[143], clinical studies have failed to find a significant improvement in mortality with the use calcium channel blockers for patients at high risk for cardiac arrhythmias[144]. The most widely used therapeutic strategy currently in clinical use for the management of ventricular arrhythmias is the surgical implantation of a defibrillator in the chest cavity, called the implantable cardioverter-defibrillator (ICD)[145]. Notably, by current clinical guidelines, ICD implantation is not indicated in the majority of patients (80%) who will die suddenly each year. Moreover, even in patients at highest risk, only 25% of implanted ICDs deliver life-saving shocks and the prolongation of life is modest, averaging 4.4 months[146]. In addition, the invasiveness of the procedure coupled with the high cost of surgery makes this treatment option less than ideal. Thus, an effective, widely applicable as well as cost-effective strategy to treat VF is strongly needed.

Since EADs are a well-established cellular trigger for VF and sudden death, the focus of this work is two-fold: i) to provide detailed mechanistic insight on the role of the $I_{Ca,L}$ in EAD formation and ii) to identify therapeutic targets to control the occurrence of EADs in cardiac myocytes. In Chapter 2, I use the dynamic clamp to replace the endogenous $I_{Ca,L}$ in rabbit ventricular myocytes with a computationally-derived $I_{Ca,L}$ in the presence of an EAD-inducing insult (oxidative stress or hypokalemia). Using this experimental setup, I present a proof-of-concept experimental paradigm whereby I demonstrate that reducing the $I_{Ca,L}$ window current by making modest shifts in the half-activation potentials of activation and inactivation (on the order of approximately 5 millivolts) are sufficient to abolish EADs without significantly distorting the Ca_i transient. Using the same experimental setup, in Chapter 3, I have used the dynamic clamp to probe the role of five additional biophysical parameters of $I_{Ca,L}$ in EAD formation. The goal of this study was to scan the sensitivity of both time-dependent as well as steady-state parameters governing $I_{Ca,L}$ on EAD occurrence. Of all remaining parameters studied, my results highlight the non-inactivating component of $I_{Ca,L}$, known as the $I_{Ca,L}$ pedestal current, as being critical for the onset of EADs. In Chapter 4, I have manipulated the $I_{Ca,L}$ window current in rabbit ventricular myocytes by a genetic means to implement the anti-arrhythmic interventions identified in Chapters 2 and 3. The findings highlight the feasibility of reducing susceptibility to triggers of cardiac arrhythmias by targeting L-type Ca^{2+} channels and their biophysical properties.

1.9 Bibliography

(1) Maltsev VA, Vinogradova TM, Lakatta EG. The emergence of a general theory of the initiation and strength of the heartbeat. *J Pharmacol Sci* 2006;100(5):338-69.

(2) Patel SP, Campbell DL. Transient outward potassium current, 'Ito', phenotypes in the mammalian left ventricle: underlying molecular, cellular and biophysical mechanisms. *J Physiol* 2005 November 15;569(Pt 1):7-39.

(3) Benitah JP, Alvarez JL, Gomez AM. L-type Ca(2+) current in ventricular cardiomyocytes. *J Mol Cell Cardiol* 2010 January;48(1):26-36.

(4) Sanguinetti MC. Dysfunction of delayed rectifier potassium channels in an inherited cardiac arrhythmia. *Ann N Y Acad Sci* 1999 April 30;868:406-13.

(5) Donald M.Bers. Excitation-Contraction Coupling and Cardiac Contractile Force. 2nd. Ed. 2001. Kluwer Academic Publishers, Dordrecht.
Ref Type: Generic

(6) John RM, Tedrow UB, Koplan BA, Albert CM, Epstein LM, Sweeney MO, Miller AL, Michaud GF, Stevenson WG. Ventricular arrhythmias and sudden cardiac death. *Lancet* 2012 October 27;380(9852):1520-9.

(7) Damiano BP, Rosen MR. Effects of pacing on triggered activity induced by early afterdepolarizations. *Circulation* 1984 May;69(5):1013-25.

(8) el-Sherif N, Bekheit SS, Henkin R. Quinidine-induced long QTU interval and torsade de pointes: role of bradycardia-dependent early afterdepolarizations. *J Am Coll Cardiol* 1989 July;14(1):252-7.

(9) Brachmann J, Scherlag BJ, Rosenshtraukh LV, Lazzara R. Bradycardia-dependent triggered activity: relevance to drug-induced multiform ventricular tachycardia. *Circulation* 1983 October;68(4):846-56.

(10) Cranefield PF. Action potentials, afterpotentials, and arrhythmias. *Circ Res* 1977 October;41(4):415-23.

(11) Katzung BG. Effects of extracellular calcium and sodium on depolarization-induced automaticity in guinea pig papillary muscle. *Circ Res* 1975 July;37(1):118-27.

(12) Marban E, Robinson SW, Wier WG. Mechanisms of arrhythmogenic delayed and early afterdepolarizations in ferret ventricular muscle. *J Clin Invest* 1986 November;78(5):1185-92.

(13) January CT, Riddle JM, Salata JJ. A model for early afterdepolarizations: induction with the Ca2+ channel agonist Bay K 8644. *Circ Res* 1988 March;62(3):563-71.

(14) Isenberg G, Klockner U. Calcium currents of isolated bovine ventricular myocytes are fast and of large amplitude. *Pflugers Arch* 1982 October;395(1):30-41.

(15) January CT, Riddle JM. Early afterdepolarizations: mechanism of induction and block. A role for L-type Ca2+ current. *Circ Res* 1989 May;64(5):977-90.

(16) Kimura J, Noma A, Irisawa H. Na-Ca exchange current in mammalian heart cells. *Nature* 1986 February 13;319(6054):596-7.

(17) Shorofsky SR, January CT. L- and T-type Ca2+ channels in canine cardiac Purkinje cells. Single-channel demonstration of L-type Ca2+ window current. *Circ Res* 1992 March;70(3):456-64.

(18) Cohen NM, Lederer WJ. Calcium current in isolated neonatal rat ventricular myocytes. *J Physiol* 1987 October;391:169-91.

(19) Szabo B, Sweidan R, Rajagopalan CV, Lazzara R. Role of Na+:Ca2+ exchange current in Cs(+)-induced early afterdepolarizations in Purkinje fibers. *J Cardiovasc Electrophysiol* 1994 November;5(11):933-44.

(20) Luo CH, Rudy Y. A model of the ventricular cardiac action potential. Depolarization, repolarization, and their interaction. *Circ Res* 1991 June;68(6):1501-26.

(21) Luo CH, Rudy Y. A dynamic model of the cardiac ventricular action potential. I. Simulations of ionic currents and concentration changes. *Circ Res* 1994 June;74(6):1071-96.

(22) Splawski I, Timothy KW, Sharpe LM, Decher N, Kumar P, Bloise R, Napolitano C, Schwartz PJ, Joseph RM, Condouris K, Tager-Flusberg H, Priori SG, Sanguinetti MC, Keating MT. Ca(V)1.2 calcium channel dysfunction causes a multisystem disorder including arrhythmia and autism. *Cell* 2004 October 1;119(1):19-31.

(23) Splawski I, Timothy KW, Decher N, Kumar P, Sachse FB, Beggs AH, Sanguinetti MC, Keating MT. Severe arrhythmia disorder caused by cardiac L-type calcium channel mutations. *Proc Natl Acad Sci U S A* 2005 June 7;102(23):8089-96.

(24) Erxleben C, Liao Y, Gentile S, Chin D, Gomez-Alegria C, Mori Y, Birnbaumer L, Armstrong DL. Cyclosporin and Timothy syndrome increase mode 2 gating of CaV1.2 calcium channels through aberrant phosphorylation of S6 helices. *Proc Natl Acad Sci U S A* 2006 March 7;103(10):3932-7.

(25) Schnabel R, Blankenberg S. Oxidative stress in cardiovascular disease: successful translation from bench to bedside? *Circulation* 2007 September 18;116(12):1338-40.

(26) Dhalla NS, Temsah RM, Netticadan T. Role of oxidative stress in cardiovascular diseases. *J Hypertens* 2000 June;18(6):655-73.

(27) Jeong EM, Liu M, Sturdy M, Gao G, Varghese ST, Sovari AA, Dudley SC, Jr. Metabolic stress, reactive oxygen species, and arrhythmia. *J Mol Cell Cardiol* 2012 February;52(2):454-63.

(28) Maier LS, Bers DM. Calcium, calmodulin, and calcium-calmodulin kinase II: heartbeat to heartbeat and beyond. *J Mol Cell Cardiol* 2002 August;34(8):919-39.

(29) Swaminathan PD, Purohit A, Hund TJ, Anderson ME. Calmodulin-dependent protein kinase II: linking heart failure and arrhythmias. *Circ Res* 2012 June 8;110(12):1661-77.

(30) Xie LH, Chen F, Karagueuzian HS, Weiss JN. Oxidative-stress-induced afterdepolarizations and calmodulin kinase II signaling. *Circ Res* 2009 January 2;104(1):79-86.

(31) Morita N, Sovari AA, Xie Y, Fishbein MC, Mandel WJ, Garfinkel A, Lin SF, Chen PS, Xie LH, Chen F, Qu Z, Weiss JN, Karagueuzian HS. Increased susceptibility of aged hearts to ventricular fibrillation during oxidative stress. *Am J Physiol Heart Circ Physiol* 2009 November;297(5):H1594-H1605.

(32) Sag CM, Wadsack DP, Khabbazzadeh S, Abesser M, Grefe C, Neumann K, Opiela MK, Backs J, Olson EN, Brown JH, Neef S, Maier SK, Maier LS. Calcium/calmodulin-dependent protein kinase II contributes to cardiac arrhythmogenesis in heart failure. *Circ Heart Fail* 2009 November;2(6):664-75.

(33) Ward CA, Giles WR. Ionic mechanism of the effects of hydrogen peroxide in rat ventricular myocytes. *J Physiol* 1997 May 1;500 (Pt 3):631-42.

(34) Song Y, Shryock JC, Wagner S, Maier LS, Belardinelli L. Blocking late sodium current reduces hydrogen peroxide-induced arrhythmogenic activity and contractile dysfunction. *J Pharmacol Exp Ther* 2006 July;318(1):214-22.

(35) Slezak J, Tribulova N, Pristacova J, Uhrik B, Thomas T, Khaper N, Kaul N, Singal PK. Hydrogen peroxide changes in ischemic and reperfused heart. Cytochemistry and biochemical and X-ray microanalysis. *Am J Pathol* 1995 September;147(3):772-81.

(36) Brown JM, Terada LS, Grosso MA, Whitman GJ, Velasco SE, Patt A, Harken AH, Repine JE. Hydrogen peroxide mediates reperfusion injury in the isolated rat heart. *Mol Cell Biochem* 1988 December;84(2):173-5.

(37) Brown JM, Terada LS, Grosso MA, Whitmann GJ, Velasco SE, Patt A, Harken AH, Repine JE. Xanthine oxidase produces hydrogen peroxide which contributes to reperfusion injury of ischemic, isolated, perfused rat hearts. *J Clin Invest* 1988 April;81(4):1297-301.

(38) Beresewicz A, Horackova M. Alterations in electrical and contractile behavior of isolated cardiomyocytes by hydrogen peroxide: possible ionic mechanisms. *J Mol Cell Cardiol* 1991 August;23(8):899-918.

(39) Zhang DM, Chai Y, Erickson JR, Brown JH, Bers DM, Lin YF. Intracellular signalling mechanism responsible for modulation of sarcolemmal ATP-sensitive potassium channels by nitric oxide in ventricular cardiomyocytes. *J Physiol* 2014 March 1;592(Pt 5):971-90.

(40) Liu Y, Gutterman DD. Oxidative stress and potassium channel function. *Clin Exp Pharmacol Physiol* 2002 April;29(4):305-11.

(41) Liu T, O'Rourke B. Regulation of the Na+/Ca2+ exchanger by pyridine nucleotide redox potential in ventricular myocytes. *J Biol Chem* 2013 November 1;288(44):31984-92.

(42) Goldhaber JI. Free radicals enhance Na+/Ca2+ exchange in ventricular myocytes. *Am J Physiol* 1996 September;271(3 Pt 2):H823-H833.

(43) Goldhaber JI, Liu E. Excitation-contraction coupling in single guinea-pig ventricular myocytes exposed to hydrogen peroxide. *J Physiol* 1994 May 15;477 (Pt 1):135-47.

(44) Bean BP. Classes of calcium channels in vertebrate cells. *Annu Rev Physiol* 1989;51:367-84.

(45) Hess P. Calcium channels in vertebrate cells. *Annu Rev Neurosci* 1990;13:337-56.

(46) Catterall WA. Voltage-gated calcium channels. *Cold Spring Harb Perspect Biol* 2011 August;3(8):a003947.

(47) Bean BP. Multiple types of calcium channels in heart muscle and neurons. Modulation by drugs and neurotransmitters. *Ann N Y Acad Sci* 1989;560:334-45.

(48) Seisenberger C, Specht V, Welling A, Platzer J, Pfeifer A, Kuhbandner S, Striessnig J, Klugbauer N, Feil R, Hofmann F. Functional embryonic cardiomyocytes after disruption of the L-type alpha1C (Cav1.2) calcium channel gene in the mouse. *J Biol Chem* 2000 December 15;275(50):39193-9.

(49) Bers DM. Cardiac excitation-contraction coupling. *Nature* 2002 January 10;415(6868):198-205.

(50) Wibo M, Bravo G, Godfraind T. Postnatal maturation of excitation-contraction coupling in rat ventricle in relation to the subcellular localization and surface density of 1,4-dihydropyridine and ryanodine receptors. *Circ Res* 1991 March;68(3):662-73.

(51) ORKAND RK, NIEDERGERKE R. HEART ACTION POTENTIAL: DEPENDENCE ON EXTERNAL CALCIUM AND SODIUM IONS. *Science* 1964 November 27;146(3648):1176-7.

(52) Mikami A, Imoto K, Tanabe T, Niidome T, Mori Y, Takeshima H, Narumiya S, Numa S. Primary structure and functional expression of the cardiac dihydropyridine-sensitive calcium channel. *Nature* 1989 July 20;340(6230):230-3.

(53) Dolphin AC. Calcium channel auxiliary alpha2delta and beta subunits: trafficking and one step beyond. *Nat Rev Neurosci* 2012 August;13(8):542-55.

(54) De Jongh KS, Warner C, Catterall WA. Subunits of purified calcium channels. Alpha 2 and delta are encoded by the same gene. *J Biol Chem* 1990 September 5;265(25):14738-41.

(55) Buraei Z, Yang J. The ss subunit of voltage-gated Ca2+ channels. *Physiol Rev* 2010 October;90(4):1461-506.

(56) Findeisen F, Tolia A, Arant R, Kim EY, Isacoff E, Minor DL, Jr. Calmodulin overexpression does not alter Cav1.2 function or oligomerization state. *Channels (Austin)* 2011 July;5(4):320-4.

(57) Dunlap K. Calcium channels are models of self-control. *J Gen Physiol* 2007 May;129(5):379-83.

(58) Halling DB, racena-Parks P, Hamilton SL. Regulation of voltage-gated Ca2+ channels by calmodulin. *Sci STKE* 2006 January 17;2006(318):er1.

(59) Foell JD, Balijepalli RC, Delisle BP, Yunker AM, Robia SL, Walker JW, McEnery MW, January CT, Kamp TJ. Molecular heterogeneity of calcium channel beta-subunits in canine and human heart: evidence for differential subcellular localization. *Physiol Genomics* 2004 April 13;17(2):183-200.

(60) Colecraft HM, Alseikhan B, Takahashi SX, Chaudhuri D, Mittman S, Yegnasubramanian V, Alvania RS, Johns DC, Marban E, Yue DT. Novel functional properties of Ca(2+) channel beta subunits revealed by their expression in adult rat heart cells. *J Physiol* 2002 June 1;541(Pt 2):435-52.

(61) Leach RN, Brette F, Orchard CH. Antisense oligonucleotide against the Ca channel beta subunit decreases L-type Ca current in rat ventricular myocytes. *Biochem Biophys Res Commun* 2007 January 19;352(3):794-8.

(62) Lee KS, Marban E, Tsien RW. Inactivation of calcium channels in mammalian heart cells: joint dependence on membrane potential and intracellular calcium. *J Physiol* 1985 July;364:395-411.

(63) Kass RS, Sanguinetti MC. Inactivation of calcium channel current in the calf cardiac Purkinje fiber. Evidence for voltage- and calcium-mediated mechanisms. *J Gen Physiol* 1984 November;84(5):705-26.

(64) Zhang JF, Ellinor PT, Aldrich RW, Tsien RW. Molecular determinants of voltage-dependent inactivation in calcium channels. *Nature* 1994 November 3;372(6501):97-100.

(65) Rasmusson RL, Morales MJ, Wang S, Liu S, Campbell DL, Brahmajothi MV, Strauss HC. Inactivation of voltage-gated cardiac K+ channels. *Circ Res* 1998 April 20;82(7):739-50.

(66) Kukuljan M, Labarca P, Latorre R. Molecular determinants of ion conduction and inactivation in K+ channels. *Am J Physiol* 1995 March;268(3 Pt 1):C535-C556.

(67) Vassilev PM, Scheuer T, Catterall WA. Identification of an intracellular peptide segment involved in sodium channel inactivation. *Science* 1988 September 23;241(4873):1658-61.

(68) Stotz SC, Zamponi GW. Identification of inactivation determinants in the domain IIS6 region of high voltage-activated calcium channels. *J Biol Chem* 2001 August 31;276(35):33001-10.

(69) Berjukow S, Marksteiner R, Sokolov S, Weiss RG, Margreiter E, Hering S. Amino acids in segment IVS6 and beta-subunit interaction support distinct conformational changes during Ca(v)2.1 inactivation. *J Biol Chem* 2001 May 18;276(20):17076-82.

(70) Barrett CF, Tsien RW. The Timothy syndrome mutation differentially affects voltage- and calcium-dependent inactivation of CaV1.2 L-type calcium channels. *Proc Natl Acad Sci U S A* 2008 February 12;105(6):2157-62.

(71) Cheng EP, Yuan C, Navedo MF, Dixon RE, Nieves-Cintron M, Scott JD, Santana LF. Restoration of normal L-type Ca2+ channel function during Timothy syndrome by ablation of an anchoring protein. *Circ Res* 2011 July 22;109(3):255-61.

(72) Burashnikov E, Pfeiffer R, Barajas-Martinez H, Delpon E, Hu D, Desai M, Borggrefe M, Haissaguerre M, Kanter R, Pollevick GD, Guerchicoff A, Laino R, Marieb M, Nademanee K, Nam GB, Robles R, Schimpf R, Stapleton DD, Viskin S, Winters S, Wolpert C, Zimmern S, Veltmann C, Antzelevitch C. Mutations in the cardiac L-type calcium channel associated with inherited J-wave syndromes and sudden cardiac death. *Heart Rhythm* 2010 December;7(12):1872-82.

(73) Hadley RW, Lederer WJ. Ca2+ and voltage inactivate Ca2+ channels in guinea-pig ventricular myocytes through independent mechanisms. *J Physiol* 1991 December;444:257-68.

(74) Imredy JP, Yue DT. Mechanism of Ca(2+)-sensitive inactivation of L-type Ca2+ channels. *Neuron* 1994 June;12(6):1301-18.

(75) Alseikhan BA, DeMaria CD, Colecraft HM, Yue DT. Engineered calmodulins reveal the unexpected eminence of Ca2+ channel inactivation in controlling heart excitation. *Proc Natl Acad Sci U S A* 2002 December 24;99(26):17185-90.

(76) Victor RG, Rusnak F, Sikkink R, Marban E, O'Rourke B. Mechanism of Ca(2+)-dependent inactivation of L-type Ca2+ channels in GH3 cells: direct evidence against dephosphorylation by calcineurin. *J Membr Biol* 1997 March 1;156(1):53-61.

(77) Zeilhofer HU, Blank NM, Neuhuber WL, Swandulla D. Calcium-dependent inactivation of neuronal calcium channel currents is independent of calcineurin. *Neuroscience* 2000;95(1):235-41.

(78) Chad JE, Eckert R. An enzymatic mechanism for calcium current inactivation in dialysed Helix neurones. *J Physiol* 1986 September;378:31-51.

(79) Cavalie A, Pelzer D, Trautwein W. Fast and slow gating behaviour of single calcium channels in cardiac cells. Relation to activation and inactivation of calcium-channel current. *Pflugers Arch* 1986 March;406(3):241-58.

(80) de LM, Wang Y, Jones L, Perez-Reyes E, Wei X, Soong TW, Snutch TP, Yue DT. Essential Ca(2+)-binding motif for Ca(2+)-sensitive inactivation of L-type Ca2+ channels. *Science* 1995 December 1;270(5241):1502-6.

(81) Rhoads AR, Friedberg F. Sequence motifs for calmodulin recognition. *FASEB J* 1997 April;11(5):331-40.

(82) Peterson BZ, DeMaria CD, Adelman JP, Yue DT. Calmodulin is the Ca2+ sensor for Ca2+ -dependent inactivation of L-type calcium channels. *Neuron* 1999 March;22(3):549-58.

(83) Zuhlke RD, Pitt GS, Deisseroth K, Tsien RW, Reuter H. Calmodulin supports both inactivation and facilitation of L-type calcium channels. *Nature* 1999 May 13;399(6732):159-62.

(84) Kilhoffer MC, Haiech J, Demaille JG. Ion binding to calmodulin. A comparison with other intracellular calcium-binding proteins. *Mol Cell Biochem* 1983;51(1):33-54.

(85) Chen YH, Li MH, Zhang Y, He LL, Yamada Y, Fitzmaurice A, Shen Y, Zhang H, Tong L, Yang J. Structural basis of the alpha1-beta subunit interaction of voltage-gated Ca2+ channels. *Nature* 2004 June 10;429(6992):675-80.

(86) Opatowsky Y, Chen CC, Campbell KP, Hirsch JA. Structural analysis of the voltage-dependent calcium channel beta subunit functional core and its complex with the alpha 1 interaction domain. *Neuron* 2004 May 13;42(3):387-99.

(87) Van PF, Clark KA, Chatelain FC, Minor DL, Jr. Structure of a complex between a voltage-gated calcium channel beta-subunit and an alpha-subunit domain. *Nature* 2004 June 10;429(6992):671-5.

(88) Zhang Y, Yamada Y, Fan M, Bangaru SD, Lin B, Yang J. The beta subunit of voltage-gated Ca2+ channels interacts with and regulates the activity of a novel isoform of Pax6. *J Biol Chem* 2010 January 22;285(4):2527-36.

(89) Gonzalez-Gutierrez G, Miranda-Laferte E, Neely A, Hidalgo P. The Src homology 3 domain of the beta-subunit of voltage-gated calcium channels promotes endocytosis via dynamin interaction. *J Biol Chem* 2007 January 26;282(4):2156-62.

(90) Witcher DR, De WM, Liu H, Pragnell M, Campbell KP. Association of native Ca2+ channel beta subunits with the alpha 1 subunit interaction domain. *J Biol Chem* 1995 July 28;270(30):18088-93.

(91) De WM, Witcher DR, Pragnell M, Liu H, Campbell KP. Properties of the alpha 1-beta anchoring site in voltage-dependent Ca2+ channels. *J Biol Chem* 1995 May 19;270(20):12056-64.

(92) De WM, Scott VE, Pragnell M, Campbell KP. Identification of critical amino acids involved in alpha1-beta interaction in voltage-dependent Ca2+ channels. *FEBS Lett* 1996 February 19;380(3):272-6.

(93) De WM, Pragnell M, Campbell KP. Ca2+ channel regulation by a conserved beta subunit domain. *Neuron* 1994 August;13(2):495-503.

(94) Canti C, Nieto-Rostro M, Foucault I, Heblich F, Wratten J, Richards MW, Hendrich J, Douglas L, Page KM, Davies A, Dolphin AC. The metal-ion-dependent adhesion site in the Von Willebrand factor-A domain of alpha2delta subunits is key to trafficking voltage-gated Ca2+ channels. *Proc Natl Acad Sci U S A* 2005 August 9;102(32):11230-5.

(95) Felix R, Gurnett CA, De WM, Campbell KP. Dissection of functional domains of the voltage-dependent Ca2+ channel alpha2delta subunit. *J Neurosci* 1997 September 15;17(18):6884-91.

(96) Dalton S, Takahashi SX, Miriyala J, Colecraft HM. A single CaVbeta can reconstitute both trafficking and macroscopic conductance of voltage-dependent calcium channels. *J Physiol* 2005 September 15;567(Pt 3):757-69.

(97) Fang K, Colecraft HM. Mechanism of auxiliary beta-subunit-mediated membrane targeting of L-type (Ca(V)1.2) channels. *J Physiol* 2011 September 15;589(Pt 18):4437-55.

(98) Shaw RM, Colecraft HM. L-type calcium channel targeting and local signalling in cardiac myocytes. *Cardiovasc Res* 2013 May 1;98(2):177-86.

(99) Takahashi SX, Miriyala J, Tay LH, Yue DT, Colecraft HM. A CaVbeta SH3/guanylate kinase domain interaction regulates multiple properties of voltage-gated Ca2+ channels. *J Gen Physiol* 2005 October;126(4):365-77.

(100) Bichet D, Cornet V, Geib S, Carlier E, Volsen S, Hoshi T, Mori Y, De WM. The I-II loop of the Ca2+ channel alpha1 subunit contains an endoplasmic reticulum retention signal antagonized by the beta subunit. *Neuron* 2000 January;25(1):177-90.

(101) Altier C, Garcia-Caballero A, Simms B, You H, Chen L, Walcher J, Tedford HW, Hermosilla T, Zamponi GW. The Cavbeta subunit prevents RFP2-mediated ubiquitination and proteasomal degradation of L-type channels. *Nat Neurosci* 2011 February;14(2):173-80.

(102) Neely A, Wei X, Olcese R, Birnbaumer L, Stefani E. Potentiation by the beta subunit of the ratio of the ionic current to the charge movement in the cardiac calcium channel. *Science* 1993 October 22;262(5133):575-8.

(103) Varadi G, Lory P, Schultz D, Varadi M, Schwartz A. Acceleration of activation and inactivation by the beta subunit of the skeletal muscle calcium channel. *Nature* 1991 July 11;352(6331):159-62.

(104) Singer D, Biel M, Lotan I, Flockerzi V, Hofmann F, Dascal N. The roles of the subunits in the function of the calcium channel. *Science* 1991 September 27;253(5027):1553-7.

(105) Reimer D, Huber IG, Garcia ML, Haase H, Striessnig J. beta subunit heterogeneity of L-type Ca(2+) channels in smooth muscle tissues. *FEBS Lett* 2000 February 4;467(1):65-9.

(106) Perez-Reyes E, Castellano A, Kim HS, Bertrand P, Baggstrom E, Lacerda AE, Wei XY, Birnbaumer L. Cloning and expression of a cardiac/brain beta subunit of the L-type calcium channel. *J Biol Chem* 1992 January 25;267(3):1792-7.

(107) Hullin R, Singer-Lahat D, Freichel M, Biel M, Dascal N, Hofmann F, Flockerzi V. Calcium channel beta subunit heterogeneity: functional expression of cloned cDNA from heart, aorta and brain. *EMBO J* 1992 March;11(3):885-90.

(108) Haase H, Pfitzmaier B, McEnery MW, Morano I. Expression of Ca(2+) channel subunits during cardiac ontogeny in mice and rats: identification of fetal alpha(1C) and beta subunit isoforms. *J Cell Biochem* 2000 January;76(4):695-703.

(109) Guo A, Zhang C, Wei S, Chen B, Song LS. Emerging mechanisms of T-tubule remodelling in heart failure. *Cardiovasc Res* 2013 May 1;98(2):204-15.

(110) Chen X, Piacentino V, III, Furukawa S, Goldman B, Margulies KB, Houser SR. L-type Ca2+ channel density and regulation are altered in failing human ventricular myocytes and recover after support with mechanical assist devices. *Circ Res* 2002 September 20;91(6):517-24.

(111) Schroder F, Handrock R, Beuckelmann DJ, Hirt S, Hullin R, Priebe L, Schwinger RH, Weil J, Herzig S. Increased availability and open probability of single L-type calcium channels from failing compared with nonfailing human ventricle. *Circulation* 1998 September 8;98(10):969-76.

(112) Beetz N, Hein L, Meszaros J, Gilsbach R, Barreto F, Meissner M, Hoppe UC, Schwartz A, Herzig S, Matthes J. Transgenic simulation of human heart failure-like L-type Ca2+-

channels: implications for fibrosis and heart rate in mice. *Cardiovasc Res* 2009 December 1;84(3):396-406.

(113) Aimond F, Alvarez JL, Rauzier JM, Lorente P, Vassort G. Ionic basis of ventricular arrhythmias in remodeled rat heart during long-term myocardial infarction. *Cardiovasc Res* 1999 May;42(2):402-15.

(114) Antoons G, Volders PG, Stankovicova T, Bito V, Stengl M, Vos MA, Sipido KR. Window Ca2+ current and its modulation by Ca2+ release in hypertrophied cardiac myocytes from dogs with chronic atrioventricular block. *J Physiol* 2007 February 15;579(Pt 1):147-60.

(115) Bito V, Heinzel FR, Biesmans L, Antoons G, Sipido KR. Crosstalk between L-type Ca2+ channels and the sarcoplasmic reticulum: alterations during cardiac remodelling. *Cardiovasc Res* 2008 January 15;77(2):315-24.

(116) Neher E, Sakmann B, Steinbach JH. The extracellular patch clamp: a method for resolving currents through individual open channels in biological membranes. *Pflugers Arch* 1978 July 18;375(2):219-28.

(117) HODGKIN AL, HUXLEY AF. A quantitative description of membrane current and its application to conduction and excitation in nerve. *J Physiol* 1952 August;117(4):500-44.

(118) Fitzhugh R. Impulses and Physiological States in Theoretical Models of Nerve Membrane. *Biophys J* 1961 July;1(6):445-66.

(119) Cannell MB, Kong CH, Imtiaz MS, Laver DR. Control of sarcoplasmic reticulum Ca2+ release by stochastic RyR gating within a 3D model of the cardiac dyad and importance of induction decay for CICR termination. *Biophys J* 2013 May 21;104(10):2149-59.

(120) Dzhura I, Neely A. Differential modulation of cardiac Ca2+ channel gating by beta-subunits. *Biophys J* 2003 July;85(1):274-89.

(121) Trayanova NA. Whole-heart modeling: applications to cardiac electrophysiology and electromechanics. *Circ Res* 2011 January 7;108(1):113-28.

(122) Xie F, Qu Z, Yang J, Baher A, Weiss JN, Garfinkel A. A simulation study of the effects of cardiac anatomy in ventricular fibrillation. *J Clin Invest* 2004 March;113(5):686-93.

(123) Tan RC, Joyner RW. Electrotonic influences on action potentials from isolated ventricular cells. *Circ Res* 1990 November;67(5):1071-81.

(124) Sharp AA, Abbott LF, Marder E. Artificial electrical synapses in oscillatory networks. *J Neurophysiol* 1992 June;67(6):1691-4.

(125) Prinz AA, Abbott LF, Marder E. The dynamic clamp comes of age. *Trends Neurosci* 2004 April;27(4):218-24.

(126) NOBLE D. Cardiac action and pacemaker potentials based on the Hodgkin-Huxley equations. *Nature* 1960 November 5;188:495-7.

(127) NOBLE D. A modification of the Hodgkin--Huxley equations applicable to Purkinje fibre action and pace-maker potentials. *J Physiol* 1962 February;160:317-52.

(128) Beeler GW, Reuter H. Reconstruction of the action potential of ventricular myocardial fibres. *J Physiol* 1977 June;268(1):177-210.

(129) Sakmann B, Neher E. Patch clamp techniques for studying ionic channels in excitable membranes. *Annu Rev Physiol* 1984;46:455-72.

(130) Mahajan A, Shiferaw Y, Sato D, Baher A, Olcese R, Xie LH, Yang MJ, Chen PS, Restrepo JG, Karma A, Garfinkel A, Qu Z, Weiss JN. A rabbit ventricular action potential model replicating cardiac dynamics at rapid heart rates. *Biophys J* 2008 January 15;94(2):392-410.

(131) O'Hara T, Virag L, Varro A, Rudy Y. Simulation of the undiseased human cardiac ventricular action potential: model formulation and experimental validation. *PLoS Comput Biol* 2011 May;7(5):e1002061.

(132) Gemmell P, Burrage K, Rodriguez B, Quinn T. Exploring the parameter space of a rabbit ventricular action potential model to investigate the effect of variation on action potential and calcium transients. *Conf Proc IEEE Eng Med Biol Soc* 2010;2010:2662-5.

(133) Garfinkel A, Kim YH, Voroshilovsky O, Qu Z, Kil JR, Lee MH, Karagueuzian HS, Weiss JN, Chen PS. Preventing ventricular fibrillation by flattening cardiac restitution. *Proc Natl Acad Sci U S A* 2000 May 23;97(11):6061-6.

(134) Goldhaber JI, Xie LH, Duong T, Motter C, Khuu K, Weiss JN. Action potential duration restitution and alternans in rabbit ventricular myocytes: the key role of intracellular calcium cycling. *Circ Res* 2005 March 4;96(4):459-66.

(135) Milberg P, Reinsch N, Osada N, Wasmer K, Monnig G, Stypmann J, Breithardt G, Haverkamp W, Eckardt L. Verapamil prevents torsade de pointes by reduction of transmural dispersion of repolarization and suppression of early afterdepolarizations in an intact heart model of LQT3. *Basic Res Cardiol* 2005 July;100(4):365-71.

(136) Belardinelli L, Shryock JC, Fraser H. Inhibition of the late sodium current as a potential cardioprotective principle: effects of the late sodium current inhibitor ranolazine. *Heart* 2006 July;92 Suppl 4:iv6-iv14.

(137) Undrovinas AI, Belardinelli L, Undrovinas NA, Sabbah HN. Ranolazine improves abnormal repolarization and contraction in left ventricular myocytes of dogs with heart failure by inhibiting late sodium current. *J Cardiovasc Electrophysiol* 2006 May;17 Suppl 1:S169-S177.

(138) Milberg P, Fink M, Pott C, Frommeyer G, Biertz J, Osada N, Stypmann J, Monnig G, Koopmann M, Breithardt G, Eckardt L. Blockade of I(Ca) suppresses early afterdepolarizations and reduces transmural dispersion of repolarization in a whole heart model of chronic heart failure. *Br J Pharmacol* 2012 May;166(2):557-68.

(139) Liu QN, Zhang L, Gong PL, Yang XY, Zeng FD. Inhibitory effects of dauricine on early afterdepolarizations and L-type calcium current. *Can J Physiol Pharmacol* 2009 November;87(11):954-62.

(140) Singh BN. The mechanism of action of calcium antagonists relative to their clinical applications. *Br J Clin Pharmacol* 1986;21 Suppl 2:109S-21S.

(141) Merillat JC, Lakatta EG, Hano O, Guarnieri T. Role of calcium and the calcium channel in the initiation and maintenance of ventricular fibrillation. *Circ Res* 1990 November;67(5):1115-23.

(142) Aliot E SBSRLR. Prevention of torsade de pointes with calcium channel blockade in an animal model. J.Am.Coll.Cardiol. 5[2s2], 492. 1985.
Ref Type: Abstract

(143) Billman GE, Hamlin RL. The effects of mibefradil, a novel calcium channel antagonist on ventricular arrhythmias induced by myocardial ischemia and programmed electrical stimulation. *J Pharmacol Exp Ther* 1996 June;277(3):1517-26.

(144) Held PH, Yusuf S, Furberg CD. Calcium channel blockers in acute myocardial infarction and unstable angina: an overview. *BMJ* 1989 November 11;299(6709):1187-92.

(145) Mirowski M, Reid PR, Mower MM, Watkins L, Gott VL, Schauble JF, Langer A, Heilman MS, Kolenik SA, Fischell RE, Weisfeldt ML. Termination of malignant ventricular arrhythmias with an implanted automatic defibrillator in human beings. *N Engl J Med* 1980 August 7;303(6):322-4.

(146) Connolly SJ, Hallstrom AP, Cappato R, Schron EB, Kuck KH, Zipes DP, Greene HL, Boczor S, Domanski M, Follmann D, Gent M, Roberts RS. Meta-analysis of the implantable cardioverter defibrillator secondary prevention trials. AVID, CASH and CIDS studies. Antiarrhythmics vs Implantable Defibrillator study. Cardiac Arrest Study Hamburg . Canadian Implantable Defibrillator Study. *Eur Heart J* 2000 December;21(24):2071-8.

Chapter 2:

Shaping a New Ca^{2+} Conductance to Suppress EADs

2.1 ABSTRACT

Sudden cardiac death (SCD) due to ventricular fibrillation (VF) is a major world-wide health problem. Common triggers of VF are abnormal repolarizations of the cardiac action potential, known as early afterdepolarizations (EADs). Here we used a hybrid biological-computational approach to investigate the dependence of EADs on the biophysical properties of the L-type Ca^{2+} current ($I_{Ca,L}$) and to explore how modifications of these properties could be designed to suppress EADs. EADs were induced in isolated rabbit ventricular myocytes by exposure to 600 μmol/L H_2O_2 (oxidative stress) or lowering the external [K^+] from 5.4 to 2.0-2.7 mmol/L (hypokalemia). The role of $I_{Ca,L}$ in EAD formation was directly assessed using the dynamic clamp technique: the paced myocyte's V_m was input to a myocyte model with tunable biophysical parameters, which computed a virtual $I_{Ca,L}$, that was injected into the myocyte in real time, replacing the endogenous $I_{Ca,L}$ which was suppressed with nifedipine. Injecting a current with the native $I_{Ca,L}$ biophysical properties restored EAD occurrence in myocytes challenged by H_2O_2 or hypokalemia. A mere 5 mV depolarizing shift in the voltage dependence of activation or a hyperpolarizing shift in the steady-state inactivation curve completely abolished EADs in myocytes while maintaining a normal Ca_i transient. We propose that modifying $I_{Ca,L}$ biophysical properties has potential as a powerful therapeutic strategy for suppressing EADs and EAD-mediated arrhythmias.

2.2 INTRODUCTION

Early afterdepolarizations (EADs) are transient reversals of normal repolarization (*i.e.*, positive dV/dt), occurring in late phase 2 or phase 3 of the cardiac action potential (AP). These events, observable both at cellular and tissue level, are recognized as triggers of cardiac arrhythmias[1,2]. When EADs propagate through cardiac tissue, they can generate premature heart beats, ventricular tachycardia (VT) and ventricular fibrillation (VF), common causes of sudden cardiac death in a variety of clinical settings[3].

EADs classically occur during bradycardia under conditions of reduced repolarization reserve, due to either abnormally decreased outward currents, increased inward currents, or both. The predominant inward currents in ventricular myocytes which have been implicated in EAD genesis are the persistent I_{Na}[4], I_{NCX}[5,6], and $I_{Ca,L}$[7]. Previous work has shown that reactivation of the L-type Ca^{2+} current ($I_{Ca,L}$) during phase 2 and 3 of the action potential (AP) plateau plays a major role in EAD formation[8], although other factors are also important[9]. Most EADs are initiated between −40 and 0 mV (Fig. 2.1), corresponding to the range of membrane potentials where the steady-state activation and inactivation curves of $I_{Ca,L}$ overlap, often referred to as the "window current" region[10,11]. As the AP repolarizes into this voltage "window", a fraction of the L-type Ca channels not inactivated may be available for reactivation to generate the upstroke of the EAD. In this study, we sought to determine the relevance of $I_{Ca,L}$ in EAD formation, and investigated whether EAD suppression can be achieved solely by manipulating $I_{Ca,L}$ without altering other ionic conductances or signaling pathways. We analyzed whether EAD formation can be suppressed by minimal perturbation of the biophysical properties of L-type Ca^{2+} channels affecting the $I_{Ca,L}$ window voltage region. Since it is difficult to control these properties experimentally with any degree of precision, we adopted a hybrid biological-computational approach using the dynamic clamp technique[12-16]. This allowed us to replace the native $I_{Ca,L}$ of the myocyte with a computed virtual $I_{Ca,L}$ with programmable properties. Our findings show that EAD formation is highly sensitive to $I_{Ca,L}$ properties and properties of the window region (such as

the slopes of the activation and inactivation curves[17], such that subtle shifts in the voltage dependence of steady-state $I_{Ca,L}$ activation or inactivation can abolish EADs. Moreover, these changes are predicted to have no significant effects on the amplitude or kinetics of the intracellular Ca transient, suggesting that pharmacological or genetic manipulation of the voltage-dependent properties of $I_{Ca,L}$ could have therapeutic potential for suppressing EAD-mediated arrhythmias without adversely affecting excitation-contraction coupling.

2.3 METHODS

Ethical approval: All animal protocols were approved by the UCLA Institutional Animal Care and Use Committee and conformed to the Guide for the Care and Use of Laboratory Animals published by the US National Institutes of Health.

Electrophysiology: Ventricular myocytes were isolated from New Zealand white rabbits as previously described[18]. All animals were anesthetized with 50 mg/mL intravenous pentobarbital, before excision of the hearts, which were subsequently submerged in Ca-free Tyrode's solution containing (in mmol/L) 136 NaCl, 5.4 KCl, 1 MgCl2, 0.33 NaH_2PO_4, 10 glucose, and 10 HEPES, adjusted to pH 7.4. The hearts were cannulated and perfused retrogradely on a Langendorff apparatus with Ca-free Tyrode's buffer containing 1.65 mg/mL collagenase and 0.8 mg/mL bovine albumin for 30–40 min. After washing out the enzyme solution, the hearts were swirled in a beaker to dissociate cells. The Ca concentration was gradually increased to 1.8 mmol/L, and the cells were stored at room temperature. This procedure typically yielded 50% rod-shaped Ca^{2+}-tolerant myocytes. Only Ca^{2+}-tolerant, rod-shaped ventricular myocytes with clear striations were randomly selected for electrophysiological studies within 8 h of isolation. All recordings were measured with AxoPatch200B (Axon Instruments). Whole-cell patch-clamp recordings (in current or voltage clamp mode) were performed at 34-36℃ using pipettes of 1-2 MΩ. The

intracellular solution contained (in mmol/L): 110 K-Aspartate, 30 KCl, 5 NaCl, 10 HEPES, 0.1 EGTA, 5 MgATP, 5 Creatine phosphate, 0.05 cAMP adjusted to pH 7.2. For $I_{Ca,L}$ recordings the solutions were as described above, except that K^+ was replaced with Cs^+ to abolish K^+ conductance and 10 µmol/L TTX was added to the extracellular solution to block Na^+ conductance. The L-type-specific Ca^{2+} current was determined by subtracting the Ca^{2+} current after 20 µmol/L nifedipine from the total Ca^{2+} current. Data were acquired and analyzed using custom-made software (G-Patch, Analysis). Currents were filtered at 1/5 of the sampling frequency. The steady-state activation curves were constructed by dividing the peak I-V curve by the driving force to calculate conductance (G) and dividing G by Gmax. The inactivation curves were constructed by plotting the normalized peak current during a test pulse at 10mV following a 300 ms inactivating pulse at various voltages. The slope and half-activation/inactivation potential of these curves were estimated by fitting to a Boltzmann distribution, and these parameters, were used to constrain the dynamic clamp model for both control and H_2O_2 conditions. These two versions of the model were then implemented for Dynamic Clamp in RTXI [19]. Sampling/computation frequency was 10 kHz.

Ca_i measurements: Myocytes were loaded with 10 µmol/L Fluo4-AM (Molecular probes) for 30 minutes at room temperature. Cells were then washed twice in regular Tyrode's solution and placed in a heated chamber at 34-36℃ for fluoresce nce and electrophysiology measurements. Ca_i transients were recorded using a CMOS camera (Silicon Imaging SI-1300).

Dynamic Clamp:

The ionic conductances included in the model are $I_{Ca,L}$, the fast sodium current I_{Na}, the Na-K pump current I_{NaK}, the Na-Ca exchange current I_{NCX} and the Ca-dependent slow component of the delayed rectifier potassium channel I_{ks}. The intracellular Ca concentration was divided into four compartments, i.e., submembrane Ca (*Cs*), cytosolic Ca (*Ci*) and network SR Ca and

junctional SR Ca. The average submembrane Ca concentration, *Cs*, is used to compute Ca^{2+}-dependent inactivation in the $I_{Ca,L}$ formulation. The Ca flux into the cell due to $I_{Ca,L}$ is given by [20]

$$J_{ca} = g_{ca} P_o i_{ca} \text{, (1);} \qquad i_{ca} = \frac{4P_{ca}VF^2}{RT} \frac{Cse^{2a} - 0.341[Ca^{2+}]_o}{e^{2a} - 1} \text{ (2);}$$

where *Cs* is the submembrane concentration in units of mmol/L. In order to facilitate shifts of the activation and inactiation curves , we replaced the Markovian calcium channel open probability P_o [20] with the Hodgkin-Huxley formulation from the Luo-Rudy dynamic model [21], where the P_o is formulated as $P_o = d \cdot f \cdot q$.

where d is the voltage dependent activation gate, *f* is the voltage dependent inactivation gate and *q* is the Ca-dependent inactivation gate. The steady states of these gating variables as functions of voltage are formulated in the following manner:

$$d_\infty = \frac{1.0}{1.0 + \exp(-(v - dhalf)/dslope)} \quad \textbf{(3)}$$

$$f_\infty = \frac{1.0 - pdest}{1.0 + \exp((v - dhalf)/dslope)} + pdest \textbf{ (4)}$$

$$q_\infty = \frac{1.0}{1.0 + (\frac{Cs}{cst})^\gamma} \textbf{ (5)}$$

$$\tau_d = \frac{d_\infty (1 - \exp(-v - (dhalf + a1)))}{a2(dslope + a2)(v - (dhalf + a1))} \textbf{ (6)}$$

$$\tau_f = b1\exp(-b2(v - (fhalf + b3))^2) + b4 \textbf{ (7)}$$

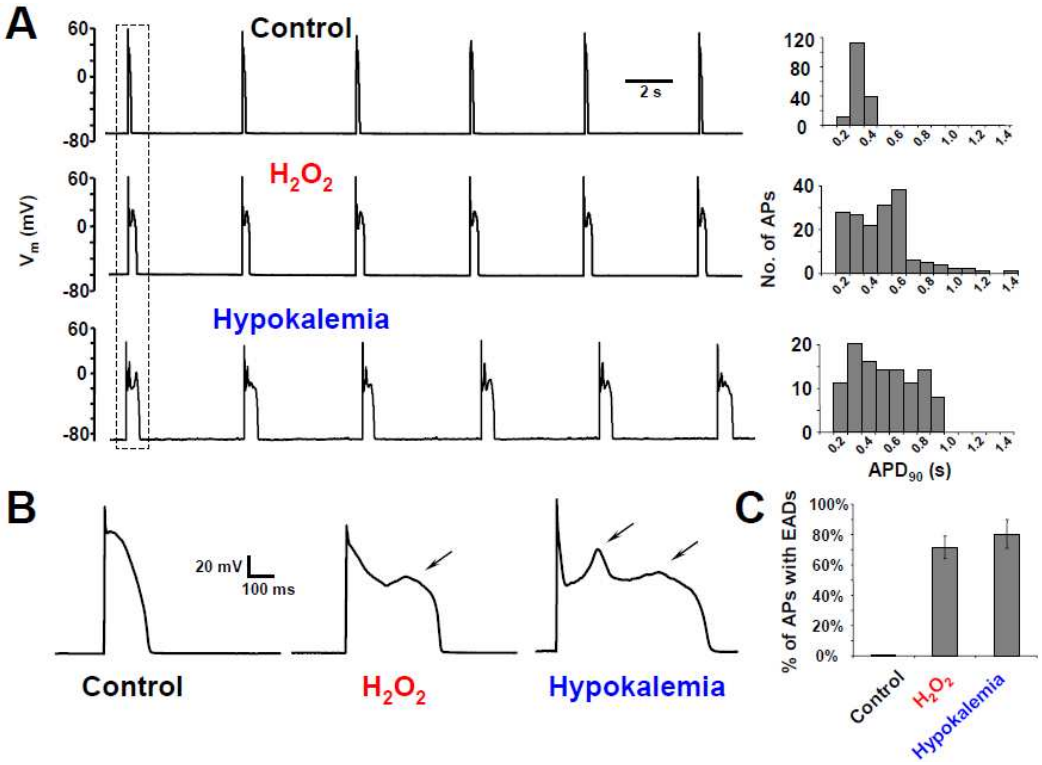

Figure 2.1. Oxidative stress and hypokalemia generate EADs in dissociated rabbit cardiomyocytes. A) Representative AP recordings in current-clamped ventricular myocytes stimulated at a pacing cycle length of 5 s. EADs, absent in control condition, were consistently induced by addition of 600 μM H_2O_2 to the bath solution or by reducing extracellular [K^+] from 5.4 mM to 2.7 mM (hypokalemia). The histogram to the left of each trace shows the distribution of action potential duration measured at 90% repolarization (APD_{90}) for each condition. B) Action potentials in the dotted box in (A) are shown on an expanded scale (arrows point to EADs). C) Percent of action potentials displaying at least one EAD in Control, H_2O_2, and hypokalemia conditions.

where τ_d and τ_f are the time constants of *d* gate and *f* gate respectively, dhalf is the half-activation voltage and dslope is the slope of the activation curve . All the parameters listed in the equations are fitted to our experimental data (the fitting parameters are shown in online supplemental materials). The Ca cycling is the same as that in the rabbit ventricular myocyte model[20], where the Ca concentration is divided into four compartments, i.e., submembrane Ca (Cs), cytosolic Ca (Ci) and network SR Ca and junctional SR Ca.

2.4 RESULTS

Oxidative stress-induced and hypokalemia-induced EADs in isolated rabbit ventricular myocytes. To determine the relevance of $I_{Ca\text{-}L}$ biophysical properties to EADs formation and/or suppression, we used two methods to induce EADs in whole-cell patch-clamped isolated rabbit ventricular myoyctes: i) oxidative stress, by exposure to 600 µmol/L H_2O_2 [22], or ii) hypokalemia, by lowering extracellular [K^+] (from 5.4 to 2.0-2.7 mmol/L). Myocytes were superfused in the recording chamber at 34-36℃, and stimulated at a p acing cycle length (PCL) of 5 s (Fig. 2.1). Under current clamp, both H_2O_2 (n = 14) and hypokalemia (n = 8) prolonged the APD significantly and consistently produced EADs in ~70% of paced APs (Figs. 2.1A & 2.1B) within

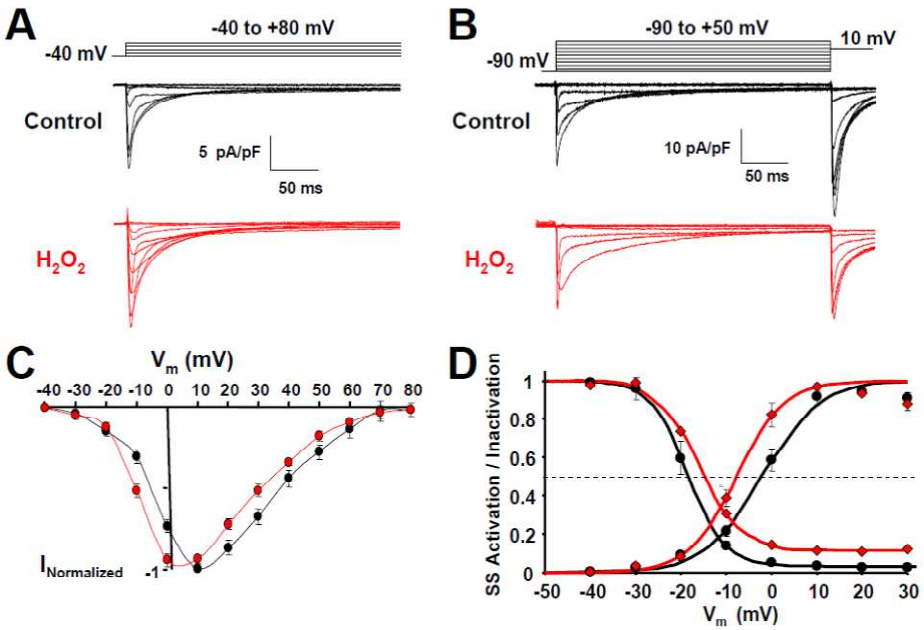

Figure 2.2. H_2O_2 alters both the time-dependent and steady-state properties of $I_{Ca,L}$ in rabbit ventricular myocytes. A) Voltage clamp recordings of nifedipine (20µM) sensitive $I_{Ca,L}$ in response to depolarizing pulses from –40mV (HP=-80mV), under control conditions (black) or after 2 minutes of exposure to 600 µM H_2O_2 (red) B). Voltage clamp recordings of nifedipine-sensitive $I_{Ca,L}$ in response to a two-pulse protocol from a holding potential of –90mV, under control conditions (black) or after 2 minutes of exposure to 600 µM H_2O_2 (red). The inactivating pulse was 300 ms to approximate the duration of a normal action potential. C) The I-V relationship for $I_{Ca,L}$ (normalized to the peak current) under control conditions (●, n=4) and H_2O_2 (●, n=5). Note the negative shift of the I-V curve in H_2O_2. D) Mean steady-state activation and inactivation curves for $I_{Ca,L}$ in control (●, n=4) and H_2O_2 conditions (♦, n=5). Note that the H_2O_2-induced shift of steady-state curves, results in a higher $I_{Ca,L}$ window area. External solution (mM): 136 NaCl, 5.4 CsCl, 1 MgCl2, 0.33 NaH_2PO4, 1.8 $CaCl_2$, 10 Glucose, 10 HEPES, and 10µM TTX, pH=7.4. Pipette solution (in mM): 100 Cs-Aspartate, 30 CsCl, 5 NaCl, 10 HEPES, 0.1 EGTA, 5 MgATP, 5 Creatine phos., 0.05 cAMP pH=7.2. Temp = 35°-37℃.

5-10 minutes. In our analysis, we individually inspected each action potential for EADs occurrence, defined as well resolved deflection of the voltage with a positive dV/dt during late phase 2 or phase 3 of the AP. EAD morphology varied among experiments and also within the same action potential as in Fig. 2.1B (under hypokalemia). Typically, we have considered EADs as a positive voltage deflection of ≥ 5 mV with durations (from inflection point to peak) between 30-150ms).

Among other effects, oxidative stress with H_2O_2 is known to promote EADs by activating Ca-Calmodulin kinase II (CaMKII)[23], which alters $I_{Ca,L}$[24] and induces late I_{Na}[25,26]. To characterize how H_2O_2 altered $I_{Ca,L}$ properties under our experimental conditions, we recorded the nifedipine-sensitive Ca^{2+} current in voltage-clamped isolated myocytes before and after exposure to 600 µmol/L H_2O_2 (n = 5)(Fig. 2): in addition to an overall slowing of inactivation (Fig. 2.2A & 2.2B), H_2O_2 shifted the peak of the current-voltage (I-V) relationship by -5mV as shown in Figure 2.2C. By constructing steady-state activation and inactivation curves, we found that H_2O_2 produced a ~+5 mV shift of the steady state half-activation potential ($V_{1/2}$ act), accompanied by a ~-5 mV shift in the steady state half-inactivation potential ($V_{1/2}$ inact) (Fig. 2.2D). Effectively, H_2O_2 increased the height of the $I_{Ca,L}$ window current region, changes which are expected to promote EAD formation[27-29].

Role of oxidative stress-mediated $I_{Ca,L}$ alterations in EAD generation.

To understand how the H_2O_2-induced changes in $I_{Ca,L}$ described above contributed to EAD formation, we next used the dynamic clamp technique[30] to replace the myocyte's native $I_{Ca,L}$ with a virtual $I_{Ca,L}$ with programmable properties. The principle of the dynamic clamp operation is illustrated in Fig. 2.3A. The recorded membrane potential of a current-clamped myocyte (V_m) is fed into a Linux-based computer with the Real-time Experimental Interface (RTXI) software[12] running the UCLA ventricular myocyte AP model[20]. The model computes, in real time, the macroscopic L-type Ca channel current, which is injected continuously into the

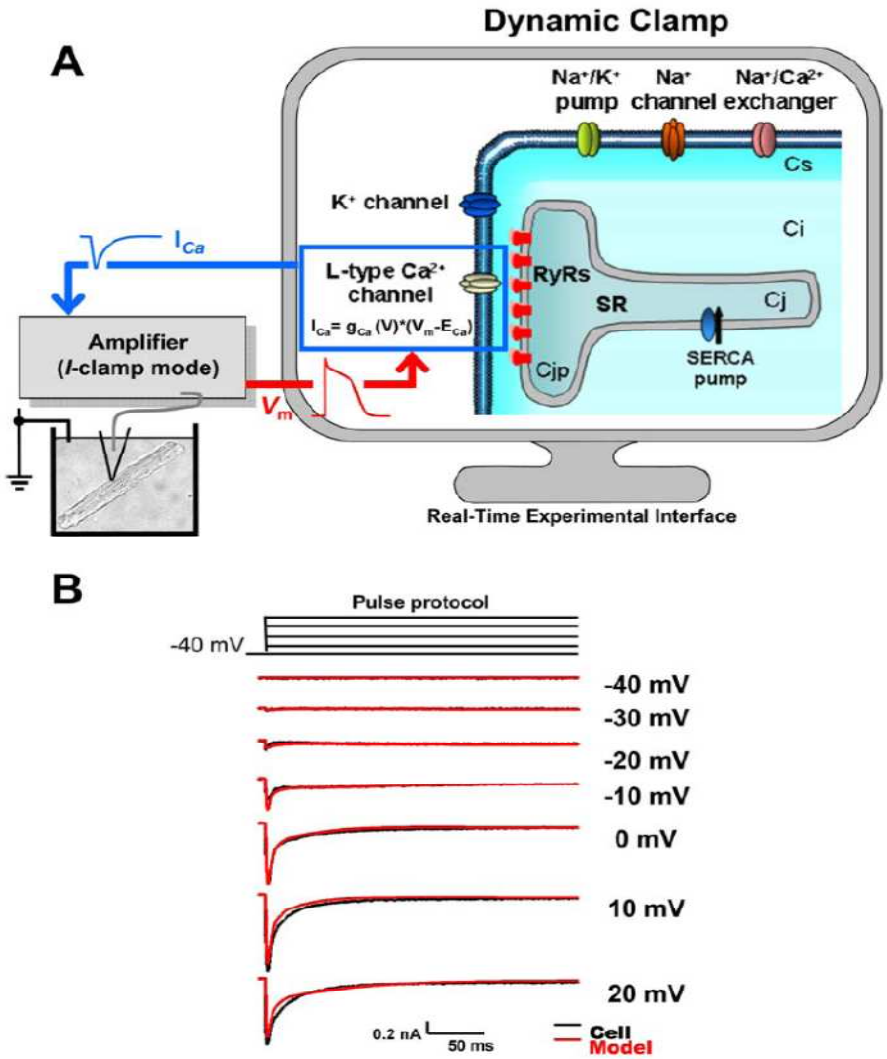

Figure 2.3. The Dynamic Patch clamp implements a virtual Ca^{2+} current computed with detailed Ca^{2+} cycling dynamics. A) Diagram of the dynamic clamp system. A ventricular myocyte is whole-cell patch-clamped with an amplifier in current-clamp mode. The myocyte's V_m signal (red arrow) is digitized and input to a computer running a cardiac action potential model (Mahajan *et al.,* 2008) containing macroscopic Hodgin-Huxley (HH) -type formulations for five conductances (I_{CaL}; the fast Na channel I_{Na}; the Na/K pump I_{NaK}; the Na/Ca exchanger I_{NCX}; and the Ca-dependent K rectifier I_{Ks}) and [Ca] in four discrete cellular compartments (Cs, Ci, Cjp, and Cj). Ionic conductances and concentrations can be fine-tuned by altering model parameters online. The calculated ionic conductances can be output in any combination to produce $I_{Command}$. In this case, $I_{Command} = I_{CaL}$ (blue arrow). $I_{Command}$ is combined with a pacing AP stimulus and converted to analog before being input to the amplifier to be injected into the clamped myocyte. This alters the myocyte V_m, which is in turn sampled for the next computation. Thus, there is a dynamic, bidirectional relationship between V_m and model conductance output, at a sampling/computation frequency of 10 kHz. B) The predicted $I_{Ca,L}$ conductance from the model in panel A (red) accurately predicts a current similar in amplitude and kinetics to experimentally recorded $I_{Ca,L}$ from rabbit cardiomyocytes (black) in response to depolarizing pulses from a holding potential of -40 mV.

myocyte, in turn changing its membrane potential. This cycle (V_m sampling → $I_{Ca,L}$ computation → $I_{Ca,L}$ injection →V_m sampling…) is iterated at 10 kHz, creating a dynamic, bidirectional relationship between the model and the cell.

The virtual $I_{Ca,L}$ computed in the AP model was tuned to fit experimental recordings of native $I_{Ca,L}$ recorded from rabbit ventricular myocytes (Fig. 2.3B). In addition to computing $I_{Ca,L}$, the model also computes all other elements of Ca_i cycling in the UCLA rabbit ventricular myocyte model[20], which is critical for simulating the effects of intracellular Ca on Ca-dependent inactivation of the virtual $I_{Ca,L}$ being injected into the myocyte. Thus, this model also generates a virtual intracellular Ca transient, which showed good agreement with the intracellular Ca transient recorded directly from a myocyte under control conditions (Fig. 2.4). The model computes Ca concentrations in four discrete subcellular compartments (Fig. 2.3A), with the average submembrane Ca concentration (Cs) used for the calculation of Ca-dependent inactivation of $I_{Ca,L}$, as described previously[20]. Although we initially used a 7-state Markovian description of $I_{Ca,L}$, we achieved equivalent accuracy of fitting the experimental $I_{Ca,L}$ data with a Hodgkin-Huxley type $I_{Ca,L}$ formulation, with the advantage that the biophysical parameters relevant to this work, could be directly modified, such as $V_{1/2}$ act and $V_{1/2}$ inact, which determine the steady-state activation and inactivation properties of the injected virtual $I_{Ca,L}$.

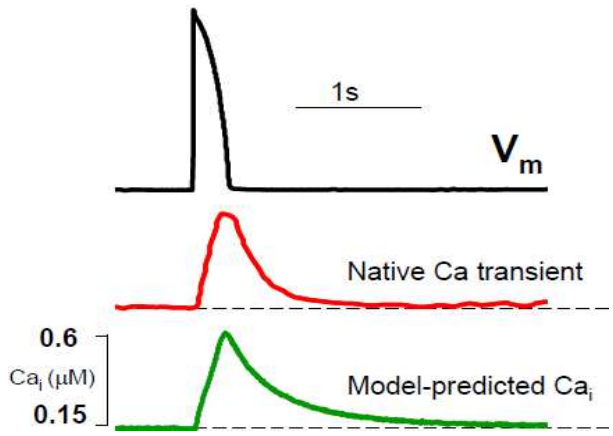

Figure 2.4. Comparison of the virtual Ca_i transient computed by the AP model with an optically measured Ca_i transient. During a paced AP (black trace), the native Ca_i transient (red) recorded from a Fluo4-AM loaded myocyte and the Ca_i transient computed by the model (green) for the same AP are comparable.

In our experimental protocol utilizing the dynamic clamp technique, we first paced a rabbit ventricular myocyte to record the AP in the current clamp mode

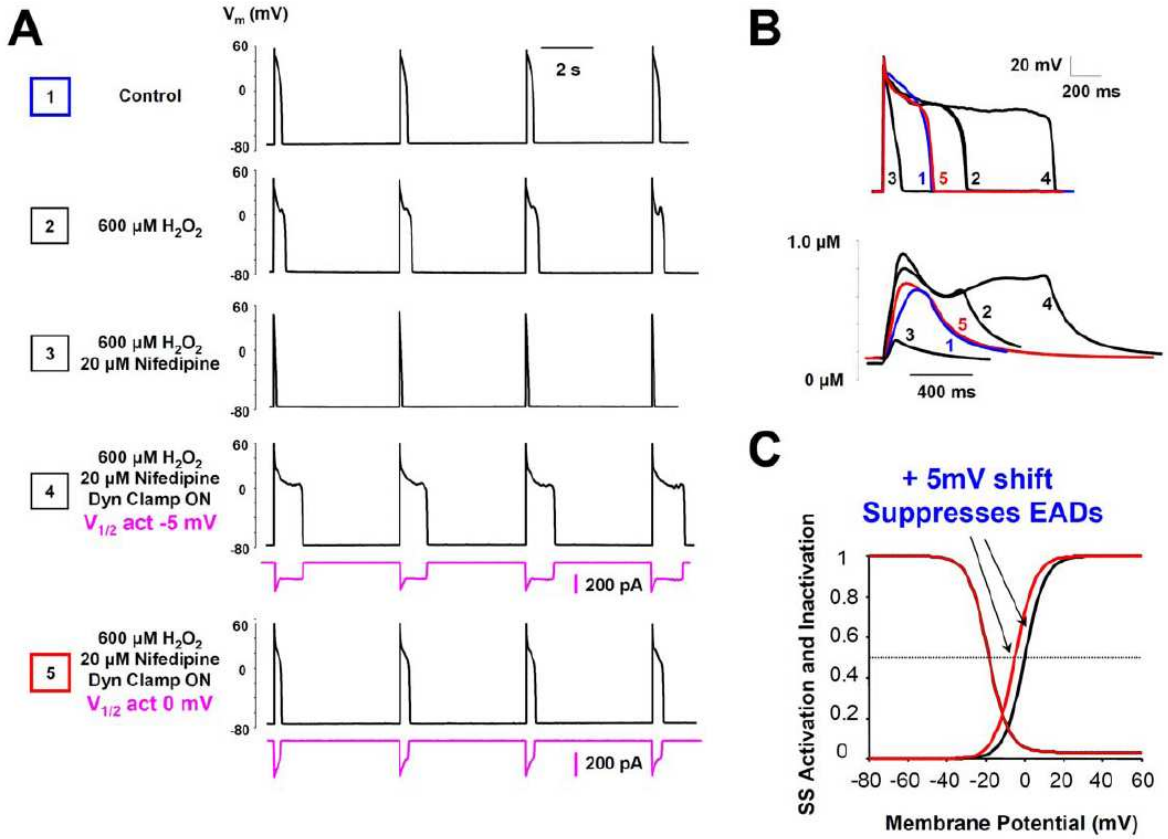

Figure 2.5. Reconstitution of EADs by a virtual $I_{Ca,L}$ and their suppression by shifting $I_{Ca,L}$ $V_{1/2}$ activation. A) APs from rabbit ventricular myocytes recorded at a pacing cycle length of 5 seconds at 36-37℃ in control conditions (1). Addition of 600 µmol/L H_2O_2 to the bath solution induced EADs within 5-10 minutes (2). Addition of 20 µmol/L Nifedipine blocked the native $I_{Ca,L}$, shortened APD and abolished EADs (3). The dynamic clamp was then turned on to inject a virtual "$I_{Ca,L}$" computed in real time (red trace), which restored EADs (4). Varying a single $I_{Ca,L}$ parameter ($V_{1/2}$ activation) by +5mV to effectively reduce the "$I_{Ca,L}$ window region" abolished EADs, despite the presence of H_2O_2 (5). B) Representative action potentials from each condition (numbered) in (A) and their corresponding virtual Ca_i transients. Note that both action potential duration and the shape and amplitude of the computed Ca_i transient in conditions (1) and (5) are similar. C) Graphical representation of the change in the overlap of the activation and steady-state inactivation curves upon a +5 mV shift in the $V_{1/2}$ of activation.

(Fig. 2.5A, trace 1). The recorded AP waveform was used to compute a virtual Ca_i transient, displayed below the AP trace (Fig. 2.5B, trace 1). The myocyte was then exposed to 600 µmol/L H_2O_2 until EADs appeared consistently (Fig. 2.5A, trace 2). Nifedipine (20 µmol/L) was then added to block the native $I_{Ca,L}$, which markedly shortened APD and abolished EADs (Fig. 2.5, trace 3). Current injection by the dynamic clamp was then turned on, adding the virtual $I_{Ca,L}$ computed from the UCLA rabbit ventricular AP cell model[20], whose properties which had been adjusted to simulate the previously analyzed effects of H_2O_2 on $I_{Ca,L}$ gating properties shown in

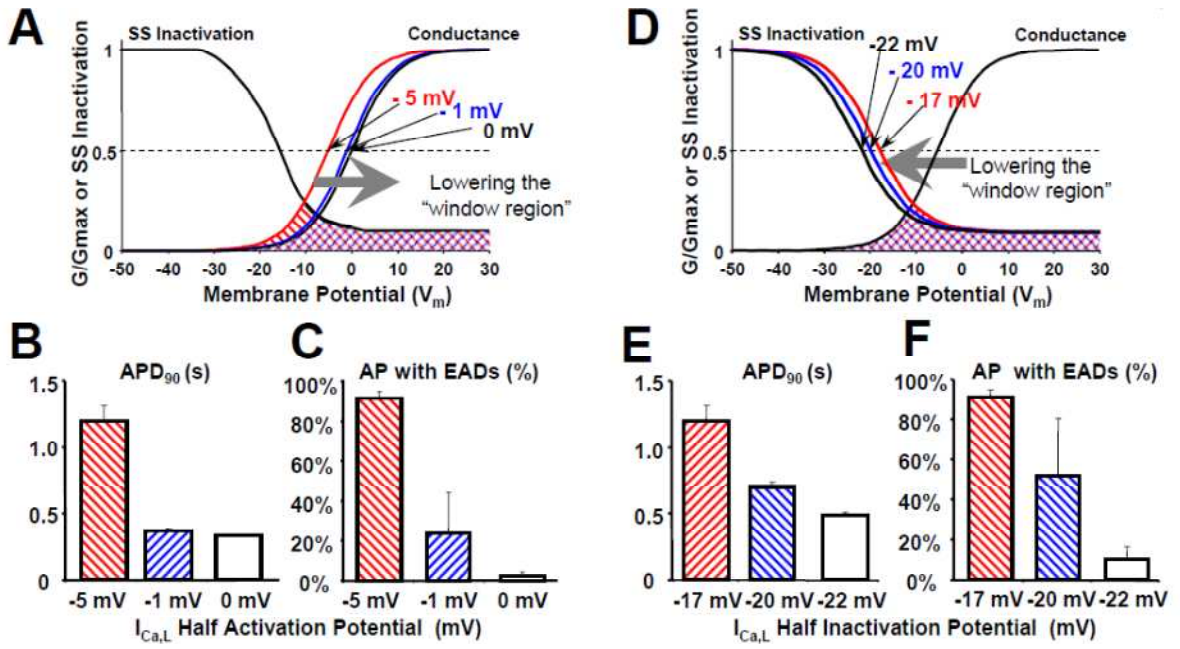

Figure 2.6 EADs induced by oxidative stress are steeply dependent on $V_{1/2}$ of activation and inactivation. A) Steady-state activation and inactivation of the virtual I_{CaL} under control conditions (black traces) and with the $V_{1/2}$ activation shifted by -1 (blue trace) or -5 mV (red trace) to partially simulate the effects of oxidative stress increasing the I_{CaL} window region (cross-hatched). B and C) APD_{90} (B) and the percentage of AP's exhibiting EADs (C) corresponding to the virtual I_{CaL} activation/inactivation properties in A, when the respective currents were injected by the dynamic clamp into ventricular myocytes in the presence of 0.6 mmol/L H_2O_2 and 20 µmol/L nifedipine. The virtual I_{CaL} corresponding to the red trace simulating oxidative stress caused marked AP prolongation and EADs, which were suppressed by returning the $V_{1/2}$ activation towards normal (blue and black traces). D) Steady-state activation and inactivation of the virtual I_{CaL} under control conditions (black traces) and with the $V_{1/2}$ inactivation shifted by +3 (blue trace) or +5 mV (red trace) to partially simulate the effects of oxidative stress increasing the I_{CaL} window region (cross-hatched). E and F) APD_{90} (E) and the percentage of AP's exhibiting EADs (F) corresponding to the virtual I_{CaL} activation/inactivation properties in A, when the respective currents were injected by the dynamic clamp into ventricular myocytes in the presence of 0.6 mmol/L H_2O_2 and 20 µmol/L nifedipine. The virtual I_{CaL} corresponding to the red trace simulating oxidative stress caused marked AP prolongation and EADs, which were suppressed by returning the $V_{1/2}$ inactivation towards normal (blue and black traces).

Fig. 2.2. Injection of this "H_2O_2- modified" virtual $I_{Ca,L}$ effectively restored the electrical properties of the myocyte membrane, resulting in AP prolongation and the reappearance of EADs (Fig.2.5, trace 4). The associated computed virtual Ca_i transients are shown in Fig. 2.5B.

To investigate the sensitivity of EAD formation to the properties of the virtual $I_{Ca,L}$, we then shifted the voltage dependence of $I_{Ca,L}$ activation ($V_{1/2}$ act) by +5 mV, to resemble the normal steady activation curve prior to H_2O_2 exposure. This small shift, which effectively suppressed the $I_{Ca,L}$ "window" current by reducing the overlap between the steady state

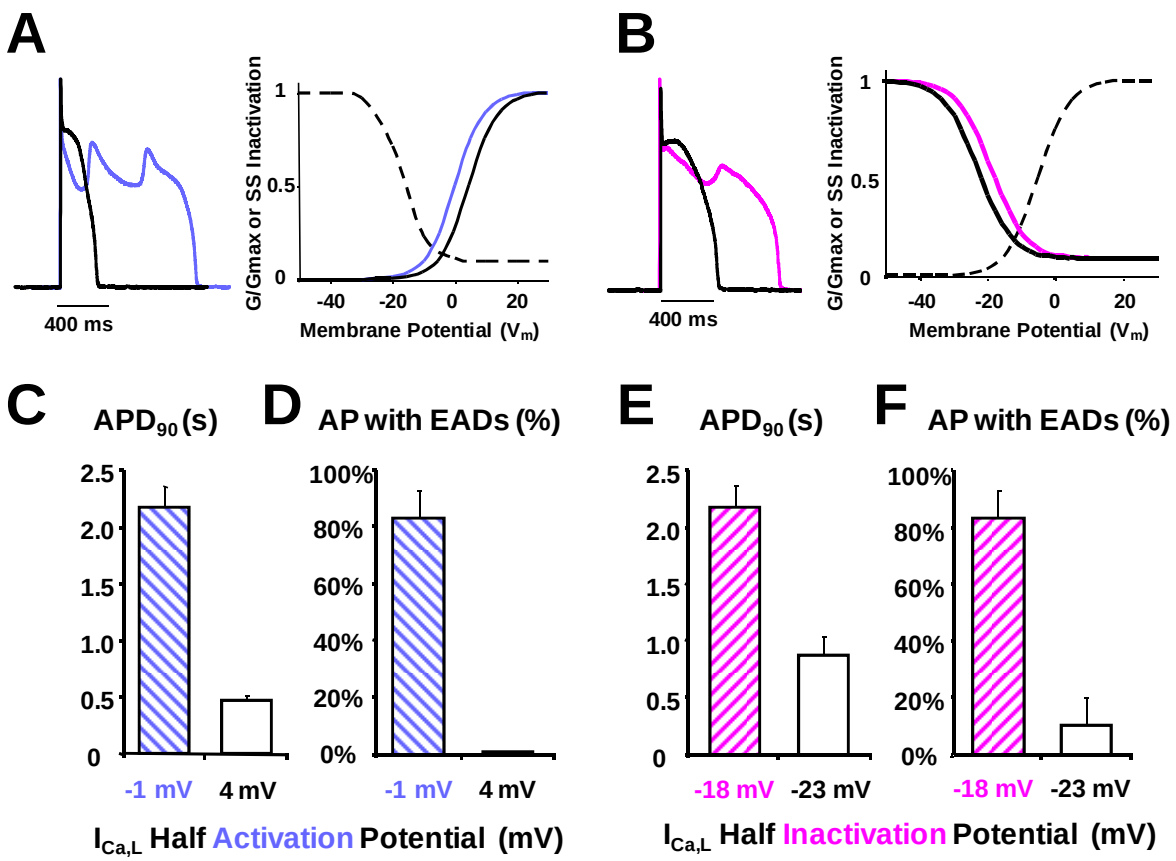

Figure 2.7. EADs induced by hypokalemia are steeply dependent on $V_{1/2}$ of activation and inactivation. A) Under hypokalemic conditions (2.0 mmol/L external K^+), EADs (blue trace) were reconstituted in the presence of 20 µmol/L nifedipine by injecting via the dynamic clamp a virtual $I_{Ca,L}$, with normal activation (blue) and inactivation (black) properties. Shifting the $V_{1/2}$ activation by +5 mV (black) to reduce the $I_{Ca,L}$ window region reversed AP prolongation and abolished EADs (solid bars). Graphs below summarize the effects on APD_{90} and percentage of AP's with EADs in myocytes subjected to the same protocol. B) Same, but with $V_{1/2}$ inactivation shifted by -5 mV to reduce the $I_{Ca,L}$ window region.

activation and inactivation curves to (Fig. 2.5C), abolished EADs and restored the AP duration towards the control value (Fig. 2.5, trace 5). Moreover, the virtual Ca_i transient (Fig. 2.5B, trace 5) had similar amplitude and kinetics to that computed for the normal control AP (Fig. 2.5B, trace 1). Similar results were also achieved by shifting the voltage dependence of $I_{Ca,L}$ *in*activation ($V_{1/2}$ inact) in the negative direction to reduce the window current region (not shown).

The overall results, summarized in Figure 2.6, demonstrate that the small shifts in the $V_{1/2}$ of steady-state activation and inactivation of $I_{Ca,L}$ strongly suppress EAD formation. A +4 mV shift of the $V_{1/2}$ act from –5mV to –1mV (Fig. 2.6A) shortened APD_{90} from 1,197±112 (n = 7)

to 373±15 ms (n = 4)(Fig. 2.6B) and suppressed EAD occurrence from 91±4% to 24±20% of paced APs (Fig. 2.6C). An additional +1 mV shift to 0 mV (Fig. 2.6A) shortened APD_{90} to 331±15 ms (n = 6) (Fig. 2.6B) and further suppressed EAD occurrence to ~2% (Fig. 2.6C). Similar results were achieved with small hyperpolarizing shifts in the $V_{1/2}$ inact. A -3 mV shift from -17mV to -20mV (Fig. 2.6D) reduced APD_{90} to 696±42 ms (n = 3) (Fig. 2.6E) and EAD occurrence to 52% (Fig. 2.6F). Further shifting $V_{1/2}$ inact by an additional -2 mV to -22mV (Fig. 2.6D) reduced APD_{90} to 488±21 ms (n = 4) (Fig. 2.6E) and EAD occurrence to 10%.

Reducing $I_{Ca,L}$ window current also suppresses hypokalemia-induced EADs

To demonstrate that the results described above are not unique to H_2O_2-induced EADs, we also assessed the effectiveness of shifting $V_{1/2}$ act or $V_{1/2}$ inact at suppressing hypokalemia-induced EADs. Lowering extracellular K^+ from 5.4 to 2.0 mmol/L hyperpolarized the resting membrane potential to nearly -100 mV and induced EADs within 5 minutes (Fig. 2.1). As with H_2O_2-induced EADs, blocking $I_{Ca,L}$ with 20 µmol/L Nifedipine abolished EADs and shortened the action potential (not shown). Adding a virtual $I_{Ca,L}$ with dynamic clamp prolonged APD_{90} to 2,170±190 ms (n = 6) (Fig. 2.7C&E, striped bars) and reconstituted EADs in 83% of APs (Fig. 2.7D&F, striped bars). A +5 mV depolarizing shift in the steady state activation curve from -1 to +4 mV shortened APD_{90} to 476±39 ms (n = 3) (Fig. 2.7C, solid bar) and reduced EAD occurrence to 0% (Fig. 2.7D, solid bar). Similarly, a hyperpolarizing shift in the steady state inactivation curve from -18 to -23 mV shortened APD_{90} to 869±167 ms (n = 3) and reduced EAD occurrence to 10% of APs.

2.5 DISCUSSION

It is widely accepted that EADs are important cellular triggers for VT and VF when repolarization reserve is reduced, as can occur clinically in acquired and congenital long QT syndromes and heart failure[31,32]. In the present study, we studied two different conditions,

oxidative stress (H_2O_2) and hypokalemia (Fig. 2.1), which reliably induce bradycardia-dependent EADs (positive dV/dt during phase 2 or 3) by different mechanisms in >90% of rabbit ventricular myocytes within 5-10 min of exposure. After blocking the native $I_{Ca,L}$ with nifedipine, we used the dynamic clamp technique to inject a virtual $I_{Ca,L}$, which successfully reconstituted EADs. Moreover, the biophysical properties of the virtual $I_{Ca,L}$ could be reprogrammed to explore its role in EAD formation. Our major findings are: 1) EAD formation is very sensitive to small shifts in the voltage sensitivity of steady state activation and inactivation of $I_{Ca,L}$, such that a +5 mV depolarizing shift in $V_{1/2}$ act, or a -5 mV hyperpolarizing shift in $V_{1/2}$ inact powerfully suppressed EAD formation (Figs. 2.5&6) ; ii) these small shifts were predicted to have minimal effects on peak $I_{Ca,L}$ during the AP, such that the Ca_i transient, hence excitation-contraction coupling and contractility, remain normal (Fig. 2.5B); 3) the same strategy was effective at suppressing EADs generated by two different mechanisms (Fig. 2.5-2.7): oxidative stress in which CaMKII activation potentiating inward Na and Ca currents plays a critical role[33, 34 35-38], and hypokalemia, in which decreased outward K^+ currents play the major role[39]. Moreover, the degree of hypokalemia used in this study is clinically relevant to values associated with EAD-mediated arrhythmias in patients[40].

These findings have therapeutic implications, namely that novel agents which alter the voltage-dependence and/or kinetics of $I_{Ca,L}$, could be developed to suppress EAD-mediated arrhythmias without adversely depressing excitation-contraction coupling.

Sensitivity of EADs to $I_{Ca,L}$ properties

In the present study, we analyzed the effects of small shifts in the $V_{1/2}$ act and $V_{1/2}$ inact on EAD formation, as a convenient way to suppress $I_{Ca,L}$ reactivation in the window voltage region. However, $I_{Ca,L}$ reactivation causing EADs during AP repolarization is not solely dependent on $V_{1/2}$ act and $V_{1/2}$ inact, but instead is a complex function of many $I_{Ca,L}$ parameters juxtaposed

with other factors, such as K^+ currents influencing the speed of repolarization [41]. With respect to $I_{Ca,L}$, other parameters in addition to $V_{1/2}$ act and $V_{1/2}$ inact influence $I_{Ca,L}$ reactivation during repolarization, including: the maximal L-type Ca current conductance; the steepness (slope factor) of voltage-dependent activation and inactivation; the time constants of activation, inactivation (both Ca-dependent and voltage-dependent), and recovery from inactivation; and the amplitude of the non-inactivating pedestal current. These factors can be combined into a single mathematical expression giving a necessary condition for EADs [42]. In the present study, our modifications to the virtual $I_{Ca,L}$ assumed that all of these other factors remained constant, allowing us to examine the isolated effects of $V_{1/2}$ act and $V_{1/2}$ inact. Thus, a major advantage of the dynamic clamp approach is that the virtual $I_{Ca,L}$ can be programmed to simulate all of the effects that a candidate agent has on these $I_{Ca,L}$ properties, once they have been characterized experimentally. The appropriately reshaped virtual $I_{Ca,L}$ can then be evaluated to determine whether or not it suppresses EADs in real myocytes when introduced by the dynamic clamp technique.

Limitations

Although the dynamic clamp provides a technique to systematically dissect the role of key ionic currents such as $I_{Ca,L}$ in EAD formation, an important limitation is that a virtual $I_{Ca,L}$ does not trigger SR Ca release, so it is not possible to directly test the effects of a modified virtual $I_{Ca,L}$ on the Ca_i transient or cell shortening. This limitation was partially offset by using an AP model incorporating detailed Ca^{2+} cycling dynamics which allowed us to make predictions about the Ca_i transient, validated by experimental recordings of the Ca_i transient in rabbit ventricular myocytes using a Ca^{2+}-sensitive fluorescent dye (Fig. 2.4). In fact, the lack of Ca^{2+} entering the cell during the virtual $I_{Ca,L}$ injection also provides an advantage, allowing us to distinguish the purely electrical effects of ionic currents from their biochemical consequences (Ca^{2+}-mediated

signaling). Thus, these results demonstrate that EADs can occur in the absence of Ca^{2+} influx or SR Ca^{2+} release and can be a purely electrical phenomenon. For example, we computed the virtual Na-Ca exchange current accompanying the virtual Ca_i transient in our model, but chose not to inject this current into the myocyte via the dynamic clamp, since our initial goal was to investigate whether $I_{Ca,L}$ alone was sufficient to reconstitute EADs without other Ca-sensitive currents. Furthermore, through the dynamic clamp, the contributions of other currents to EAD formation can be analyzed systematically, assuming they have been accurately formulated in the model.

Therapeutic implications

Our study demonstrates "proof-of-concept" for a hybrid biological-computational approach designed to predict how modifications of ion channel properties affect cellular arrhythmogenic phenomena such as EADs. Thus, in this study, the dynamic clamp has highlighted potential therapeutic targets (i.e. $I_{Ca,L}$ properties such as $V_{1/2}$ act, $V_{1/2}$ inact,) for new drugs or genetic interventions to suppress EAD-mediated arrhythmias.

Interstingly, whereas pharmacological agents may have off-target effects in both cardiac and noncardiac tissue, a specific way to target $I_{Ca,L}$ could be to take advantage of the modulatory accessory subunits of the L-type Ca^{2+} channel [43-45] such as $\alpha_2\delta$ or β subunits. These accessory subunits are highly specific for the channel and are known to modulate its biophysical properties [46-48]. Thus, genetic interventions to tune the biophysical properties of $I_{Ca,L}$ by altering its subunit composition could be a promising approach to suppress EAD formation in a highly specific manner.

2.6 Bibliography

(1) Sato D, Xie LH, Sovari AA, Tran DX, Morita N, Xie F, Karagueuzian H, Garfinkel A, Weiss JN, Qu Z. Synchronization of chaotic early afterdepolarizations in the genesis of cardiac arrhythmias. *Proc Natl Acad Sci U S A* 2009 March 3;106(9):2983-8.

(2) Weiss JN, Garfinkel A, Karagueuzian HS, Chen PS, Qu Z. Early afterdepolarizations and cardiac arrhythmias. *Heart Rhythm* 2010 December;7(12):1891-9.

(3) Weiss JN, Chen PS, Qu Z, Karagueuzian HS, Garfinkel A. Ventricular fibrillation: how do we stop the waves from breaking? *Circ Res* 2000 December 8;87(12):1103-7.

(4) Maltsev VA, Sabbah HN, Higgins RS, Silverman N, Lesch M, Undrovinas AI. Novel, ultraslow inactivating sodium current in human ventricular cardiomyocytes. *Circulation* 1998 December 8;98(23):2545-52.

(5) Volders PG, Kulcsar A, Vos MA, Sipido KR, Wellens HJ, Lazzara R, Szabo B. Similarities between early and delayed afterdepolarizations induced by isoproterenol in canine ventricular myocytes. *Cardiovasc Res* 1997 May;34(2):348-59.

(6) Szabo B, Sweidan R, Rajagopalan CV, Lazzara R. Role of Na+:Ca2+ exchange current in Cs(+)-induced early afterdepolarizations in Purkinje fibers. *J Cardiovasc Electrophysiol* 1994 November;5(11):933-44.

(7) January CT, Riddle JM. Early afterdepolarizations: mechanism of induction and block. A role for L-type Ca2+ current. *Circ Res* 1989 May;64(5):977-90.

(8) January CT, Riddle JM, Salata JJ. A model for early afterdepolarizations: induction with the Ca2+ channel agonist Bay K 8644. *Circ Res* 1988 March;62(3):563-71.

(9) Weiss JN, Garfinkel A, Karagueuzian HS, Chen PS, Qu Z. Early afterdepolarizations and cardiac arrhythmias. *Heart Rhythm* 2010 December;7(12):1891-9.

(10) January CT, Riddle JM. Early afterdepolarizations: mechanism of induction and block. A role for L-type Ca2+ current. *Circ Res* 1989 May;64(5):977-90.

(11) Antoons G, Volders PG, Stankovicova T, Bito V, Stengl M, Vos MA, Sipido KR. Window Ca2+ current and its modulation by Ca2+ release in hypertrophied cardiac myocytes from dogs with chronic atrioventricular block. *J Physiol* 2007 February 15;579(Pt 1):147-60.

(12) Dorval AD, Christini DJ, White JA. Real-Time linux dynamic clamp: a fast and flexible way to construct virtual ion channels in living cells. *Ann Biomed Eng* 2001 October;29(10):897-907.

(13) Berecki G, Zegers JG, Bhuiyan ZA, Verkerk AO, Wilders R, Van Ginneken AC. Long-QT syndrome-related sodium channel mutations probed by the dynamic action potential clamp technique. *J Physiol* 2006 January 15;570(Pt 2):237-50.

(14) Berecki G, Zegers JG, Verkerk AO, Bhuiyan ZA, de Jonge B, Veldkamp MW, Wilders R, Van Ginneken AC. HERG channel (dys)function revealed by dynamic action potential clamp technique. *Biophys J* 2005 January;88(1):566-78.

(15) Berecki G, Zegers JG, Wilders R, Van Ginneken AC. Cardiac channelopathies studied with the dynamic action potential-clamp technique. *Methods Mol Biol* 2007;403:233-50.

(16) Wilders R. Dynamic clamp: a powerful tool in cardiac electrophysiology. *J Physiol* 2006 October 15;576(Pt 2):349-59.

(17) Tran DX, Sato D, Yochelis A, Weiss JN, Garfinkel A, Qu Z. Bifurcation and chaos in a model of cardiac early afterdepolarizations. *Phys Rev Lett* 2009 June 26;102(25):258103.

(18) Mahajan A, Sato D, Shiferaw Y, Baher A, Xie LH, Peralta R, Olcese R, Garfinkel A, Qu Z, Weiss JN. Modifying L-type calcium current kinetics: consequences for cardiac excitation and arrhythmia dynamics. *Biophys J* 2008 January 15;94(2):411-23.

(19) Lin RJ, Bettencourt J, Wha IJ, Christini DJ, Butera RJ. Real-time experiment interface for biological control applications. *Conf Proc IEEE Eng Med Biol Soc* 2010;2010:4160-3.

(20) Mahajan A, Shiferaw Y, Sato D, Baher A, Olcese R, Xie LH, Yang MJ, Chen PS, Restrepo JG, Karma A, Garfinkel A, Qu Z, Weiss JN. A rabbit ventricular action potential model replicating cardiac dynamics at rapid heart rates. *Biophys J* 2008 January 15;94(2):392-410.

(21) Luo CH, Rudy Y. A dynamic model of the cardiac ventricular action potential. I. Simulations of ionic currents and concentration changes. *Circ Res* 1994 June;74(6):1071-96.

(22) Xie LH, Chen F, Karagueuzian HS, Weiss JN. Oxidative-stress-induced afterdepolarizations and calmodulin kinase II signaling. *Circ Res* 2009 January 2;104(1):79-86.

(23) Xie LH, Chen F, Karagueuzian HS, Weiss JN. Oxidative-stress-induced afterdepolarizations and calmodulin kinase II signaling. *Circ Res* 2009 January 2;104(1):79-86.

(24) Dzhura I, Wu Y, Colbran RJ, Balser JR, Anderson ME. Calmodulin kinase determines calcium-dependent facilitation of L-type calcium channels. *Nat Cell Biol* 2000 March;2(3):173-7.

(25) Wagner S, Dybkova N, Rasenack EC, Jacobshagen C, Fabritz L, Kirchhof P, Maier SK, Zhang T, Hasenfuss G, Brown JH, Bers DM, Maier LS. Ca2+/calmodulin-dependent protein kinase II regulates cardiac Na+ channels. *J Clin Invest* 2006 December;116(12):3127-38.

(26) Wagner S, Ruff HM, Weber SL, Bellmann S, Sowa T, Schulte T, Grandi E, Bers DM, Backs J, Belardinelli L, Maier LS. Reactive Oxygen Species-Activated Ca/Calmodulin Kinase II{delta} Is Required for Late INa Augmentation Leading to Cellular Na and Ca Overload. *Circ Res* 2011 January 20.

(27) Antoons G, Volders PG, Stankovicova T, Bito V, Stengl M, Vos MA, Sipido KR. Window Ca2+ current and its modulation by Ca2+ release in hypertrophied cardiac myocytes from dogs with chronic atrioventricular block. *J Physiol* 2007 February 15;579(Pt 1):147-60.

(28) Qi X, Yeh YH, Chartier D, Xiao L, Tsuji Y, Brundel BJ, Kodama I, Nattel S. The calcium/calmodulin/kinase system and arrhythmogenic afterdepolarizations in bradycardia-related acquired long-QT syndrome. *Circ Arrhythm Electrophysiol* 2009 June;2(3):295-304.

(29) Tran DX, Sato D, Yochelis A, Weiss JN, Garfinkel A, Qu Z. Bifurcation and chaos in a model of cardiac early afterdepolarizations. *Phys Rev Lett* 2009 June 26;102(25):258103.

(30) Tan RC, Joyner RW. Electrotonic influences on action potentials from isolated ventricular cells. *Circ Res* 1990 November;67(5):1071-81.

(31) Huffaker R, Lamp ST, Weiss JN, Kogan B. Intracellular calcium cycling, early afterdepolarizations, and reentry in simulated long QT syndrome. *Heart Rhythm* 2004 October;1(4):441-8.

(32) Maruyama M, Lin SF, Xie Y, Chua SK, Joung B, Han S, Shinohara T, Shen MJ, Qu Z, Weiss JN, Chen PS. Genesis of Phase 3 Early Afterdepolarizations and Triggered Activity in Acquired Long-QT Syndrome. *Circ Arrhythm Electrophysiol* 2011 February 1;4(1):103-11.

(33) Anderson ME. Calmodulin kinase and L-type calcium channels; a recipe for arrhythmias? *Trends Cardiovasc Med* 2004 May;14(4):152-61.

(34) Koval OM, Guan X, Wu Y, Joiner ML, Gao Z, Chen B, Grumbach IM, Luczak ED, Colbran RJ, Song LS, Hund TJ, Mohler PJ, Anderson ME. CaV1.2 beta-subunit coordinates CaMKII-triggered cardiomyocyte death and afterdepolarizations. *Proc Natl Acad Sci U S A* 2010 March 16;107(11):4996-5000.

(35) Xie LH, Chen F, Karagueuzian HS, Weiss JN. Oxidative-stress-induced afterdepolarizations and calmodulin kinase II signaling. *Circ Res* 2009 January 2;104(1):79-86.

(36) Dzhura I, Wu Y, Colbran RJ, Balser JR, Anderson ME. Calmodulin kinase determines calcium-dependent facilitation of L-type calcium channels. *Nat Cell Biol* 2000 March;2(3):173-7.

(37) Wagner S, Dybkova N, Rasenack EC, Jacobshagen C, Fabritz L, Kirchhof P, Maier SK, Zhang T, Hasenfuss G, Brown JH, Bers DM, Maier LS. Ca2+/calmodulin-dependent protein kinase II regulates cardiac Na+ channels. *J Clin Invest* 2006 December;116(12):3127-38.

(38) Wagner S, Ruff HM, Weber SL, Bellmann S, Sowa T, Schulte T, Grandi E, Bers DM, Backs J, Belardinelli L, Maier LS. Reactive Oxygen Species-Activated Ca/Calmodulin Kinase II{delta} Is Required for Late INa Augmentation Leading to Cellular Na and Ca Overload. *Circ Res* 2011 January 20.

(39) Sato D, Xie LH, Nguyen TP, Weiss JN, Qu Z. Irregularly appearing early afterdepolarizations in cardiac myocytes: random fluctuations or dynamical chaos? *Biophys J* 2010 August 4;99(3):765-73.

(40) Osadchii OE. Mechanisms of hypokalemia-induced ventricular arrhythmogenicity. *Fundam Clin Pharmacol* 2010 October;24(5):547-59.

(41) Tran DX, Sato D, Yochelis A, Weiss JN, Garfinkel A, Qu Z. Bifurcation and chaos in a model of cardiac early afterdepolarizations. *Phys Rev Lett* 2009 June 26;102(25):258103.

(42) Tran DX, Sato D, Yochelis A, Weiss JN, Garfinkel A, Qu Z. Bifurcation and chaos in a model of cardiac early afterdepolarizations. *Phys Rev Lett* 2009 June 26;102(25):258103.

(43) Birnbaumer L, Qin N, Olcese R, Tareilus E, Platano D, Costantin J, Stefani E. Structures and functions of calcium channel beta subunits. *J Bioenerg Biomembr* 1998 August;30(4):357-75.

(44) Davies A, Hendrich J, Van Minh AT, Wratten J, Douglas L, Dolphin AC. Functional biology of the alpha(2)delta subunits of voltage-gated calcium channels. *Trends Pharmacol Sci* 2007 May;28(5):220-8.

(45) Dolphin AC. Calcium channel diversity: multiple roles of calcium channel subunits. *Curr Opin Neurobiol* 2009 June;19(3):237-44.

(46) Birnbaumer L, Qin N, Olcese R, Tareilus E, Platano D, Costantin J, Stefani E. Structures and functions of calcium channel beta subunits. *J Bioenerg Biomembr* 1998 August;30(4):357-75.

(47) Olcese R, Qin N, Schneider T, Neely A, Wei X, Stefani E, Birnbaumer L. The amino terminus of a calcium channel beta subunit sets rates of channel inactivation independently of the subunit's effect on activation. *Neuron* 1994 December;13(6):1433-8.

(48) Platano D, Qin N, Noceti F, Birnbaumer L, Stefani E, Olcese R. Expression of the alpha(2)delta subunit interferes with prepulse facilitation in cardiac L-type calcium channels. *Biophys J* 2000 June;78(6):2959-72.

Chapter 3:
The Late Component of the L-type Ca Current is a Critical Target To Suppress Cardiac Early Afterdepolarizations.

3.1 ABSTRACT

Aims: Early afterdepolarizations (EADs) are voltage oscillations during phase 2 or 3 of the cardiac action potential (AP) that can trigger lethal cardiac arrhythmias. Reactivation of the L-type Ca^{2+} current ($I_{Ca,L}$) plays a key role in EAD formation. Therefore, L-type Ca^{2+} channels (LTCCs) may represent an ideal therapeutic target to suppress EAD formation.

Methods & Results: We established a consistent EAD regime in rabbit ventricular myocytes exposed to H_2O_2. Next, to systematically identify modifications of steady-state and time-dependent biophysical properties of $I_{Ca,L}$ to suppress EADs without impairing excitation-contraction coupling, we used the dynamic clamp technique to replace the endogenous ICa,L with a virtual $I_{Ca,L}$ (with tunable parameters). We then probed the sensitivity of EADs to changes in the i) slope of the voltage-dependent activation; ii) slope of the voltage-dependent inactivation; iii) time constant of voltage-dependent activation; iv); time constant of voltage-dependent inactivation and v) the amplitude of the non-inactivating pedestal current. We found that only a reduction in the amplitude of the $I_{Ca,L}$ non-inactivating pedestal current was potently effective at suppressing EADs and restoring action potential duration to a normal range. These modifications did not affect the Ca_i transient properties, preserving myocyte contractility.

Conclusions: These results, together with our previous work, highlight the potential of the steady-state biophysical properties of $I_{Ca,L}$ as powerful therapeutic targets for EAD suppression. The hybrid experimental/computational approach illustrates the potential utility of the dynamic clamp to guide a drug discovery or gene therapy strategy by identifying and targeting subtle and selective aspects of LTCC function.

3.2 INTRODUCTION

Early afterdepolarizations (EADs) are arrhythmogenic membrane potential oscillations that occur before repolarization of the cardiac action potential (AP) is complete. While the mechanistic link between EADs in single cells and triggered arrhythmias in the heart is still a subject of intense investigation, their arrhythmogenic effects have traditionally been associated with focal excitation[1, 2] and more recently with reentrant waves caused by premature ventricular complexes (PVCs) or prolongation of the action potential duration [3-7]. Several experimental and theoretical studies have suggested that EADs are capable of triggering fatal arrhythmias such as polymorphic ventricular tachycardia, torsade de pointes and ventricular fibrillation[5, 8-11]. Interestingly, the onset of EADs (i.e the reversal of the normal repolarization phase of the AP) occurs over a range of membrane potentials where the steady-state activation and inactivation curves of the L-type Ca^{2+} current ($I_{Ca,L}$) overlap, known as the $I_{Ca,L}$ window current region [12]. In this membrane potential range $I_{Ca,L}$ can reactivate, thus reversing the normal repolarization phase and playing a major role in EAD formation[13]. While other ionic currents can also contribute to EAD formation depending on the cellular context, a regenerative inward current such as $I_{Ca,L}$ is required for EADs to propagate in tissue [14, 15]. Based on the relevance of $I_{Ca,L}$ to EAD formation and propagation, we sought to identify the biophysical properties of $I_{Ca,L}$ that could be targeted to suppress EAD formation.

Using the dynamic clamp technique [16] in dissociated rabbit ventricular myocytes, we recently demonstrated that EADs are highly sensitive to subtle changes in the half-activation or half-inactivation potentials of $I_{Ca,L}$, suggesting that a reduction of the $I_{Ca,L}$ window current may represent an effective maneuver to suppress EADs without blocking the early peak $I_{Ca,L}$ required to maintain normal excitation-contraction coupling [17]. The dynamic clamp is a powerful technique which allows one to introduce a model conductance such as $I_{Ca,L}$ with programmable properties into a cell in real time to study its effects on action potential characteristics (Fig 3.1E).

The proof-of-concept provided by our initial study[17] prompted us to perform a more thorough analysis of biophysical parameters influencing the time- and voltage-dependent properties of $I_{Ca,L}$, in order to identify the most sensitive parameters involved in EAD formation. In addition to the half-activation and half-inactivation potentials, we systematically investigated the slopes of

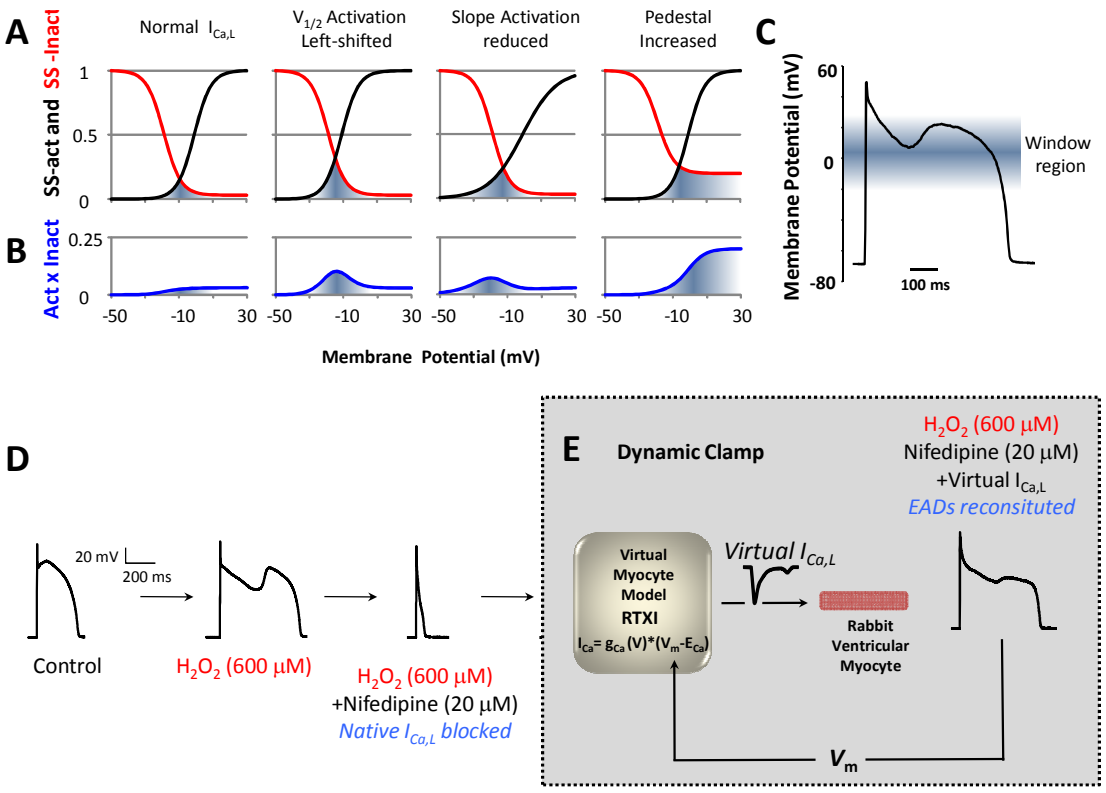

Figure 3.1 The $I_{Ca,L}$ window current region and the experimental design for dynamic clamp. A) Changing steady-state biophysical properties of $I_{Ca,L}$, such as the half-activation potential ($V_{1/2}$ activation), the slope of the activation curve or the non-inactivating pedestal of the inactivation curve has a large impact on the $I_{Ca,L}$ window region, i.e., the area (shaded) subtended by the intersection of the voltage-dependent activation and inactivation curves. B) The window region quantified as a product of the steady-state activation and steady-state inactivation curves (SS-act x SS-Inact). C) A typical rabbit ventricular myocyte action potential after exposure to 600 µmol/L H_2O_2, displaying a large-amplitude early afterdepolarization (EAD). EADs often occur within the range of membrane potentials defined by the window current (around 30 to 20 mV). D) Representative action potentials for the experimental protocol used in this study: Cardiac myocytes (paced at 5 s, left) were exposed to 600 µmol/L H_2O_2 to induce EADs (center). Addition of 20 µmol/L nifedipine blocked the native $I_{Ca,L}$ (right). . Under dynamic clamp (E) the myocyte membrane potential is fed into the model, which computes and injects a virtual $I_{Ca,L}$ into the cell in real time and reconstitutes EADs in the continuous presence of H_2O_2.

the voltage dependence of activation and inactivation, the non-inactivating pedestal current and the time constants of activation and inactivation, all of which are important in determining the shape, amplitude and rate of growth of the $I_{Ca,L}$ window current (Fig. 3.1A-C) during the action potential.

The results demonstrate that of all the biophysical parameters of $I_{Ca,L}$ explored in this and previous work [17], only three are effective at suppressing EADs without adversely affecting action potential duration (APD): the half-activation and half-inactivation potentials and the non-inactivating pedestal current. Collectively, these findings provide a drug discovery target to search for new antiarrhythmic agents to suppress EAD-mediated arrhythmias. Moreover, this study demonstrates a novel hybrid experimental/computational approach incorporating the dynamic clamp technique to predict how subtle alterations in biophysical properties of ionic currents such as $I_{Ca,L}$ affect cardiac electrophysiology and arrhythmogenic phenomena.

3.3 METHODS

Ethical approval: All animal handling protocols were approved by the UCLA Institutional Animal Care and Use Committee and conformed to the Guide for the Care and Use of Laboratory Animals published by the US National Institutes of Health.

Electrophysiology: Three to four month old New Zealand male rabbits were euthanized by an intravenous injection of heparin sulfate (1000 U) and sodium pentobarbital (100 mg/kg); adequacy of anesthesia was confirmed by the lack of pedal withdrawal reflex, corneal reflex, and motor response to pain stimuli. Ventricular myocytes were dissociated using a retrograde Langendorff perfusion system as previously described [18], and washed and bathed in Tyrode's solution containing (in mmol/L): 136 NaCl, 5.4 KCl, 1 $MgCl_2$, 0.33 NaH_2PO_4, 1.8 $CaCl_2$, 10

Glucose, and 10 HEPES adjusted to pH 7.4. The intracellular solution contained (in mmol/L): 110 K-Aspartate, 30 KCl, 5 NaCl, 10 HEPES, 0.1 EGTA, 5 MgATP, 5 Creatine phosphate, 0.05 cAMP adjusted to pH 7.2. All recordings were made using an Axopatch 200B amplifier (Axon Instruments). Whole-cell patch-clamp recordings were performed in current-clamp mode at ~36℃ with 1-2 MΩ pipettes. Data were acquired and analyzed using custom-made software (G-Patch, Analysis).

Dynamic Clamp: The myocyte model used computes all Ca^{2+}-dependent ionic conductances including $I_{Ca,L}$, the fast sodium current I_{Na}, the Na-K pump current I_{NaK}, the Na-Ca exchange current I_{NCX} and the Ca^{2+}-dependent slow component of the delayed rectifier potassium channel $I_{Ks,}$ as described previously [19] [17]. Briefly, the Ca^{2+} flux into the cell due to $I_{Ca,L}$ is given by

$$J_{ca} = g_{ca} P_o i_{ca}, \textbf{(1)}; \qquad i_{ca} = \frac{4P_{ca}V_m F^2}{RT} \frac{Cse^{2a} - 0.341[Ca^{2+}]_o}{e^{2a} - 1} \textbf{(2)};$$

where *Cs* is the submembrane concentration in units of mmol/L. P_o was formulated as

$$P_o = d \cdot f \cdot q$$

where *d* is the voltage-dependent activation gate, *f* is the voltage-dependent inactivation gate and *q* is the Ca^{2+}-dependent inactivation gate. The steady states of these gating variables as functions of the membrane potential (V_m) were formulated as follows:

$$d_\infty = \frac{1.0}{1.0 + \exp(-(V_m - dhalf)/dslope)} \quad \textbf{(3)}$$

$$f_\infty = \frac{1.0 - pdest}{1.0 + \exp((V_m - fhalf)/fslope)} + pdest \textbf{(4)}$$

$$q_\infty = \frac{1.0}{1.0 + (\frac{Cs}{cst})^\gamma} \quad \textbf{(5)}$$

$$\tau_d = \frac{d_\infty (1 - \exp(-V_m - (dhalf + a1))}{a2(dslope + a2)(V_m - (dhalf + a1))} \quad \textbf{(6)}$$

$$\tau_f = 1/[b1\exp(-b2(V_m - (fhalf + b3))^2) + b4] \quad \textbf{(7)}$$

where τ_d and τ_f are the time constants of the *d* gate and the *f* gate, respectively, *pdest* is the non-inactivating pedestal and *dslope* and *fslope* are the steepness of the voltage-dependence of activation and inactivation, respectively. These two parameters are called slope factors (k) in this study, which were calculated as RT/*z*, where R is the gas constant, T is temperature and *z* is the effective charge (e^0). We change the slope factors by changing the effective charge. The control parameters in the $I_{Ca,L}$ formulation were determined by fitting formulated current to experimental nifedipine-sensitive $I_{Ca,L}$ records[17] using Berkeley Madonna and then implemented for dynamic clamp in RTXI [20] (www.rtxi.org). The sampling/computation frequency was 10 kHz.

Data analysis: APD at 90% repolarization (APD_{90}) was calculated using custom-made software, while EAD amplitude was calculated manually by measuring the difference in V_m from the inflection point where dV/dt is 0 to the peak of the EAD where dV/dt is also 0. In APs that displayed multiple EADs, only the EAD with the largest voltage excursion was included in the analysis. EAD occurrence is reported as the percentage of APs that displayed at least one EAD. Error bars show the standard error of the mean (SEM).

Computer simulations: The Markovian L-type Ca^{2+} open channel probability P_o was replaced by the Hodgkin-Huxley formulation for P_o, as used in the dynamic clamp experiments described

above. The formulation of I_{to} was replaced by that of Dong *et al.*[21] as modified by Zhao *et al*[22] to more accurately reflect experimental data of Zhao *et al.* on APD restitution. In the rabbit ventricular myocyte, the APD restitution curve is biphasic, as the APD at intermediate heart rates is greater than at fast and slow heart rates[22]. This has been attributed to the slow recovery of I_{to} in this type of cell[23].

To model the effects of H_2O_2, we made several changes to ionic currents (see below). We implemented a late I_{Na} current with a magnitude approximately 1% of peak I_{Na} based on the findings of Song *et al* [24]of increased late I_{Na} in presence of 200 µmol/L H_2O_2 in isolated rabbit ventricular myocytes.

We increased maximum conductance of $I_{Ca,L}$ by a factor of 2.0, which is within the range reported by Xie *et al* [25]who found that in rabbit ventricular myocytes the peak $I_{Ca,L}$ increased from 7.3 ± 0.8 pA/pF in a control environment to 12.1 ± 1.8 pA/pF in the presence of 1mmol/L H_2O_2.

We also increased maximum conductance of I_{to} by a factor of 1.57 based on experimental data from Zhao *et al.* [22] on isolated rabbit ventricular myocytes. Finally, we increased the maximum conductance of I_{NCX} by a factor of 1.5 following the mathematical model of Zhao *et al.*[22].

Maximum ionic conductances: Following Zhao *et al.* [22], the maximal conductance of $I_{Ca,L}$ was increased by a factor of 2.0, and that of NCX was increased by a factor of 1.5.

$I_{Ca,L}$ formulation: The same model used for the dynamic clamp was also used for computer simulations.

Late I_{Na} formulation*:* A late I_{Na} current was implemented by changing the formulation of I_{Na} to:

$$I_{Na} = \overline{G}_{Na} m^3 [\alpha + (1-\alpha)h][\alpha + (1-\alpha) j](V - E_{Na}) \quad \textbf{(8)}$$

where α reflects a non-inactivating component of the channel. For the H_2O_2 model, α = 0.01.

I_{to} formulation: The formulation of I_{to} was based on that of Dong *et al*[21], as modified by Zhao *et al.* [22]to better fit rabbit ventricular myocytes:

$$I_{to} = g_{to}(mhjR + \alpha)(V - E_K) \quad \textbf{(9)}$$

$$R = e^{V/300} \quad \textbf{(10)}$$

$$\alpha_m = \frac{4}{1+e^{-(V-25)/20}}\ ,\ \beta_m = \frac{3.5}{1+e^{(V+110)/29.5}}\ ,\ m_\infty = \frac{1}{1+e^{-(V+13.9)/8}} \quad \textbf{(11)}$$

$$\alpha_h = \frac{0.016}{1+e^{(V+59)/5.5}}\ ,\ \beta_h = \frac{0.11}{1+e^{-(V+27)/6.5}}\ ,\ h_\infty = \frac{1}{1+e^{(V+50.3)/3.9}} \quad \textbf{(12)}$$

$$j_\infty = h_\infty \quad \textbf{(13)}$$

$$\tau_h = \frac{1}{\alpha_h + \beta_h} + 50 \text{ for control} \quad \textbf{(14a)}$$

$$\tau_h = \frac{1}{\alpha_h + \beta_h} + 70 \text{ for } H_2O_2 \quad \textbf{(14b)}$$

$$\tau_j = \frac{7000}{1+e^{(V+30)/10}} + 400 \text{ for control} \quad \textbf{(15a)}$$

$$\tau_j = \frac{6000}{1+e^{(V+30)/10}} + 250 \text{ for } H_2O_2 \quad \textbf{(15b)}$$

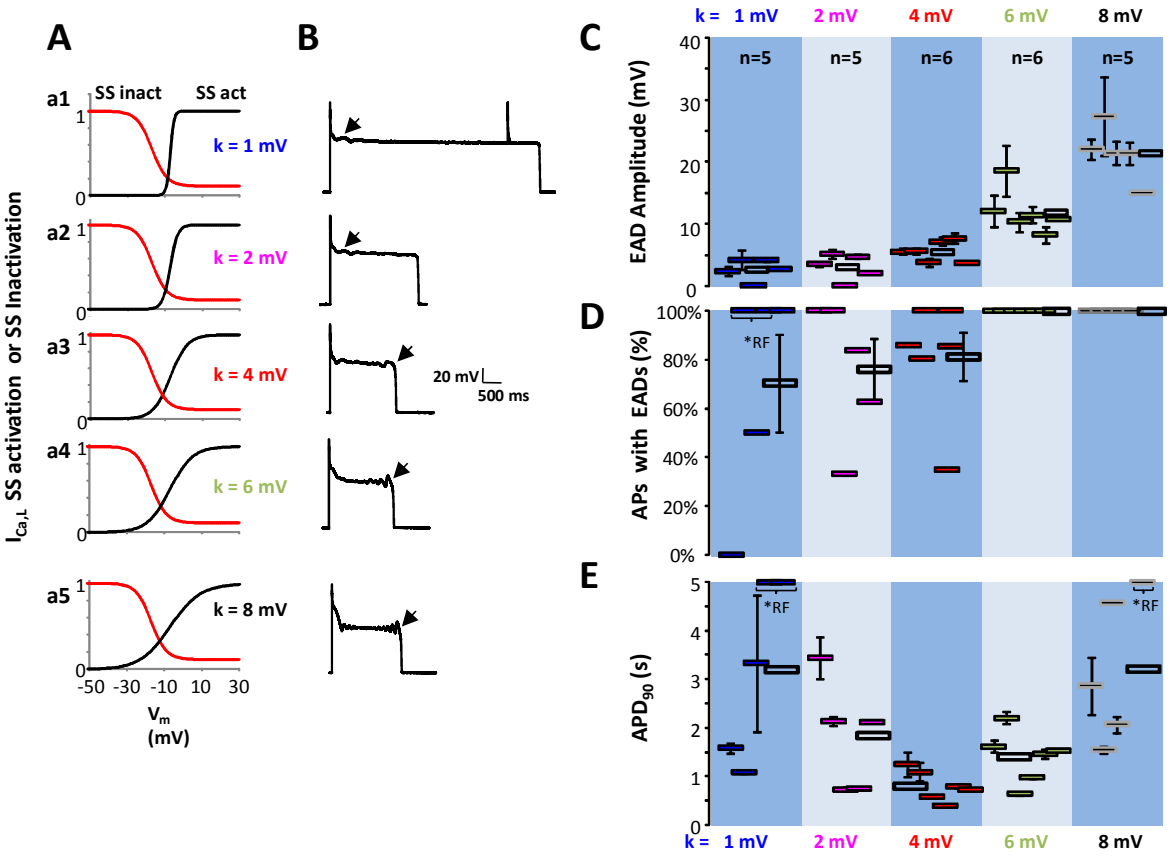

Figure 3.2. EAD amplitude is sensitive to changes in the slope of the steady-state voltage dependence of activation of $I_{Ca,L}$ A) Under dynamic clamp and in the presence of H_2O_2, we evaluated the effects of varying the slope (k) of the steady-state activation curve (black). Steady-state inactivation properties were unperturbed, while the slope of the steady-state activation curve was varied under dynamic clamp from z = 1 mV (a1) to z = 8 mV (a5). The set of curves in the center, z = 4 mV (a3) correspond to the native $I_{Ca,L}$ modified by H_2O_2. B) Representative APs obtained for each k value studied, displaying EADs (arrows). For each value of k tested, the mean EAD amplitude (C), EAD occurrence (D) and APD_{90} (E) are shown. Individual experiments are shown as solid rectangles, the means for all experiments are plotted as an open rectangles (n = 5-6 cells, from 5-6 rabbits). Error bars indicate SEM. *Instances when the AP failed to repolarize before the next pacing stimulus are reported as RF (repolarization failure). Note that EAD amplitude grows as k is increased (slope becomes shallower).

Gto = 0.07 for control

Gto = 0.11 for H_2O_2

To model the experimentally reported differences in AP duration and ionic current strength between the epicardial, endocardial, and M cell, we created 3 model cells with different combinations of maximal conductances for I_{to} and I_{Ks}. Fedida et al.[26] reported isolated rabbit endocardial cells to have a maximum I_{to} current that was 85% of that of epicardial cells, which is

reflected in the model. Idriss *et al.* [27] reported APDs of rabbit endocardial and M cells to be 12% and 18% longer, respectively, than APs of epicardial cells. The control endocardial and M cells have APDs that are 13% and 17% longer, respectively, than the epicardial cell.

Cell model code was written in the C++ language format and implemented using Microsoft Visual Studio 2008. The model, which consists of 22 differential equations, was integrated using the Euler method with an adaptive time step ranging from 0.1 to 0.01 ms. Analysis was performed using custom scripts written in MATLAB.

Transmural I_{Ks} and I_{to} gradients: To establish epi, endo, and M cell types, 3 different cell models were created by scaling the original values for the maximal conductances of I_{ks} and I_{to} by different scaling factors. These scaling factors were chosen to reflect the transmural I_{to} gradient reported by Fedida et al.[26], as well as the transmural APD gradient reported by Idriss *et al*.[27].

3.4 RESULTS

Sensitivity of EADs to the Steepness of Steady-State Activation and Inactivation Curves. In our previous study using the dynamic clamp technique [17] we showed that modest shifts (<5 mV) in the half-activation and half-inactivation potentials of $I_{Ca,L}$, which both reduced the overlap between steady-state activation and inactivation curves (i.e., the window current region, Fig. 3.1A), potently suppressed EADs, without adversely altering APD or the intracellular Ca_i transient. However, the half-activation and half-inactivation potentials are only two of the many biophysical parameters that affect the voltage dependence, amplitude and rate of growth of the $I_{Ca,L}$ window current. To explore systematically how other biophysical parameters such as the slopes and time constants of activation and inactivation affect EAD formation, we used the same experimental design as previously described [17] Briefly, myocytes were paced at a 5 second cycle length and superfused with 600 µmol/L H_2O_2 until EADs appeared consistently. The native $I_{Ca,L}$ was then blocked with 20 µmol/L nifedipine, which eliminated EADs and markedly shortened the APD (Fig. 3.1D). Next, the dynamic clamp was engaged to inject, in

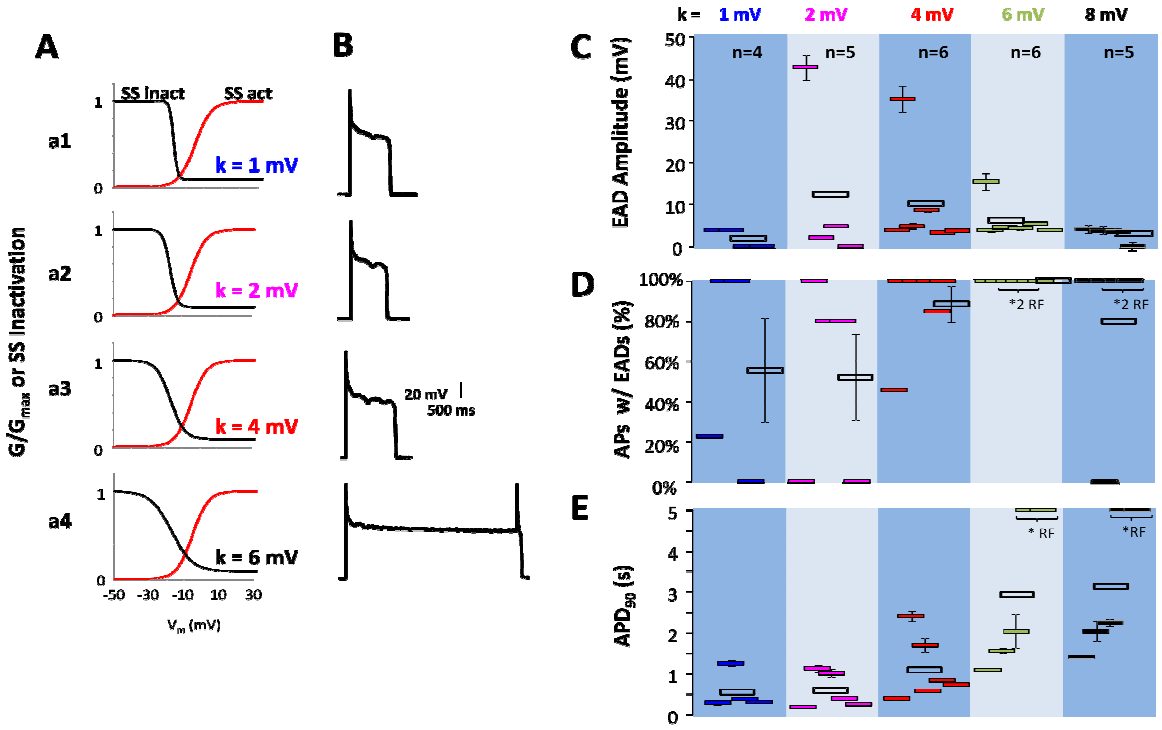

Figure 3.3 Relevance of the slope of $I_{Ca,L}$ steady-state inactivation curve to EADs and APD. A) Under dynamic clamp and in the presence of H_2O_2, we evaluated the effects of varying the slope (k) of the steady-state inactivation curve (black). The steady-state activation curve was kept constant, while the slope of the steady-state inactivation curve was varied under dynamic clamp from k = 1 mV (a1) to z = 8 mV. The pair of curves in the center, k = 4 mV (a3) correspond to the native $I_{Ca,L}$ modified by H_2O_2. B) Representative APs obtained for each k values studied. For each value of k tested, the mean EAD amplitude (C), EAD occurrence (D) and APD_{90} (E) are shown. Individual experiments are shown as solid rectangles, the means for all experiments are plotted as an open rectangles. Error bars indicate SEM. *Instances when the AP failed to repolarize before the next pacing stimulus are reported as RF (repolarization failure).

real time, a virtual $I_{Ca,L}$ computed from Eqs.1-7 using the membrane potential of the myocyte (Fig. 3.1E), which incorporated previously measured H_2O_2-induced changes in $I_{Ca,L}$ [17], causing EADs to reappear (Fig 3.1E). Thus, all the experiments in dynamic clamp were carried out in the constant presence of the H_2O_2, maintaining a pathological state which resulted in EAD formation.

Following reconstitution of the EADs with dynamic clamp in the presence of H_2O_2 in the superfusate, the first intervention was to examine the effects of altering the effective valence, *z* (slope), of the voltage dependence of activation from $z = 5.7\ e^0$ (slope factor, k = 4 mV) to $z = 25.6\ e^0$ (k = 1 mV) to increase, or to $3.2\ e^0$ (k = 8 mV) to decrease, the steepness of the voltage

dependence of activation (Fig. 3.2A). We found that at greater steepness, EAD amplitudes decreased from 5.6±0.7mV to 3.1±1.0mV (for z =12.8 e^0 , k = 2 mV) or 2.6±0.8 mV (for z =25.6 e^0, k = 1 mV) (Fig. 3.2B and 3.2C). Also, for the largest z we used (z =25.6 e^0, k = 1 mV), APD became prolonged such that, in some cases, the AP failed to repolarize before the next pacing stimulus (Fig. 3.2B). Conversely, when the effective charge of the activation curve was reduced from z=5.7e^0 (k= 4 mV) to z=4.3e^0 (k = 6 mV) EAD amplitude increased from 5.6±0.7 mV to 12.3±1.4 mV (Fig. 3.2B and 3.C). This effect was even more pronounced for z=3.2e^0 (k=8 mV) such that mean EAD amplitude increased to 21.4±2.0 mV (Fig. 3.2B and 3.C), although no significant changes in percentage of APs with EADs were observed (Fig. 3.2D) and APD_{90} remained prolonged for these maneuvers (Fig. 3.2E).

We also investigated the effects of changing the slope of the voltage dependence of inactivation (Fig. 3.3A) by increasing or decreasing the effective charge to z=25.6 e^0 (k=1 mV) or z = 3.2 e^0 (k=8 mV), respectively. We did not observe a significant difference in either EAD amplitude, or in percentage of APs with EADs (Fig. 3.3C and 3.3D). APD_{90} prolonged from 1104±319 ms to 3140±771 ms (Fig. 3.3B and 3.3E) as the steepness of the inactivation curve was reduced from z = 5 e^0 (k= 4 mV) to z = 3.2 e^0 (k= 8 mV)(Fig. 3.3A,a4).

τ_d	% APs with EADs	APD_{90} (ms)
τ_d x 0.1	77 ± 10 %	1104 ± 0165
τ_d x 0.5	79 ± 15%	1122 ± 126
τ_d x 1	76 ± 8%	1376 ± 200
τ_d x 2	91 ± 4%	1550 ± 130
τ_d x 10	100%	2711 ± 548
τ_f	% EADs	APD_{90} (ms)
τ_f x 0.1	85 ± 8 %	2433 ± 291
τ_f x 0.5	70 ± 16%	1838 ± 435
τ_f x 1	76 ± 8%	1376 ± 200
τ_f x 2	24 ± 14%	802 ± 183
τ_f x 10	73 ± 24%	1506 ± 102

Table 3.1 EAD occurrence and APD_{90} for changes in the time constant of $I_{Ca,L}$ activation.

Sensitivity of EADs to the kinetics of $I_{Ca,L}$ activation and inactivation. EADs depend on a transient mismatch of inward and outward currents [28] [29]. Since the inward current carried by

$I_{Ca,L}$ during the AP plateau depends on its kinetic properties, we next studied the effects of altering the time constants of $I_{Ca,L}$ activation and inactivation in the dynamic clamp model on EAD formation during oxidative stress. Overall, we found that changes in the rates of $I_{Ca,L}$ activation or inactivation by up to 10-fold had limited efficacy at suppressing EADs induced by H_2O_2 (Figs. 3.4 and 3.5).

Specifically, in the presence of 600 µmol/L H_2O_2, slowing the activation rate of $I_{Ca,L}$ by

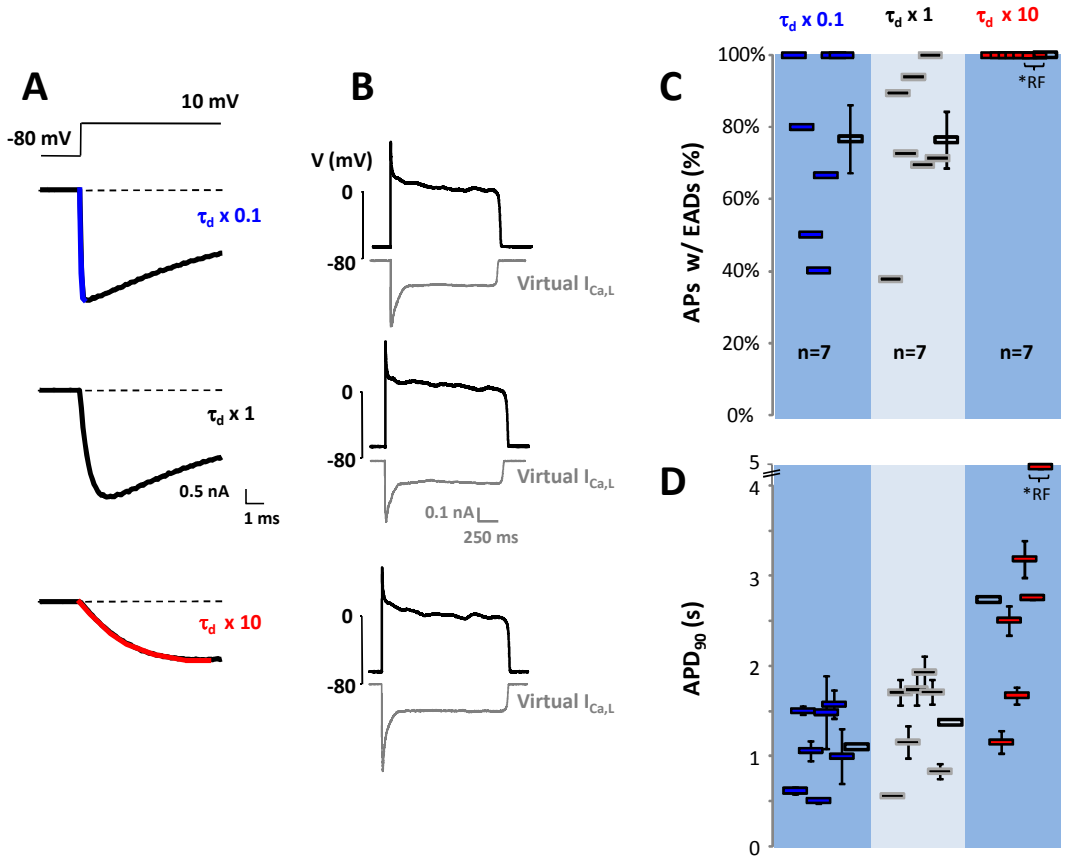

Figure 3.4 Time constant of $I_{Ca,L}$ activation has a limited effect on H_2O_2-induced EADs. A) The output of the $I_{Ca,L}$ model in response to a depolarizing pulse from ~80 mV to 10 mV using three different time constants of activation (τ_d). B) Representative action potentials recorded under dynamic clamp conditions from myocytes in which the endogenous $I_{Ca,L}$ was replaced with a virtual $I_{Ca,L}$ with modified activation time constants. The injected virtual $I_{Ca,L}$ in dynamic clamp is shown under each AP trace. Increasing or decreasing $I_{Ca,L}$ activation rate by a factor of 10 did not shorten APD or suppress EADs. For each value of τ_d tested, EAD occurrence (C) and APD_{90} (D) are shown. Individual experiments are shown as solid rectangles, the means for all experiments are plotted as open rectangles (n =7, from 5-6 rabbits). Note that in all cases APD_{90} was prolonged (≥ 500 ms). Error bars indicate SEM. *Instances when the AP failed to repolarize before the next pacing stimulus are reported as RF (repolarzation failure).

two-fold (τ_d×2) maintained an average APD_{90} of 1550±130 ms and EAD occurrence remained high at 91% (Table 3.1). A 10-fold slowing of the rate of activation of $I_{Ca,L}$ (τ_d×10), prolonged APD_{90} from 1376±200 ms to 2710±548 ms, while EAD occurrence increased from 76±8% to 100%. Conversely, accelerating the rate of activation of $I_{Ca,L}$ by two-fold ($\tau_d \times 0.5$) (Table 3.1) or by 10-fold ($\tau_d \times 0.1$) had only modest impacts on both APD_{90} (1121±126 ms or 1104±165 ms) and EAD occurrence (80% or 77%), respectively (Fig.3.4).

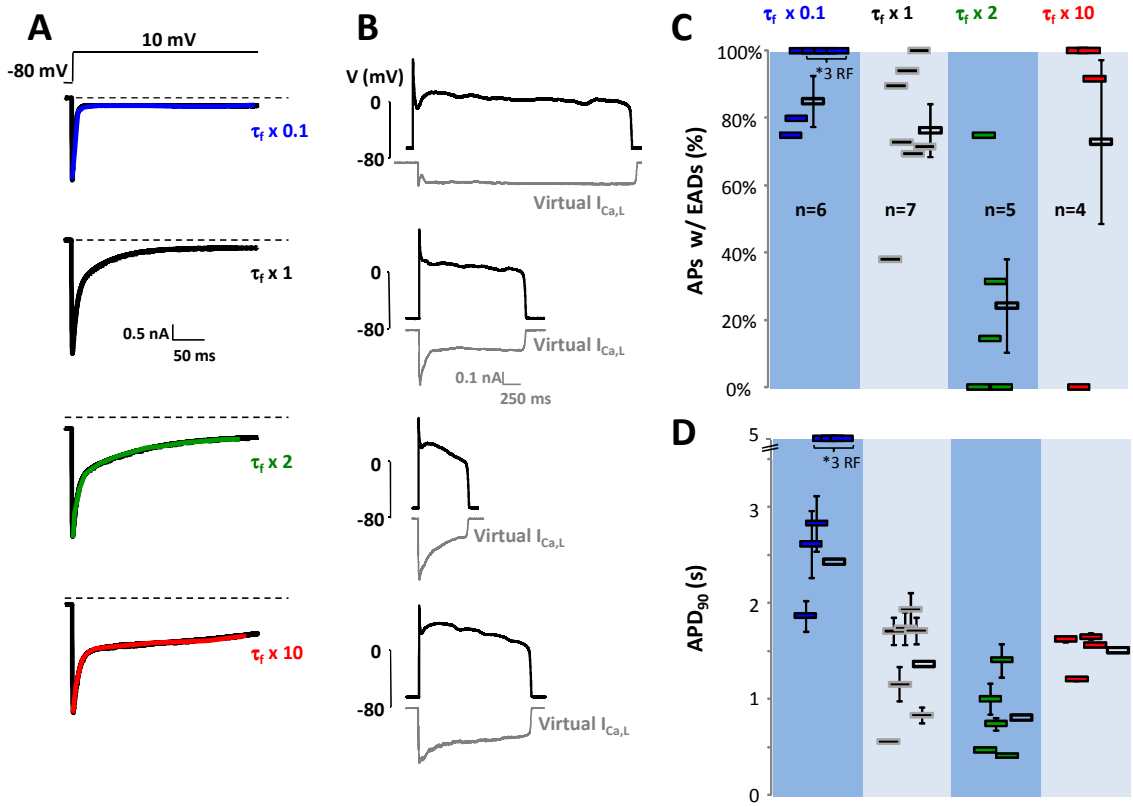

Figure 3.5 $I_{Ca,L}$ time constant of inactivation has limited efficacy for suppressing EADs induced by H_2O_2. A) The output of the $I_{Ca,L}$ model in response to a depolarizing pulse from 80 mV to 10 mV using four different time constants of inactivation (τ_f). B) Representative action potentials recorded under dynamic clamp conditions from myocytes in which the endogenous $I_{Ca,L}$ was replaced with a virtual $I_{Ca,L}$ with modified inactivation time constants. The injected virtual $I_{Ca,L}$ in dynamic clamp is shown under each AP trace. For each value of τ_f tested, EAD occurrence (C) and APD_{90} (D) are shown. Individual experiments are shown as solid rectangles, the means for all experiments are plotted as open rectangles (n= 4-7, from 3-5 rabbits). Note that in all cases APD_{90} is prolonged (> 500 ms). Error bars indicate SEM. *Instances when the AP failed to repolarize before the next pacing stimulus are reported as RF (repolarization failure). A limited favorable effect on EAD occurrence is observed for decreasing τ_f by a factor of 2; however, on average, APs remained prolonged (> 500 ms).

When the rate of voltage-dependent inactivation (VDI) in the dynamic clamp model was accelerated two-fold (τ_f ×0.5), neither APD_{90} (from 1376±199ms to 1838±434ms) nor EAD occurrence (from 76±8% to 70±16%) were dramatically altered. Accelerating the rate of VDI by ten-fold (τ_f ×0.1) (Fig 3.5A) increased APD_{90} (to 2433±290 ms) (Fig 3.5D) and also increased EAD occurrence to 85±8% (Fig 3.5C).

Conversely, decreasing the rate of VDI by two-fold (τ_f ×2) (Fig 3.5A) reduced EAD occurrence to 24±14% (Fig 3.5C), but APD_{90} remained prolonged (802±183 ms) (Fig 3.5D). Further slowing the rate of inactivation by ten-fold (τ_f×10), on the other hand, did not reduce EAD occurrence (73±24% of APs), and significantly prolonged APD_{90} (1506±102 ms) (Fig 3.5C and 3.5D).

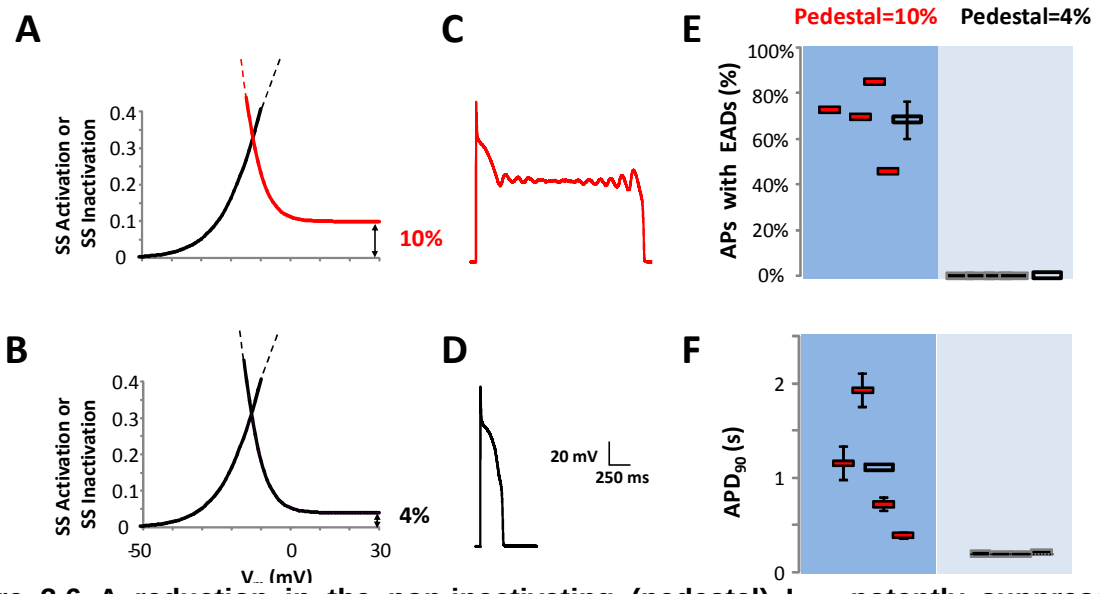

Figure 3.6 A reduction in the non-inactivating (pedestal) $I_{Ca,L}$ potently suppresses EADs and restores APD. A, B) Enlarged view of the steady-state activation and inactivation curves of $I_{Ca,L}$ shows changes made to the non-inactivating component (pedestal). Under dynamic clamp and in the presence of H_2O_2, we evaluated the effect of lowering the non-inactivating pedestal from 10% (A) to 4% of the peak current (B). C) Representative AP recorded in dynamic clamp under the conditions shown in (A). Note that lowering the pedestal current to 4% (B) eliminated EADs and restored a normal APD (D). E) The proportion of APs displaying EADs under two different pedestal amplitudes. F) APD_{90} under two different pedestal amplitudes. Individual experiments are shown as solid rectangles, the means for all experiments are plotted as open rectangles (n = 4, from 4 rabbits). Error bars indicate SEM.

Sensitivity of EADs to the non-inactivating pedestal of $I_{Ca,L}$. The inactivation of $I_{Ca\text{-}L}$, due to VDI and Ca-dependent (CDI) mechanisms [30] is incomplete during the time course of an AP. A residual, non-inactivating component known as the pedestal $I_{Ca,L}$ [31 32] has a large impact on the voltage level and duration of the AP plateau. Since one of the effects of H_2O_2 in producing EADs is to enhance the non-inactivating component of $I_{Ca,L}$ pedestal from ~3% to ~10% of the peak current [17], we explored the effects of altering the pedestal current of the dynamic clamp-generated $I_{Ca,L}$. Reducing the pedestal current from 10% to 4% completely suppressed EAD occurrence (Fig 3.6D and 3.6E) and shortened APD to 186±2 ms (Fig. 3.6D and 3.6F), without attenuating the amplitude of the predicted Ca_i transient (Fig. 3.7) compared to control conditions.

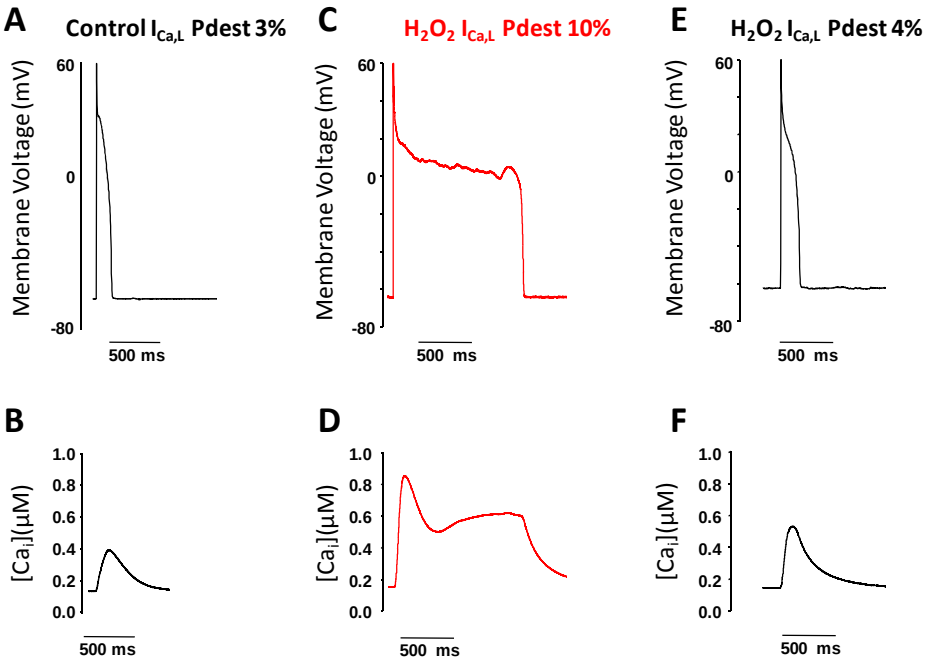

Figure 3.7 Predicted Ca_i Transient Before and After Reduction of the $I_{Ca,L}$ Pedestal. A) A representative AP recorded in control conditions. B) The predicted Ca_i transient upon action potential clamp of the ventricular AP model with the AP waveform in (A). C) Representative AP recorded in dynamic clamp in the presence of H_2O_2 (10% $I_{Ca,L}$ pedestal) reconstituted EADs and prolonged the APD. D) The ventricular AP model predicts the Ca_i transient in real time during the AP recorded in (C). (E) Upon a reduction in the $I_{Ca,L}$ pedestal to 4% the AP is restored to ~250 ms and EADs are abolished. (F) The ventricular AP model predicts the Ca_i transient in real time during the AP recorded in (E). Note that the expected amplitude and shape of the Ca_i transient is also restored compared to control conditions shown in (B).

Effect of non-inactivating pedestal of $I_{Ca,L}$ on epicardial, endocardial and M cell types. Considering that there are regional differences in the ionic basis underlying ventricular action potentials, we explored whether a therapeutic reduction in the $I_{Ca,L}$ pedestal can be effective at suppressing EADs in various cell types of the myocardium. We first paced our 3 cell models at a 5s cycle length under control conditions, with a 3% $I_{Ca,L}$ pedestal current (Fig. 3.8A). This resulted in APDs of 229ms, 258ms, and 268ms, for the epi, endo, and M cell respectively. We next modeled the effects of H_2O_2 as described above, including increasing the $I_{Ca,L}$ pedestal current to 10%. The AP was prolonged to 540ms/504ms/811ms in epi/endo/M and EADs appeared in all three cell types (Fig. 3.8B). When we decreased the $I_{Ca,L}$ pedestal current back

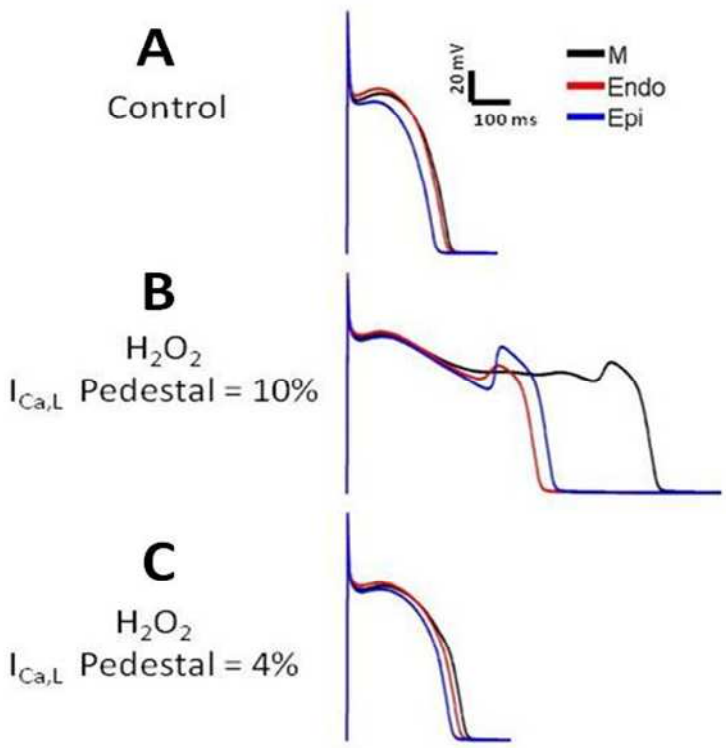

Figure 3.8 Reducing the non-inactivating $I_{Ca,L}$ pedestal is an effective maneuver to suppress simulated H_2O_2-induced EADs in a computer model of rabbit ventricular cell layer types. A) Action potentials for M, endocardial, and epicardial versions of the Mahajan cell model under control conditions. B) Modeling the effects of H_2O_2 produces AP prolongation and EADs in all cell models. C) Lowering the $I_{Ca,L}$ pedestal current from 10% to 4%, while maintaining other H_2O_2 effects, suppresses EADs and restores normal APDs in all cell models.

to 4%, while maintaining all other H_2O_2 effects APD shortened to 273ms/293ms/309ms in epi/endo/M and EADs disappeared (Fig. 3.8C). Thus, suppressing the I_{CaL} pedestal current was effective at eliminating EADs irrespective of transmural AP morphological differences.

3.5 DISCUSSION

Although many ionic currents can contribute to EAD formation, reactivation of $I_{Ca,L}$ plays a central role in providing a regenerative inward current required for EADs to propagate, thereby causing triggered activity in multicellular tissue [13, 33]. The main finding of the present study is that, even though H_2O_2 is likely to affect other ionic currents such as I_{Na} [34], the modification of $I_{Ca,L}$ is sufficient to prevent EADs even in the presence of H_2O_2. Furthermore, this maneuver does not diminish the amplitude of the predicted Ca_i transient (Fig. 3.7) and therefore is expected to maintain cell contractility. Conventional Ca^{2+} channel blockers such as nifedipine, which indiscriminately block both peak and window $I_{Ca,L}$, are highly effective at suppressing EADs (e.g. Fig. 3.1D). However, by blocking peak $I_{Ca,L}$, these drugs also potently suppress excitation-contraction coupling, precluding clinical usefulness for EAD suppression. The ideal Ca^{2+} channel agent for suppressing EAD-mediated arrhythmias would leave peak $I_{Ca,L}$ intact to preserve normal excitation-contraction coupling, and selectively block the late $I_{Ca,L}$ reactivated during repolarization when AP plateau enters the window voltage range.

In this study, we applied the dynamic clamp technique to systematically evaluate the hypothesis that EADs can be suppressed by selectively targeting the biophysical properties regulating the $I_{Ca,L}$ window current. Figure 3.9 summarizes the effects of the various parameter changes on both APD and EAD occurrence, illustrating the three parameters (half-activation potential, half-inactivation potential and pedestal current) that both effectively suppress EADs and restore APD towards a normal value. From these findings, we predict that drugs or genetic interventions that reproduce these desired effects on $I_{Ca,L}$ properties will leave peak $I_{Ca,L}$ and

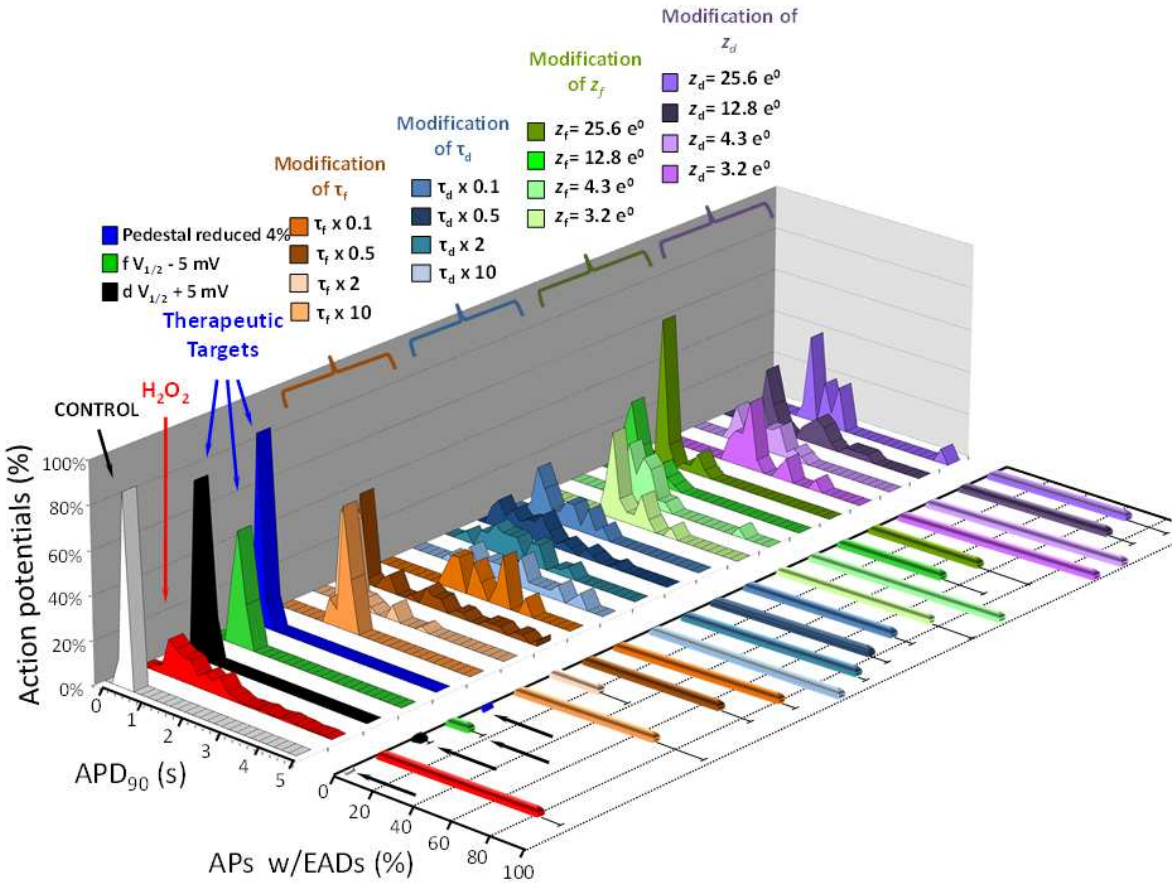

Figure 3.9 The effects of modification of $I_{Ca,L}$ time-dependent and steady-state biophysical properties on APD_{90} and EAD formation. 3D plot showing the action potential duration (APD) distribution for each experimental condition (n = 4-28, from 4-14 rabbits). The histograms show the percentage of action potentials that fall within 200 ms bins up to 5 seconds. APs in control conditions (white) have a narrow duration distribution with most APs ca. 250 ms . Under dynamic clamp, in the presence of H2O2, the APD distribution becomes broad as most APs are longer than 1 second (red). Changes in the slope of the steady-state activation curve (purple), the steady-state inactivation curve (green), the time constant of activation (blue), or the time constant of inactivation (brown) maintain broad APD distributions. A 6% reduction of the pedestal current (indigo), a 5 mV leftward shift in the half-inactivation potential (green), or a 5 mV rightward shift in the half-activation potential (black) restore APD distributions to around 250 ms 49. The corresponding EAD occurrence for each condition is shown as a plot perpendicular to the Y-axis and on the same plane as the floor of the histogram. EAD occurrence is plotted as the percentage of action potentials with EADs in each experimental condition. In control conditions, no EADs are present (white bar). EAD occurrence is high for all maneuvers studied except for a reduction in the pedestal (indigo bar), or favorable shifts in the half-inactivation (green) and half-activation potentials (black).

hence excitation-contraction coupling intact, yet suppress the late $I_{Ca,L}$ reactivation in the window region that plays such a critical role in EAD formation. An important novel contribution of the present study is the finding that the $I_{Ca,L}$ pedestal current has an equivalent promise to the half-activation and half-inactivation potentials as a novel anti-arrhythmic target to suppress EAD formation, which is robust across the spectrum of simulated transmural AP differences in the ventricular epicardial, M cell and endocardial layers (Fig. 3.8). This finding is intriguing because of the precedent in Na channels, in which selective blockers of the late Na current (I_{Na}), which leave the peak I_{Na} intact, are already in clinical use [35]. Given the overall structural similarities between Na and Ca^{2+} channels, the likelihood that analogous agents that selectively block late $I_{Ca,L}$ can be also identified seems high. Moreover, since late I_{Na} can also play an important role in EAD formation [36, 37], we can further speculate that the combination of a late I_{Na} blocker with a late $I_{Ca,L}$ blocker might be a particularly efficacious anti-arrhythmic combination to prevent EAD-mediated arrhythmias.

The effects of the various $I_{Ca,L}$ on APD and EADs observed in this study can be understood in terms of the dynamical theory of EAD formation as a dual Hopf-homoclinic bifurcation [28]. In this theory, the membrane voltage oscillations characterizing EADs depend critically on the amount of time that the membrane voltage dwells in the window region during repolarization. This dwell time which must be long enough for the voltage- and time-dependent growth rate of $I_{Ca,L}$ in the window range to overcome counterbalancing repolarizing currents such as I_{Ks}, thereby generating the upstroke of the EAD. As membrane voltage approaches 0 mV, the diminishing amplitude of $I_{Ca,L}$ and voltage-dependent growth of I_{Ks} force the repolarization phase of the EAD, with this tug-of-war generating successive oscillations. Sensitivity analysis shows that EAD amplitude is a function of the slope of the voltage dependence of activation (Fig. 3.2), consistent with the dynamical theory stating that membrane oscillations (EADs) occur due to instability of the L-type Ca^{2+} current in the window current

voltage range via a Hopf bifurcation [28]. EAD formation is more susceptible to interventions which limit the maximum steady-state amplitude that the late $I_{Ca,L}$ can achieve during repolarization (shifts in half-activation and half-inactivation potential and pedestal current) than to interventions that change the rate of growth (time constants of activation and inactivation) or shape of the window $I_{Ca,L}$ (slopes of inactivation and inactivation): While EAD occurrence could be diminished with small changes in steady-state parameters (<5 mV shifts in half-activation and half-inactivation potential or 60% reduction in the pedestal current), kinetic parameters required order-of-magnitude changes to produce modest effects, often causing excessive changes in APD.

A recent theoretical study predicted that reducing $I_{Ca,L}$ pedestal current has a biphasic effect on APD: while a moderate reductions of $I_{Ca,L}$ pedestal shortens APD and suppresses EADs (in congruence with this work), a more pronounced reduction results in a prolonged APD, without EADs formation [32]. In this work, we show that as long as the AP plateau voltage remains above the $I_{Ca,L}$ window range (i.e., > 0 mV), APD can prolong markedly without any significant oscillations in voltage. For example, steepening the I_{Ca-L} activation curve dampened EAD amplitude, but APD was remained very prolonged (Fig. 3.2). Thus theoretical and experimental data support the notion that APD prolongation and EAD occurrence are not causally linked. While the occurrence of EADs prolongs APD, prolongation of the AP by itself does not necessarily lead to EADs. These findings are consistent with previous observations that AP triangulation is more likely to cause EADs than AP prolongation per se [38].

Limitations and Implications

Several limitations of this study should be noted. This study was performed in rabbit ventricular myocytes, which differ in some respects from human myocytes. However, the L-type Ca^{2+} current properties are generally similar [39, 40]. Although we investigated the sensitivity of

EAD formation over a wide array of steady-state and time-dependent $I_{Ca,L}$ biophysical properties, our analysis has focused on EADs induced by oxidative stress. It will be important to test whether EADs induced by other interventions show the same pattern of sensitivity. We also speculate that altering the time constant of CDI (similar to the calmodulin CaM_{1234} mutation [41]) will likely impact EAD occurrence, as demonstrated in a recent theoretical study [42]; however the effects of Ca^{2+}-dependent inactivation were not evaluated in this work.

Futhermore, while it was possible to account for cell size in the dynamic clamp model (by scaling the computed $I_{Ca,L}$ by the clamped cell membrane capacitance),the model used in this work assumed a fixed $I_{Ca,L}$ density and therefore did not take into account the regional cell-to-cell variability. To validate these findings in the different ventricular myocyte populations, we have modeled regional differences of ionic conductances in the ventricular action potentials based on data reported in the literature (Fig 3.8). We have incorporated the changes in H_2O_2-modified parameters to induce EADs in these cell types and confirmed the efficacy of reducing the $I_{Ca,L}$ pedestal current as an EAD-suppressing maneuver.

Finally, to replace the endogenous native $I_{Ca,L}$ with a virtual programmable $I_{Ca,L}$ using the dynamic clamp required blocking the native $I_{Ca,L}$ with nifedipine, while the current injected by the dynamic clamp did not carry Ca^{2+} ions. Therefore, the injected virtual $I_{Ca,L}$ did not trigger SR Ca^{2+} release. Nevertheless the depolarizing current had the shape and duration dictated by the $I_{Ca,L}$ model parameters and the membrane voltage. While this can be viewed as a limitation, the opposite is also true: EAD formation can have a purely electrical etiology that does not involve the biochemical consequences of Ca^{2+} influx . Nevertheless, we are aware that the Ca^{2+} cycling dynamics also play a large role in determining susceptibility to EADs; as such, the model accounted for Ca^{2+}-dependent $I_{Ca,L}$ inactivation, by computing the Ca^{2+} transient in real time. This approach allowed us to acquire the predicted Ca_i transient for each experiment, to ensure that anti-EAD maneuvers did not significantly perturb the predicted Ca^{2+} release from the SR.

Despite these limitations, we believe that this approach outlines a useful new strategy for drug discovery, potentially adaptable to high throughput screening of small molecules or genetic interventions, to identify new antiarrhythmic agents. In this context, the dynamic clamp approach represents a powerful method to move beyond simple screening for indiscriminate ion channel blockers and towards identifying and targeting subtle and selective aspects of ion channel biophysics to guide drug discovery.

3.6 Bibliography

(1) Wit AL, Rosen MR. Pathophysiologic mechanisms of cardiac arrhythmias. *Am Heart J* 1983 October;106(4 Pt 2):798-811.

(2) Rosen MR. Mechanisms for arrhythmias. *Am J Cardiol* 1988 January 15;61(2):2A-8A.

(3) el-Sherif N, Caref EB, Yin H, Restivo M. The electrophysiological mechanism of ventricular arrhythmias in the long QT syndrome. Tridimensional mapping of activation and recovery patterns. *Circ Res* 1996 September;79(3):474-92.

(4) Antzelevitch C, Sicouri S. Clinical relevance of cardiac arrhythmias generated by afterdepolarizations. Role of M cells in the generation of U waves, triggered activity and torsade de pointes. *J Am Coll Cardiol* 1994 January;23(1):259-77.

(5) Yan GX, Wu Y, Liu T, Wang J, Marinchak RA, Kowey PR. Phase 2 early afterdepolarization as a trigger of polymorphic ventricular tachycardia in acquired long-QT syndrome : direct evidence from intracellular recordings in the intact left ventricular wall. *Circulation* 2001 June 12;103(23):2851-6.

(6) Yang PC, Kurokawa J, Furukawa T, Clancy CE. Acute effects of sex steroid hormones on susceptibility to cardiac arrhythmias: a simulation study. *PLoS Comput Biol* 2010 January;6(1):e1000658.

(7) Xie Y, Sato D, Garfinkel A, Qu Z, Weiss JN. So little source, so much sink: requirements for afterdepolarizations to propagate in tissue. *Biophys J* 2010 September 8;99(5):1408-15.

(8) Bapat A, Nguyen TP, Lee JH, Sovari AA, Fishbein MC, Weiss JN, Karagueuzian HS. Enhanced sensitivity of aged fibrotic hearts to angiotensin II- and hypokalemia-induced

early afterdepolarization-mediated ventricular arrhythmias. *Am J Physiol Heart Circ Physiol* 2012 June 1;302(11):H2331-H2340.

(9) Wu J, Wu J, Zipes DP. Early afterdepolarizations, U waves, and torsades de pointes. *Circulation* 2002 February 12;105(6):675-6.

(10) Antzelevitch C. Ionic, molecular, and cellular bases of QT-interval prolongation and torsade de pointes. *Europace* 2007 September;9 Suppl 4:iv4-15.

(11) Choi BR, Burton F, Salama G. Cytosolic Ca2+ triggers early afterdepolarizations and Torsade de Pointes in rabbit hearts with type 2 long QT syndrome. *J Physiol* 2002 September 1;543(Pt 2):615-31.

(12) January CT, Riddle JM, Salata JJ. A model for early afterdepolarizations: induction with the Ca2+ channel agonist Bay K 8644. *Circ Res* 1988 March;62(3):563-71.

(13) January CT, Riddle JM, Salata JJ. A model for early afterdepolarizations: induction with the Ca2+ channel agonist Bay K 8644. *Circ Res* 1988 March;62(3):563-71.

(14) Chang MG, Sato D, de LE, Lee JH, Karagueuzian HS, Garfinkel A, Weiss JN, Qu Z. Bi-stable wave propagation and early afterdepolarization-mediated cardiac arrhythmias. *Heart Rhythm* 2012 January;9(1):115-22.

(15) Zeng J, Rudy Y. Early afterdepolarizations in cardiac myocytes: mechanism and rate dependence. *Biophys J* 1995 March;68(3):949-64.

(16) Dorval AD, Christini DJ, White JA. Real-Time linux dynamic clamp: a fast and flexible way to construct virtual ion channels in living cells. *Ann Biomed Eng* 2001 October;29(10):897-907.

(17) Madhvani RV, Xie Y, Pantazis A, Garfinkel A, Qu Z, Weiss JN, Olcese R. Shaping a new Ca(2) conductance to suppress early afterdepolarizations in cardiac myocytes. *J Physiol* 2011 December 15;589(Pt 24):6081-92.

(18) Chen PS, Wu TJ, Ting CT, Karagueuzian HS, Garfinkel A, Lin SF, Weiss JN. A tale of two fibrillations. *Circulation* 2003 November 11;108(19):2298-303.

(19) Mahajan A, Shiferaw Y, Sato D, Baher A, Olcese R, Xie LH, Yang MJ, Chen PS, Restrepo JG, Karma A, Garfinkel A, Qu Z, Weiss JN. A rabbit ventricular action potential model replicating cardiac dynamics at rapid heart rates. *Biophys J* 2008 January 15;94(2):392-410.

(20) Lin RJ, Bettencourt J, Wha IJ, Christini DJ, Butera RJ. Real-time experiment interface for biological control applications. *Conf Proc IEEE Eng Med Biol Soc* 2010;2010:4160-3.

(21) Dong M, Sun X, Prinz AA, Wang HS. Effect of simulated I(to) on guinea pig and canine ventricular action potential morphology. *Am J Physiol Heart Circ Physiol* 2006 August;291(2):H631-H637.

(22) Zhao Z, Xie Y, Wen H, Xiao D, Allen C, Fefelova N, Dun W, Boyden PA, Qu Z, Xie LH. Role of the transient outward potassium current in the genesis of early afterdepolarizations in cardiac cells. *Cardiovasc Res* 2012 August 1;95(3):308-16.

(23) Bassani RA, Altamirano J, Puglisi JL, Bers DM. Action potential duration determines sarcoplasmic reticulum Ca2+ reloading in mammalian ventricular myocytes. *J Physiol* 2004 September 1;559(Pt 2):593-609.

(24) Song YH, Cho H, Ryu SY, Yoon JY, Park SH, Noh CI, Lee SH, Ho WK. L-type Ca(2+) channel facilitation mediated by H(2)O(2)-induced activation of CaMKII in rat ventricular myocytes. *J Mol Cell Cardiol* 2010 April;48(4):773-80.

(25) Xie LH, Chen F, Karagueuzian HS, Weiss JN. Oxidative-stress-induced afterdepolarizations and calmodulin kinase II signaling. *Circ Res* 2009 January 2;104(1):79-86.

(26) Fedida D, Giles WR. Regional variations in action potentials and transient outward current in myocytes isolated from rabbit left ventricle. *J Physiol* 1991 October;442:191-209.

(27) Idriss SF, Wolf PD. Transmural action potential repolarization heterogeneity develops postnatally in the rabbit. *J Cardiovasc Electrophysiol* 2004 July;15(7):795-801.

(28) Tran DX, Sato D, Yochelis A, Weiss JN, Garfinkel A, Qu Z. Bifurcation and chaos in a model of cardiac early afterdepolarizations. *Phys Rev Lett* 2009 June 26;102(25):258103.

(29) Weiss JN, Garfinkel A, Karagueuzian HS, Chen PS, Qu Z. Early afterdepolarizations and cardiac arrhythmias. *Heart Rhythm* 2010 December;7(12):1891-9.

(30) Catterall WA. Structure and regulation of voltage-gated Ca2+ channels. *Annu Rev Cell Dev Biol* 2000;16:521-55.

(31) Rose WC, Balke CW, Wier WG, Marban E. Macroscopic and unitary properties of physiological ion flux through L-type Ca2+ channels in guinea-pig heart cells. *J Physiol* 1992 October;456:267-84.

(32) Qu Z, Chung D. Mechanisms and determinants of ultralong action potential duration and slow rate-dependence in cardiac myocytes. *PLoS One* 2012;7(8):e43587.

(33) January CT, Riddle JM. Early afterdepolarizations: mechanism of induction and block. A role for L-type Ca2+ current. *Circ Res* 1989 May;64(5):977-90.

(34) Song Y, Shryock JC, Wagner S, Maier LS, Belardinelli L. Blocking late sodium current reduces hydrogen peroxide-induced arrhythmogenic activity and contractile dysfunction. *J Pharmacol Exp Ther* 2006 July;318(1):214-22.

(35) Karwatowska-Prokopczuk E, Wang W, Cheng ML, Zeng D, Schwartz PJ, Belardinelli L. The risk of sudden cardiac death in patients with non-ST elevation acute coronary syndrome and prolonged QTc interval: effect of ranolazine. *Europace* 2013 March;15(3):429-36.

(36) Yang T, Atack TC, Stroud DM, Zhang W, Hall L, Roden DM. Blocking Scn10a channels in heart reduces late sodium current and is antiarrhythmic. *Circ Res* 2012 July 20;111(3):322-32.

(37) Xie LH, Chen F, Karagueuzian HS, Weiss JN. Oxidative-stress-induced afterdepolarizations and calmodulin kinase II signaling. *Circ Res* 2009 January 2;104(1):79-86.

(38) Hondeghem LM, Carlsson L, Duker G. Instability and triangulation of the action potential predict serious proarrhythmia, but action potential duration prolongation is antiarrhythmic. *Circulation* 2001 April 17;103(15):2004-13.

(39) Grandi E, Pasqualini FS, Bers DM. A novel computational model of the human ventricular action potential and Ca transient. *J Mol Cell Cardiol* 2010 January;48(1):112-21.

(40) Verkerk AO, Baartscheer A, de G, Jr., Wilders R, Coronel R. Etiology-dependency of ionic remodeling in cardiomyopathic rabbits. *Int J Cardiol* 2011 April 14;148(2):154-60.

(41) Alseikhan BA, DeMaria CD, Colecraft HM, Yue DT. Engineered calmodulins reveal the unexpected eminence of Ca2+ channel inactivation in controlling heart excitation. *Proc Natl Acad Sci U S A* 2002 December 24;99(26):17185-90.

(42) Corrias A, Giles W, Rodriguez B. Ionic mechanisms of electrophysiological properties and repolarization abnormalities in rabbit Purkinje fibers. *Am J Physiol Heart Circ Physiol* 2011 May;300(5):H1806-H1813.

Chapter 4:
Modification of L-type Ca^{2+} Channel Subunit Composition as an Approach to Control EAD-mediated Arrhythmias

4.1 ABSTRACT

Early afterdepolarizations (EADs) are transient reversals of the membrane voltage during phase 2 or phase 3 of a cardiac action potential (AP), that can trigger an extra beat and cause arrhythmias in heart tissue. Based on previous dynamic clamp results, we investigated whether L-type Ca^{2+} channels (LTCCs) and their biophysical properties, specifically the L-type Ca^{2+} window current, can be favorably modified to suppress EADs in cardiac myocytes by targeting the modulatory auxiliary subunits. To identify subunit compositions that favorably alter steady-state properties of the L-type Ca^{2+} current ($I_{Ca,L}$), we heterologously expressed LTCCs (α_{1C}) with different β subunit subtypes. Co-expression of three Ca^{2+} channel β subunits (β_{2a}, β_{2b}, and β_3) elicited a robust $I_{Ca,L}$ in *Xenopus* oocytes, in the virtual absence of any significant contaminant endogenous Ca^{2+} current, allowing us to accurately estimate both steady-state and kinetic effects resulting from the expression of different subunit compositions. Furthermore, we tested whether overexpression of β_{2a} vs. β_3, which each alter the $I_{Ca,L}$ window current in opposite directions, can be an effective anti-EAD strategy in cardiac myocytes using an adenoviral gene delivery method. Our results show that β_3 not only produced a more complete inactivation at the end of 300 ms depolarizing pulses when compared to β_{2a}, but voltage clamp protocols demonstrate that it also produces less reactivation following a variety of repolarization rates simulated by ramp protocol. Recordings of action potentials also confirmed that, despite an increase in overall current density, cardiac myocytes expressing β_3 displayed fewer EADs than those expressing β_{2a}. These findings demonstrate that manipulation of the subunit composition can be an effective strategy for modifying the steady-state properties of $I_{Ca,L}$. Moreover, a "narrower" $I_{Ca,L}$ window current could diminish the probability of EAD formation by preventing channel reopening. Thus, our results highlight the use of genetic engineering as a therapeutic avenue for the treatment of EAD-related cardiac arrhythmias.

4.2 INTRODUCTION

Cardiac L-type Ca^{2+} channels (LTCCs) are multimeric complexes found at invaginations of the sarcolemma of cardiomyocytes called T-tubules. They are made up of a pore-forming α_1 subunit (encoded by the $Ca_V1.2$ gene) that co-assembles with modulatory subunits such as β and $\alpha_2\delta^1$ (Figure 4.1). The α_1 subunit encodes all the structural elements required for a functional voltage-gated Ca^{2+} channel including voltage dependence of activation and inactivation, Ca^{2+} permeability and selectivity, Ca^{2+}-dependent inactivation, and the major pharmacological properties such as sensitivity to dihydropyridines and BayK8644[2]. These voltage-gated channels are critical players in the excitation-contraction response in cardiac tissue (among others), in that they activate at depolarized membrane potentials to conduct an inward flow of Ca^{2+} ions, which in turn induce the release of Ca^{2+} from intracellular stores and hence initiate a cascade of cellular events leading to cell contraction[3]. The primary role of $Ca_V1.2$ in heart function is demonstrated by the targeted disruption of the channel which is lethal during embryonic development[4].

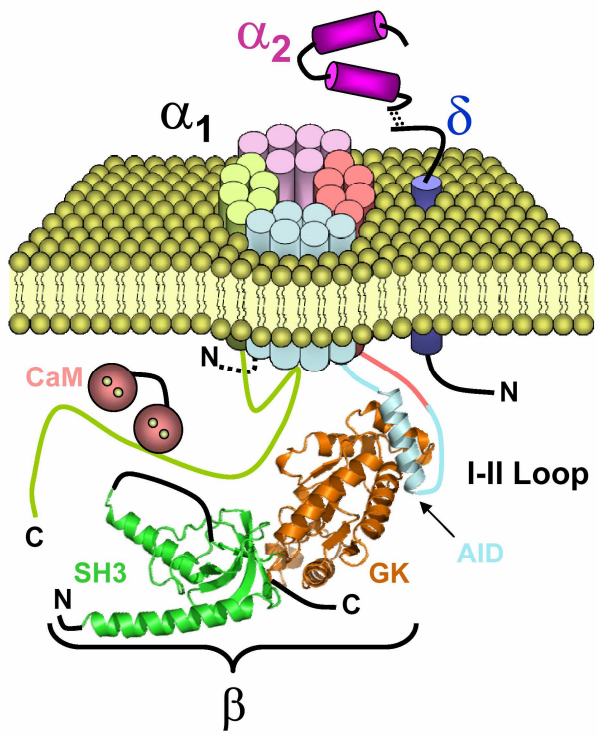

Figure 4.1 Ca^{2+} Channel β Subunits Modulate Biophysical Properties of $I_{Ca,L}$ (A) The L-type Ca^{2+} channel consists of a pore-forming and voltage sensing α subunit, one modulatory β subunit that binds intracellularly and a third subunit, $\alpha_2\delta$, is a single gene product cleaved post-translationally into a_2 and δ peptides, which remain coupled by disulfide bonds. Calmodulin (CaM), constitutively bound to the C- terminus of the a_1 subunit, mediates the Ca-dependent inactivation process.

While functional LTCCs can be obtained by expressing the α_1 subunit

alone in heterologous systems[5], co-expression with the other regulatory subunits (β and $\alpha_2\delta$) profoundly modifies its biophysical properties, increasing surface membrane expression, open probability, and modulating voltage dependence and kinetics[6]. Four LTCC β subunit isoforms have been identified, each encoded by a single gene. Each isoform, β_1-β_4, has a large diversity of splice variants, which alter surface membrane expression levels as well as the voltage dependence and kinetic properties of the channel[6].

In the heart, the L-type Ca^{2+} current ($I_{Ca,L}$) is one of the major conductances responsible for maintaining the cardiac action potential (AP) plateau, which depends upon a delicate balance of inward and outward currents[7]. Therefore, modest deviations in the open probability of LTCCs during steady-state conditions can create a substantial change in AP morphology. Aberrations of the cardiac AP that are well-established cellular triggers for cardiac arrhythmias such as ventricular fibrillation (VF) are transient depolarizations during the AP plateau, called early afterdepolarizations (EADs)[7]. Many groups have characterized the cellular mechanisms which give rise to EADs, leading to a debate within the field whether Na^+ channels[8, 9] , the Na/Ca^{2+} exchanger [10, 11] or LTCCs[12-14] are the primary conductances that contribute to the EAD upstroke under pathophysiological conditions.

We have recently probed the sensitivity of oxidative stress-induced EADs to changes in the biophysical properties of LTCCs using a hybrid computational-electrophysiological system called the Dynamic Patch clamp to determine whether we could suppress EADs by selectively targeting the $I_{Ca,L}$ "window current"[15]. Our findings, that small changes in key LTCC steady-state parameters which reduce the $I_{Ca,L}$ "window current" (the half-activation and half-inactivation potentials ($V_{1/2}$s), and the non-inactivating pedestal component) can potently suppress EADs, highlights LTCC biophysical properties as ideal therapeutic targets for controlling arrhythmogenic triggers such as EADs. Our work, as well as that of others, has shown the

importance of the steady-state and kinetic properties of LTCCs and their subunits in cardiac wave stability, which is highly relevant for the initiation and maintenance of VF[16]. Notably, Koval *et al*, have shown that the pro-EAD effects mediated by the β_{2a} subunit are due to phosphorylation of two different residues by CaMKII[17].

Here, we are testing the hypothesis that manipulating the β subunit composition of LTCCs is a tractable means to fine-tune the $I_{Ca,L}$ "window current" in both, heterologous expression systems as well as in cardiomyocytes, and can serve as an effective approach to control the occurrence of EADs. We have used a heterologous *Xenopus* oocyte expression system to determine how changes in the β subunit composition impact the $I_{Ca,L}$ window current in the absence of other contaminating conductances during a time frame that is relevant for the cardiac action potential. Based on findings from this read-out system, we selected two different β subunits, β_{2a} and β_3, which alter the window current in opposite ways, and overexpressed them in dissociated rabbit ventricular myocytes in culture using an adenoviral expression system to assess the impact on AP morphology and EAD susceptibility. Our findings demonstrate a striking difference in EAD occurrence from these myocytes, with those overexpressing β_3 displaying a lower incidence of EADs, despite an increase in total $I_{Ca,L}$ current density. These results illustrate that EAD suppression in cardiomyocytes can be achieved by targeting the LTCC subunit composition in such a way that the $I_{Ca,L}$ window current is minimized.

4.3 METHODS

Ethical approval: All animal handling protocols were approved by the UCLA Institutional Animal Care and Use Committee and conformed to the Guide for the Care and Use of Laboratory Animals published by the US National Institutes of Health.

Adenovirus construction: We used a replication-deficient recombinant adenoviral construct which expresses either β_{2a} or β_3 tagged with yellow fluorescent protein (YFP) to monitor relative expression levels, via fluorescent intensity, and determine which cells have been successfully infected.

Myocyte Isolation & Cell Culture: Ventricular myocytes were dissociated from male New Zealand white rabbits using a retrograde Langendorff perfusion system as previously described [18], washed and bathed in Tyrode's solution containing (in mmol/L): 136 NaCl, 5.4 KCl, 1 $MgCl_2$, 0.33 NaH_2PO_4, 1.8 $CaCl_2$, 10 Glucose, and 10 HEPES adjusted to pH 7.4. For culture, cardiomyocytes were washed in 1X MEM + Earle's Salts (Invitrogen) with 1% Pen/Strep, 5% FBS, 10 mM BDM and plated on Geltrex (Invitrogen) coated glass coverslips and allowed to attach for 1 hour. Cells were then washed with 1X MEM with 1% Pen/Strep, 5% FBS, (10 mM BDM) and 1X ITS (BD) and infected with Adenovirus expressing either β_{2a}-YFP, β_3-YFP, or uninfected control. Cultured myocytes were mounted for electrophysiology ~36-48 hrs after infection.

Electrophysiology: Xenopus laevis oocytes (stage V-VI) were prepared and injected with 50 nl of cRNA containing concentrations of 0.1 to 1 mg/ml of each subunit in equal molarity. Injected oocytes were maintained at 18ºC in an amphibian saline solution supplemented with 50 mg/ml Gentamycin for 4-7 days before experiments. Immediately prior to experiments, each oocyte was injected with 100 nl of 50 mM BAPTA. Electrophysiological recordings were performed using the cut-open oocyte voltage clamp technique. The external solution contained the following in mM: 105 NaMES, 10 CaMES, 10 HEPES, and 0.1 Oubain (pH 7.0). The internal solution contained 110 mM K-Glutamate and 10 mM HEPES (pH 7.0). Data was acquired using GPatch and analyzed using a customized program developed in our Division. Currents were filtered at 2 and 10 kHz. Steady-state inactivation curves were fit with a Bolztmann distribution

given by the following equation: (Imax-Imin)/(1+e(z(Vm-V1/2)/(RT/f))) +Imin Steady state activation curves were fit to a Boltzmann given by the following: (Imax-Imin)/(1+e(z(Vm-V1/2)/(RT/f))) +Imin

For action potential recordings, cultured ventricular myocytes infected with adenovirus or control (uninfected) were washed with Tyrode's solution and mounted for whole-cell patch clamp recordings. The intracellular solution contained (in mmol/L): 110 K-Aspartate, 30 KCl, 5 NaCl, 10 HEPES, 0.1 EGTA, 5 MgATP, 5 Creatine phosphate, 0.05 cAMP adjusted to pH 7.2. All recordings were made using an Axopatch 200B amplifier (Axon Instruments). Recordings were performed in current clamp mode at ~36℃ with 1-2 MΩ pipettes. Data were acquired and analyzed using custom-made software (G-Patch, Analysis).

Real-Time PCR & Immunocytochemistry: RNA was isolated from freshly dissociated adult rabbit cardiomyocytes using TRI reagent (Sigma). The PCR product was monitored using SYBR green (BioRad) dye and a MyiQ single color Real-time PCR Detection system was used for temperature cycling (BioRad). Quantitative analysis of relative expression of β_{2a} and β_3 (n=2) calculated by taking the difference in cycle numbers at Fluorescence intensity=100, (x), and raising 2 by the difference in cycle numbers (2x). For immunocytochemistry, freshly isolated myocytes were fixed in cold acetone for 10 min at -20℃. Isolated cells were incubated with 10% normal goat serum and 0.1% Triton X-100 in PBS for 30 min at room temp. to block background. Cells were then incubated with appropriate primary antibodies, either mouse monoclonal for β_2 (Abcam) or rabbit polyclonal for β3 (Alomone) in 1% normal goat serum, 0.1% Triton X-100 in PBS at 4℃ overnight. Cells were th en incubated with Alexa 488 goat anti-rabbit or Alexa 568 goat anti-mouse secondary antibodies in 1% normal goat serum, 0.1% Triton X-100 for 1 hr at room temp. in the dark, and then mounted onto slides using Prolong Gold

antifade reagent. Images were acquired at 0.0575 mm per pixel with a confocal microscope (Olympus Fluoview).

4.4 RESULTS

$I_{Ca,L}$ Window Current with various LTCC β subunits.

To identify subunit compositions that alter steady-state biophysical properties of LTCCs, such as the $V_{1/2}$ of activation or inactivation or the non-inactivating pedestal current (all of which

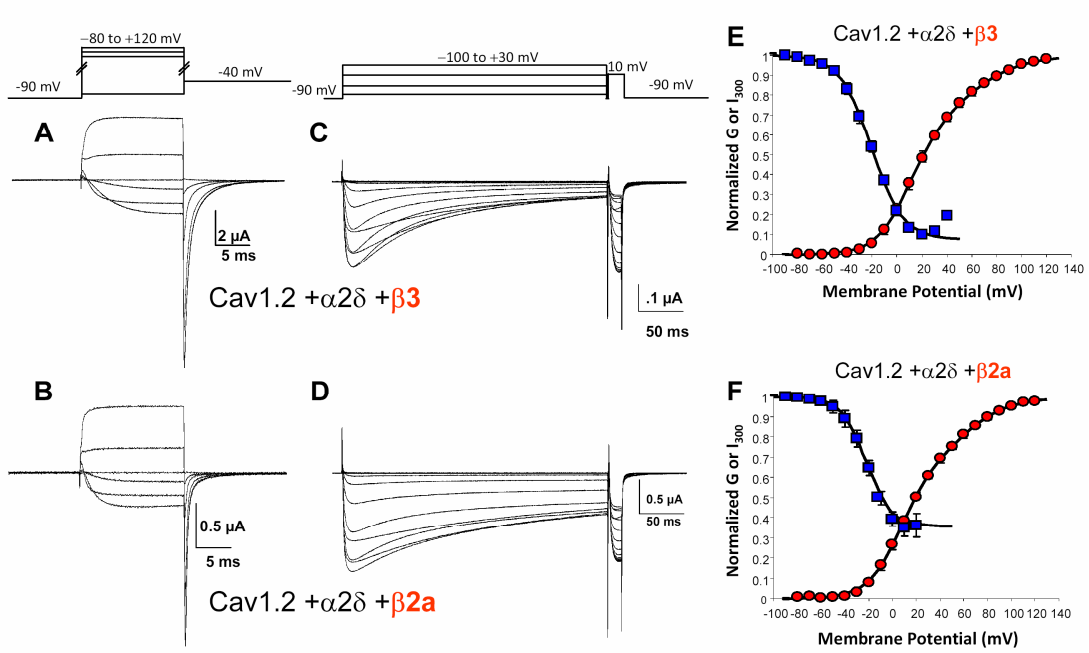

Figure 4.2. Cav β_3 And β_{2a} Subunits Have Profoundly Different Effects On The "Window" Current of L-type Ca^{2+} Channels. (A & B) Shows Ca^{2+} current recordings from human L-type Ca^{2+} channels composed of α_{1C} + $\alpha_2\delta$ in association with β_3 (A) or β_{2a} (B) expressed in *Xenopus* oocytes to dissect their modulatory differences. The activation curves were constructed by plotting the normalized peak tail current during the repolarization at -40mV(E and F, circles). (C and D) show typical $I_{Ca,L}$ recording elicited by a two-pulse protocol used to construct quasi-steady state inactivation curves shown in (E) and (F) (squares). Note the large effect on inactivation kinetics produced by the β_3 subunit (C) as compared to β_{2a} (D). The activation curves (red circles) for both subunits compositions are shown superimposed to their corresponding steady-state inactivation curves in (E) and (F). Besides accelerating the time course of inactivation, β_3 produced a more complete inactivation, as shown by its steady-state inactivation curve (E, squares) as compared to β_{2a} (F, squares). Note that the area subtended by the activation (red squares) and inactivation (blue circles) curves is greatly affected by the two different β subunits. Cut-open voltage clamp in 10 mM external Ca^{2+}.

dictate the $I_{Ca,L}$ window current, see Fig. 3.1), we heterologously expressed human L-type Ca^{2+} channels (α_{1C} or $Ca_V1.2$) with different β subunit subtypes in *Xenopus* oocytes and recording Ca^{2+} currents using the cut-open voltage clamp technique[19]. Co-expression of one of two Ca^{2+} channel subunits (β_{2a}, and β_3) elicited a robust $I_{Ca,L}$, in the virtual absence of any significant contaminant endogenous Ca^{2+} current (Fig. 4.2A-D), allowing us to accurately estimate both steady-state and kinetic effects resulting from the expression of different subunit compositions. Tail currents from 20 ms pulses (Fig. 4.2A,B) were used to construct steady-state activation curves (Fig. 4.2E,F). Furthermore, considering that the average duration of a human cardiac AP is approximately 300 ms, we assessed the availability of channels (the inactivation curves) at this time point using a two-pulse protocol (Fig. 4.2 C,D). The data shown in Fig. 4.2 demonstrates the modulatory effects of the two β subunits on the biophysical properties of $I_{Ca,L}$. For example, in addition to the evident change in the time course of inactivation, β_3 produced a more complete inactivation at the end of the 300 ms depolarizing pulses, as shown by the steady-state inactivation curve (Fig. 4.2E) when compared to β_{2a} (Fig. 4.2F), producing a lower $I_{Ca,L}$ pedestal current. Additionally, in the presence of β_3, the half-activation and half-inactivation potentials of $I_{Ca,L}$ are 10 and -20 mVs, respectively (Fig. 4.2E, n=14). In the presence of β_{2a}, in addition to the noticeable slowing of inactivation (Fig. 4.2D) the half-inactivation potential is shifted by ~ 5 mVs to the right (n=5), and the non-inactivating pedestal current is heightened to 36%, greatly enlarging the $I_{Ca,L}$ window current. Thus, the window area subtended by the activation and inactivation curves is greatly dependent on the isoform of β subunit co-expressed. Therefore, each subunit composition has its own “signature” in regard to the window $I_{Ca,L}$ region. This is evident in Fig. 4.3A, in which activation and inactivation curves for four different subunit compositions are plotted, including $\alpha_1+\alpha_2\delta$ alone (green circles, n=3) or $\alpha_1+\alpha_2\delta$ co-expressed with three different β subunits: β_{2a} (blue diamonds, n=5), β_{2b} (red squares, n=5), or β_3 (purple triangles, n=14). Each combination produced a unique window region due to small shifts in the half-activation or half-inactivation potentials and the pedestal component (Fig.

A

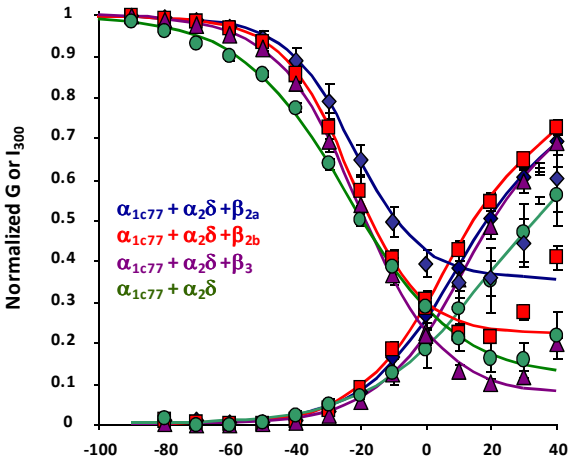

B

LTCC subunits	$V_{1/2}$ act (mV)	z act	$V_{1/2}$ inact (mV)	z inact	pedestal (%
$\alpha_{1c} + \alpha_2\delta + \beta_{2a}$	22.51	1.20	-22.09	2.42	36%
$\alpha_{1c} + \alpha_2\delta + \beta_{2b}$	17.99	1.26	-22.98	2.39	22%
$\alpha_{1c} + \alpha_2\delta + \beta_3$	24.71	1.23	-20.52	1.99	7%
$\alpha_{1c} + \alpha_2\delta$	34.64	1.03	-23.65	1.54	12%

Figure 4.3 Influence of Subunit Composition on the Biophysical Properties of LTCCs. (A) The experimental steady-state activation and quasi-steady-state inactivation curves from various L-type Ca^{2+} channels compositions. The pore forming α_{1C} subunit was expressed with the modulatory subunit $\alpha_2\delta$ (green circle). The addition of a β subunit (β_{2a}, β_{2b} and β_3) specifically altered activation and inactivation curves producing significant variation in the window current. (B) A table showing the mean half-activation ($V_{1/2}$ act) and half-inactivation ($V_{1/2}$ inact) potentials and z (slope) values for each subunit combination shown in (A).

4.3B). Note that the modulatory subunits were expressed in excess compared to the α_1, so that the differences observed are genuine and not due to different levels of expression. These findings demonstrate that manipulation of the subunit composition can be an effective strategy for modifying the steady-state properties of $I_{Ca,L}$, which we have previously shown to be an effective strategy to control EAD occurrence[15]. In other words, a "narrower" $I_{Ca,L}$ window current region obtained by altering the subunit composition of LTCCs may lower the probability of EAD formation by preventing channel reopening during the AP plateau.

$I_{Ca,L}$ Reactivation as a function of kinetic influences during the cardiac AP.

In the characterization of altered subunit compositions described above, we used standard square voltage clamp pulse protocols to analyze $I_{Ca,L}$ properties. However, $I_{Ca,L}$ reactivation is also very sensitive to kinetics parameters. For example, even if the steady state $I_{Ca,L}$ window region is very large, $I_{Ca,L}$ reactivation during AP repolarization will remain very small if the kinetics of recovery from inactivation are too slow[20]. Accordingly, we have designed voltage-

clamp protocols to study $I_{Ca,L}$ reactivation as a function of the AP repolarization rate, as illustrated in Fig. 4.4. In this protocol, successive depolarizations to +10 mV for 300 ms are followed by a series of repolarizing voltage ramps at variable rates from +10 to -30mV or +10 to -20 mV. Several gating processes, including activation, inactivation and reactivation, all take place simultaneously to determine the number of L-type Ca^{2+} channels available to reactivate at the end of the ramp. This makes it problematic to interpret the actual current during the ramp, in which the Ca^{2+} driving force is changing as well as $I_{Ca,L}$ gating properties. However, the number of L-type Ca^{2+} channels available to reactivate can be assessed by a brief, square "test" pulse to 10 mV following the ramp. As the 300ms depolarizing pulse and the test pulse are both to 10 mV, a direct comparison of the $I_{Ca,L}$ amplitude immediately before the ramp ("I1" in Fig 4.4 A & C) and during the test pulse ("I2") gives an accurate indication of the fraction of the channels that can be re-activated, as a function of the rate of repolarization during the ramp. Figure 4.4 shows the availability of $I_{Ca,L}$ following a ramp which ends at -30 mV (Fig. 4.4A) as well as a second protocol in which the ramp ends at -20 mV (Fig. 4.4C). Both of these potentials were chosen to assess the subunit-dependent $I_{Ca,L}$ recovery from inactivation at membrane potentials where EAD amplitudes are the largest. Furthermore, the rate at which the change in membrane potential occurred (dV/dt) was varied (Fig. 4.4B&D, inset). The analysis, shown in Fig. 4.4B & D, clearly demonstrates that subunit composition greatly affects the current that can be reactivated following the ramp. Of note, the β_{2a} subunit, which is upregulated during heart failure[21, 22], produces the most reactivation (n=4), especially at slow repolarization rates, which may be relevant to the increased predisposition of the failing heart to EADs. On the other hand, co-expression with β_{2b} or β_3 each produced less reactivation under the same conditions (Fig. 4.4D). Thus, collectively, our voltage clamp experiments consistently identify the β_3 subunit as the most effective at minimizing channel $I_{Ca,L}$ reactivation at all repolarization rates, and β_{2a} as highly effective at enhancing it.

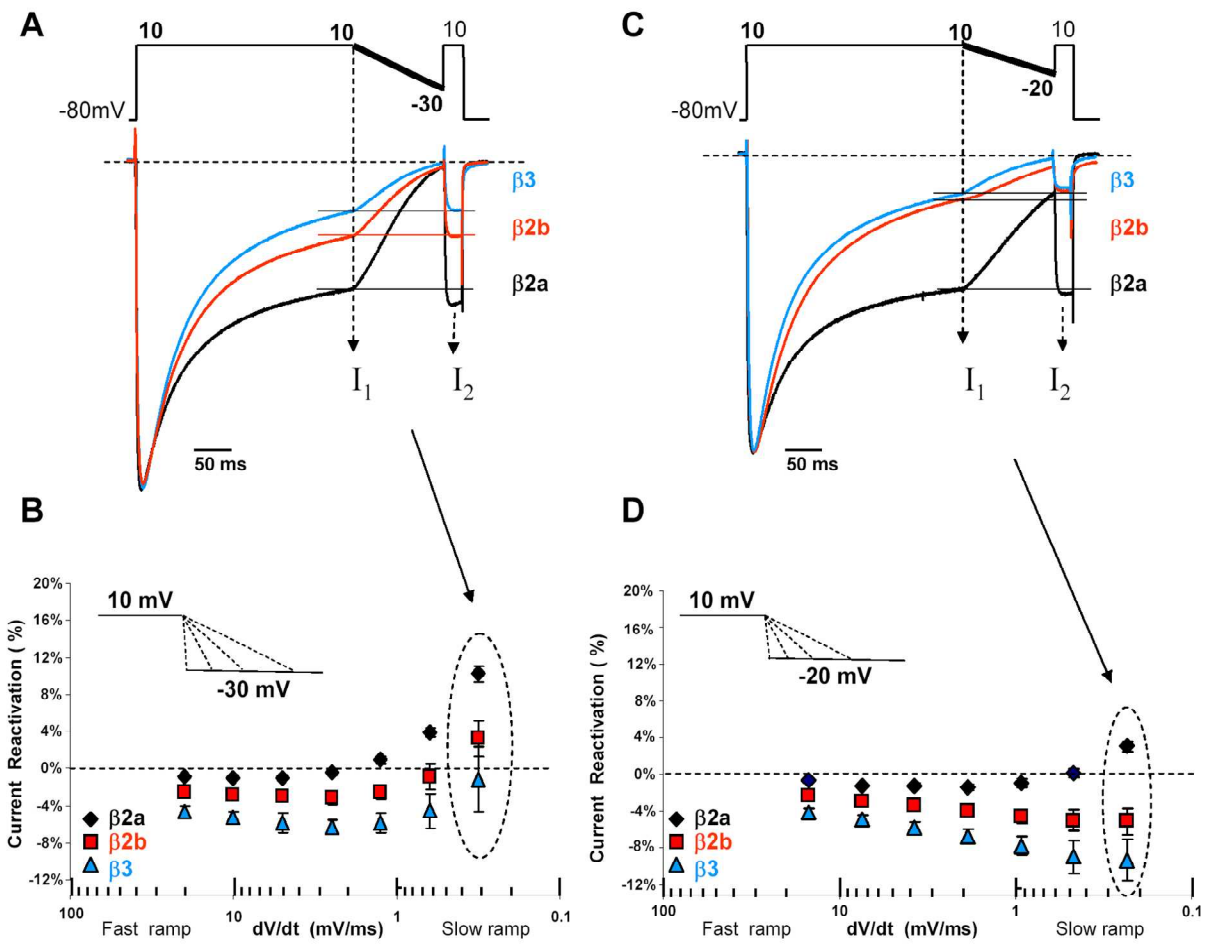

Figure 4.4 Reactivation of the $I_{Ca,L}$ Current Depends on the Subunit Composition. (A and C) Representative Ca^{2+} current traces for human cardiac $Ca_V1.2$ channels expressed with $\alpha_2\delta$ and different β subunits. The initial 300 ms depolarization to 10 mV inactivates the current. A ramp of variable duration from +10 to -30mV (A) or +10 to -20mV (B) is applied to partially repolarize the membrane and allow for closing/recovery of the channels, simulating different repolarization rate as in AP prolongation. A short test pulse (25 ms to 10 mV) follows the ramp to estimate the extent of channel reactivation. The traces in (A) and (B) show current recording using ramps of 128ms. The plots in (B) and (D) summarize the extent of current recovery as a function of the steepness of the ramp. Recovery was estimated as 1-(I2/I1) were I1 is the current at time 300 ms (just before the ramp) and I2 is the peak current during the test pulse. As shown, fast ramps (large dV/dT, left side of the plot) do not allow for channel reopening (% recovery <0) (B) and (D). Note that the extent of current inhibition is significantly dependent on the type of subunit. Slower ramps allowed significant recovery only with the β_{2a} subunit (% recovery >0).

Identification and subcellular localization of β_{2a} and β_3 in dissociated rabbit ventricular myocytes.

Based on our findings thus far, that heterogously expressed LTCCs associated with β_3 have a smaller steady-state window current (Figs. 4.2 & 4.3), and are less likely to reactivate following

a variety of repolarization rates (Fig. 4.4) compared to β_{2a}, we sought to determine *i)* whether both β_{2a} and β_3 are present in dissociated ventricular myocytes, *ii)* in what ratio, and *iii)* where they are localized. Several groups have demonstrated that the β_2 subunits are the most abundant in the heart[21, 23]. Most of these studies, however, have quantified mRNA or protein levels from whole tissue extracts, where smooth muscle cells (from vascularization in the heart), fibroblasts and other types of cells may also be present. Although it is well known that multiple β subunits are present in the heart[24, 25], we focused our attention on β_{2a} and β_3 due to our observation that they each endow LTCCs with a window current region which is highly divergent from each other, where channels associated with β_3 show a narrower window current (Figures 4.2 & 4.3). Using quantitative real-time PCR, we detected the presence of both β_{2a} and β_3 in dissociated rabbit ventricular myocytes (Fig. 4.5A). Our analyses revealed that β_{2a} transcripts are 20-fold more abundant compared to β_3 (Fig. 4.5B) (see methods). Furthermore, we carried out immunocytochemistry experiments using antibodies against each of these proteins to pinpoint the subcellular localization of each these

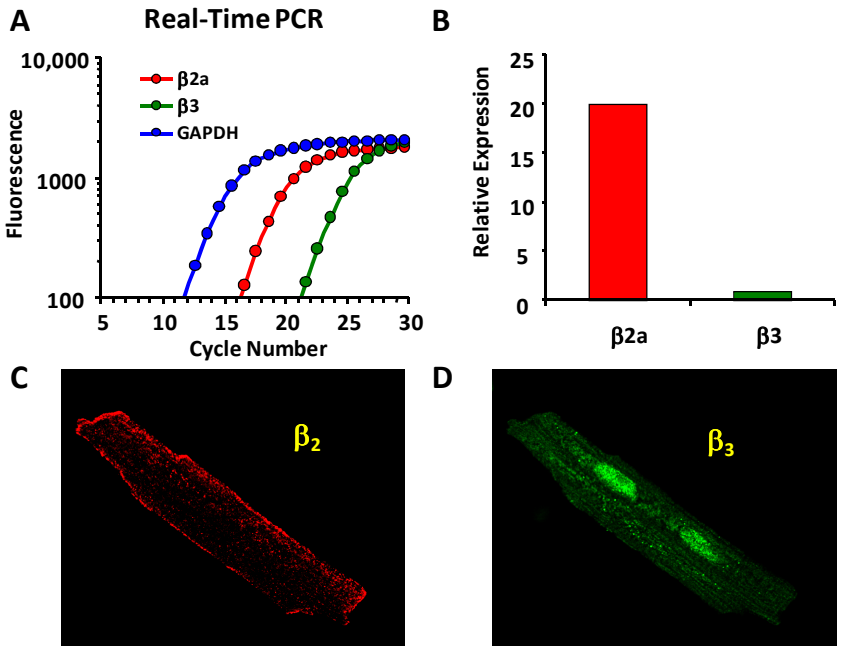

Figure 4.5 Quantitative Real-Time RT-PCR Detects Higher Levels of β_{2a} Transcripts Compared To β_3, in Dissociated Rabbit Ventricular Myocytes. (A) Fluorescence intensity versus cycle number for β_{2a}, β_3 and GAPDH. (B). Quantitative analysis of relative expression of β_{2a} and β_3 (n=2) calculated from (A) by taking the difference in cycle numbers at Fluorescence intensity=100, (x), and raising 2 by the difference in cycle numbers (2x). (C & D) Confocal images of a rabbit ventricular myocyte incubated with β_2 (Abcam) & β_3 (Alomone) primary antibodies. Secondary antibodies are Alexa 488 and 568 respectively.

β subunits. Our results demonstrate the difference in localization of the two βs: while β_3 was mainly intracellular and concentrated in the nuclei, consistent with reports that it can act as a transcription factor [26], β_{2a} was found predominantly at the surface membrane, likely due to its propensity to be palmitoylated[27, 28]. Thus, both expression levels and localization of these two β subunits are very different and therefore may explain their functional differences in shaping the $I_{Ca,L}$ window current.

EAD incidence can be controlled by manipulating LTCC β subunit expression in cardiomyocytes.

Previous work from our laboratory has demonstrated that a smaller $I_{Ca,L}$ window current due to shifts in the steady-state activation and inactivation curves or lowering the non-inactivating pedestal current results in a significantly lower propensity for EAD occurrence[15]. This, combined with our findings that β_3 produces a more favorable $I_{Ca,L}$ window current (Fig. 4.2 & 4.3), renders LTCCs less prone to reactivation (Fig. 4.4) and is expressed relatively weakly in ventricular cells compared to β_{2a} (Fig. 4.5), we tested the hypothesis that overexpressing β_3 may suppress the incidence of EADs in ventricular myocytes. We have used an adenoviral expression system to over-express either β_3 or β_{2a} subunits tagged with YFP in rabbit cardiomyocytes (Fig. 4.6A). We found that overexpression of either subunit resulted in an increase in overall current density from 14.2±1.7 (n=6) in uninfected cells to 35.2±2.1 pA/pF (n=6) or 21.2±2.2 pA/pF (n=15) for cells expressing β_3 or β_{2a}, respectively (Fig. 4.6B). However, when cells with similar levels of current density were compared, there was a clear difference in AP morphology (Fig. 4.6C) as well as an overall decrease in EAD occurrence under baseline conditions such that 26.3% of APs had EADs in cells overexpressing β_3, compared to 56.6% of APs in cells overexpressing β_{2a} (Fig. 4.6D). Therefore, consistent with our hypothesis, over-expression of β_3 appears to reduce the occurrence of EADs regardless of the increase in current density. On the other hand,

over-expression of β_{2a} increases the occurrence of EADs, even in the absence of H_2O_2 or hypokalemia.

4.5 DISCUSSION

Despite decades of intense investigation of the molecular and cellular mechanisms of cardiac arrhythmias, no biological therapy has yet emerged with comparable efficacy to the implantable cardioverter-defibrillator (ICD). Sudden cardiac death (SCD) due to VF is a world-wide public health issue, and current forms of therapy, such as ICD implantation, are costly, not indicated in a majority of patients who succumb to SCD annually. Furthermore, even in the high risk patient population, only 28% of implanted ICDs deliver life-saving shocks, prolonging life by approximately 4.4 months, on average[29]. Therefore, there is an unmet need for therapeutic agents or interventions which can effectively suppress or prevent cardiac arrhythmias such as VF while maintaining normal cardiac function.

Previous work from our laboratory has identified three main steady-state properties that can be tuned to reduce the $I_{Ca,L}$ "window current" to suppress EADs while maintaining normal excitation-contraction coupling [15]. In the present study we have demonstrated that β subunits are strong modulators of the $I_{Ca,L}$ window current and therefore overexpressing them in myocytes produces varying degrees of susceptibility to EADs, depending on the β subunit expressed. Our findings are consistent with previous reports demonstrating the pro-EAD effects of the β_{2a} subunits, particularly due to phosphorylation by CaMKII[17]. CaMKII phosphorylation of amino acid residues within β_{2a} push the channel into mode 2 gating and facilitation[30], all of which are thought to promote the occurrence of EADs and cardiac arrhythmias[31-33]. A novel finding in this study was that expressing β_3 in cardiomyocytes protects against EAD occurrence despite an increase in total $I_{Ca,L}$ current. Furthermore, the results indicate that given the heterogeneity and modularity of L-type Ca^{2+} channel auxiliary subunits and their diverse effects

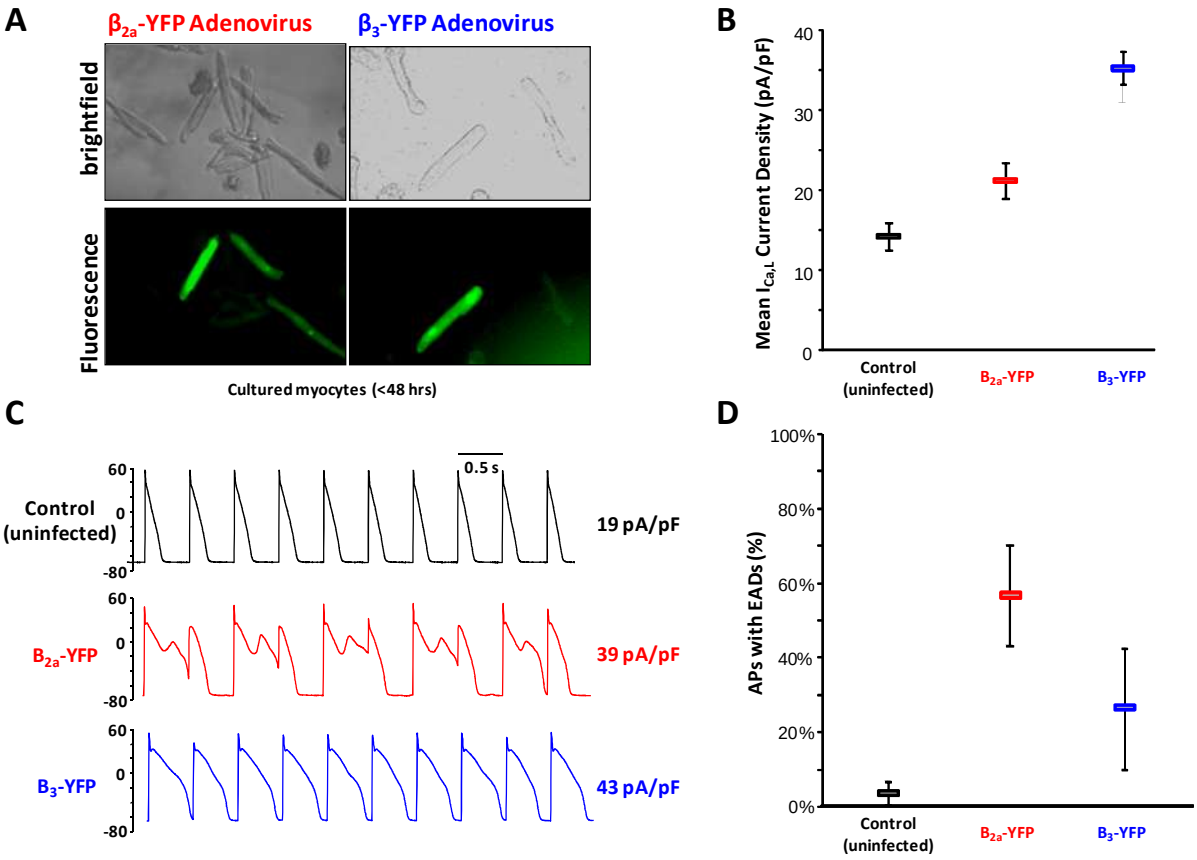

Figure 4.6 EADs Occur More Frequently in Myocytes Overexpressing β_{2a} vs. β_3. (A) show bright field and fluorescence images of ventricular myocytes ~48 hrs after adenoviral infection with β_{2a}-YFP and β_3-YFP, respectively. (B) Average current density of $I_{Ca,L}$ in rabbit ventricular myocytes following <48 hrs in culture under control conditions (black), expressing β_3 (blue), or expressing β_{2a} (red). (C) Representative AP recordings from cultured (<48hrs) ventricular myocytes. Note that although over-expression of any β subunit increases $I_{Ca,L}$ current density, β_{2a} over-expression greatly increased EAD occurrence compared to over-expression of β_3. PCL=0.5s (D) Percent of APs in each condition that displayed EADs.

on channel gating, it seems plausible that a multi-protein complex which has a diminished $I_{Ca,L}$ window current can be assembled *in vivo* to prevent arrhythmogenic outcomes. A major potential advantage of using β subunits to alter the biophysical properties of LTCCs is their high selectivity for the pore-forming α_1 subunit, minimizing off-target effects common to standard drug therapy.

Several studies have characterized the β subunits isoforms expressed in mammalian and human heart. Foell and collaborators have identified 18 splice variants of β subunits that are expressed in the canine and human heart and suggested that β_{1b}, β_2 and β_3 seem predominant in T tubules of ventricular myocytes[24]. Other quantitative studies have suggested that in heart β_{2b} expression is higher than β_3 and β_{2a}[21]. These observations are in general agreement with evidence from over-expression studies of different β subunits in rat myocytes, which concluded that β_{2b} subunits reconstitute the kinetic properties of native $I_{Ca,L}$[23]. Interestingly, upregulation of β_{2a}, which is also a target for PKA phosphorylation[34], has been reported in failing human cardiomyocytes[21, 22]. The relevance of the β_2 gene for cardiac function is also emphasized by knockout studies showing that, cardiac specific destruction of the β_2 gene is lethal during embryonic development[35], while deletion of β_1, β_3 and β_4 do not induce a significant cardiac phenotype[35-37].

The modulatory effects produced by β subunits primarily take place through interaction with the AID domain on the α_1 subunit, located in the loop connecting repeats I and II[38]. Along the same line, decoy β subunits, which retain the β interaction domain (BID) but lack functional domains, have been successfully constructed and utilized to modulate contractile function in myocytes by displacing the full length, native β subunits[39, 40]. In addition, global β antisense oligonucleotides have been successfully used to inhibit β expression, causing a positive shift in voltage dependence of $I_{Ca,L}$, activation. Our results, showing the substantial narrowing of the window current due to shifts in the steady-state activation and inactivation curves and a lower non-inactivating pedestal upon expression of the channel without any β subunits (Fig. 4.3), are consistent with these findings. Furthermore, if the decoy β subunits can maintain channel trafficking without the β-dependent changes in channel gating, such a strategy may characterize an ideal way to achieve a therapeutic window current while maintaining total current density.

The importance of β subunit expression for cardiac function has been highlighted by a number of studies showing that the properties of the native $I_{Ca,L}$ can be controlled by manipulating the expression of the β subunits. For example, the Marbán group at John Hopkins has used shRNA in a lentiviral vector to knockdown the expression of β_2, resulting in inhibition of $I_{Ca,L}$, and attenuation of the hypertrophic response in an aortic-banded rat model of hypertrophy, without compromising systolic performance[41]. On the other hand, Meissner *et. al.* demonstrated that a conditional heart-specific β_2 knockout mouse did not considerably impair LTCC function in adult myocytes and is physiologically well tolerated[42].

Limitations and Implications

Our finding that cells overexpressing β_3 are less prone to EADs despite an increase in $I_{Ca,L}$ current density compared to cells overexpressing β_{2a}, is promising as a therapeutic strategy to control EAD-related arrhythmias in cardiac tissue. However, the increase in trafficking of the channel, which causes the increase in current density, can be highly arrhythmogenic by itself. An alternative strategy may be to reduce the expression of native β_{2a} subunits using a knock-down approach, which, according to our results, produces a larger $I_{Ca,L}$ window current and greater likelihood of $I_{Ca,L}$ reactivation during the action potential. Conversely, this can lead to a reduced $I_{Ca,L}$ current density, which may impair excitation-contraction coupling and cell contractility, especially considering that quantitative real-time PCR results demonstrate that β_{2a} is more abundant than β_3 in cardiac myocytes. Due to this possibility, it will be important to measure the Ca_i transient in all cells to ensure that contractility is not compromised.

Another important consideration in our experimental design is the use of adenovirus, which can be highly toxic to cells and thus may produce artifacts. For our control conditions, we have used cells that were not subjected to these toxic conditions and therefore are not entirely suitable for comparison with cells that have been infected with adenovirus which takes over the transcription

and translation machinery of the cell to overexpress the given protein. A more appropriate control would be to use an adenovirus which delivers only YFP.

Finally, since our experiments were conducted in dissociated myocytes, it is possible that our findings may not directly apply to whole heart preparations or in animal models. Systemic influences such as β-adrenergic stimulation by the nervous system or hormonal regulation mechanisms may alter the outcome of gene therapy. Further investigation using animal models is critical to assess the anti-arrhythmic potential of altering LTCC function using auxiliary subunit manipulation in the heart.

4.6 Bibliography

(1) Shaw RM, Colecraft HM. L-type calcium channel targeting and local signalling in cardiac myocytes. *Cardiovasc Res* 2013 May 1;98(2):177-86.

(2) Catterall WA. Structure and regulation of voltage-gated Ca2+ channels. *Annu Rev Cell Dev Biol* 2000;16:521-55.

(3) Bers DM. Cardiac excitation-contraction coupling. *Nature* 2002 January 10;415(6868):198-205.

(4) Seisenberger C, Specht V, Welling A, Platzer J, Pfeifer A, Kuhbandner S, Striessnig J, Klugbauer N, Feil R, Hofmann F. Functional embryonic cardiomyocytes after disruption of the L-type alpha1C (Cav1.2) calcium channel gene in the mouse. *J Biol Chem* 2000 December 15;275(50):39193-9.

(5) Neely A, Wei X, Olcese R, Birnbaumer L, Stefani E. Potentiation by the beta subunit of the ratio of the ionic current to the charge movement in the cardiac calcium channel. *Science* 1993 October 22;262(5133):575-8.

(6) Birnbaumer L, Qin N, Olcese R, Tareilus E, Platano D, Costantin J, Stefani E. Structures and functions of calcium channel beta subunits. *J Bioenerg Biomembr* 1998 August;30(4):357-75.

(7) Weiss JN, Garfinkel A, Karagueuzian HS, Chen PS, Qu Z. Early afterdepolarizations and cardiac arrhythmias. *Heart Rhythm* 2010 December;7(12):1891-9.

(8) Song Y, Shryock JC, Belardinelli L. An increase of late sodium current induces delayed afterdepolarizations and sustained triggered activity in atrial myocytes. *Am J Physiol Heart Circ Physiol* 2008 May;294(5):H2031-H2039.

(9) Boutjdir M, el-Sherif N. Pharmacological evaluation of early afterdepolarisations induced by sea anemone toxin (ATXII) in dog heart. *Cardiovasc Res* 1991 October;25(10):815-9.

(10) Szabo B, Sweidan R, Rajagopalan CV, Lazzara R. Role of Na+:Ca2+ exchange current in Cs(+)-induced early afterdepolarizations in Purkinje fibers. *J Cardiovasc Electrophysiol* 1994 November;5(11):933-44.

(11) Sipido KR, Bito V, Antoons G, Volders PG, Vos MA. Na/Ca exchange and cardiac ventricular arrhythmias. *Ann N Y Acad Sci* 2007 March;1099:339-48.

(12) January CT, Riddle JM, Salata JJ. A model for early afterdepolarizations: induction with the Ca2+ channel agonist Bay K 8644. *Circ Res* 1988 March;62(3):563-71.

(13) January CT, Riddle JM. Early afterdepolarizations: mechanism of induction and block. A role for L-type Ca2+ current. *Circ Res* 1989 May;64(5):977-90.

(14) Hirano Y, Moscucci A, January CT. Direct measurement of L-type Ca2+ window current in heart cells. *Circ Res* 1992 March;70(3):445-55.

(15) Madhvani RV, Xie Y, Pantazis A, Garfinkel A, Qu Z, Weiss JN, Olcese R. Shaping a new Ca(2) conductance to suppress early afterdepolarizations in cardiac myocytes. *J Physiol* 2011 December 15;589(Pt 24):6081-92.

(16) Gudzenko V, Shiferaw Y, Savalli N, Vyas R, Weiss JN, Olcese R. Influence of channel subunit composition on L-type Ca2+ current kinetics and cardiac wave stability. *Am J Physiol Heart Circ Physiol* 2007 September;293(3):H1805-H1815.

(17) Koval OM, Guan X, Wu Y, Joiner ML, Gao Z, Chen B, Grumbach IM, Luczak ED, Colbran RJ, Song LS, Hund TJ, Mohler PJ, Anderson ME. CaV1.2 beta-subunit coordinates CaMKII-triggered cardiomyocyte death and afterdepolarizations. *Proc Natl Acad Sci U S A* 2010 March 16;107(11):4996-5000.

(18) Chen PS, Wu TJ, Ting CT, Karagueuzian HS, Garfinkel A, Lin SF, Weiss JN. A tale of two fibrillations. *Circulation* 2003 November 11;108(19):2298-303.

(19) Stefani E, Bezanilla F. Cut-open oocyte voltage-clamp technique. *Methods Enzymol* 1998;293:300-18.

(20) Altamirano J, Bers DM. Effect of intracellular Ca2+ and action potential duration on L-type Ca2+ channel inactivation and recovery from inactivation in rabbit cardiac myocytes. *Am J Physiol Heart Circ Physiol* 2007 July;293(1):H563-H573.

(21) Hullin R, Khan IF, Wirtz S, Mohacsi P, Varadi G, Schwartz A, Herzig S. Cardiac L-type calcium channel beta-subunits expressed in human heart have differential effects on single channel characteristics. *J Biol Chem* 2003 June 13;278(24):21623-30.

(22) Hullin R, Matthes J, von VS, Bodi I, Rubio M, D'Souza K, Friedrich K, I, Rottlander D, Hoppe UC, Mohacsi P, Schmitteckert E, Gilsbach R, Bunemann M, Hein L, Schwartz A, Herzig S. Increased expression of the auxiliary beta(2)-subunit of ventricular L-type Ca(2)+ channels leads to single-channel activity characteristic of heart failure. *PLoS One* 2007;2(3):e292.

(23) Colecraft HM, Alseikhan B, Takahashi SX, Chaudhuri D, Mittman S, Yegnasubramanian V, Alvania RS, Johns DC, Marban E, Yue DT. Novel functional properties of Ca(2+) channel beta subunits revealed by their expression in adult rat heart cells. *J Physiol* 2002 June 1;541(Pt 2):435-52.

(24) Foell JD, Balijepalli RC, Delisle BP, Yunker AM, Robia SL, Walker JW, McEnery MW, January CT, Kamp TJ. Molecular heterogeneity of calcium channel beta-subunits in canine and human heart: evidence for differential subcellular localization. *Physiol Genomics* 2004 April 13;17(2):183-200.

(25) Hullin R, Singer-Lahat D, Freichel M, Biel M, Dascal N, Hofmann F, Flockerzi V. Calcium channel beta subunit heterogeneity: functional expression of cloned cDNA from heart, aorta and brain. *EMBO J* 1992 March;11(3):885-90.

(26) Zhang Y, Yamada Y, Fan M, Bangaru SD, Lin B, Yang J. The beta subunit of voltage-gated Ca2+ channels interacts with and regulates the activity of a novel isoform of Pax6. *J Biol Chem* 2010 January 22;285(4):2527-36.

(27) Chien AJ, Zhao X, Shirokov RE, Puri TS, Chang CF, Sun D, Rios E, Hosey MM. Roles of a membrane-localized beta subunit in the formation and targeting of

functional L-type Ca2+ channels. *J Biol Chem* 1995 December 15;270(50):30036-44.

(28) Chien AJ, Carr KM, Shirokov RE, Rios E, Hosey MM. Identification of palmitoylation sites within the L-type calcium channel beta2a subunit and effects on channel function. *J Biol Chem* 1996 October 25;271(43):26465-8.

(29) Connolly SJ, Hallstrom AP, Cappato R, Schron EB, Kuck KH, Zipes DP, Greene HL, Boczor S, Domanski M, Follmann D, Gent M, Roberts RS. Meta-analysis of the implantable cardioverter defibrillator secondary prevention trials. AVID, CASH and CIDS studies. Antiarrhythmics vs Implantable Defibrillator study. Cardiac Arrest Study Hamburg . Canadian Implantable Defibrillator Study. *Eur Heart J* 2000 December;21(24):2071-8.

(30) Dzhura I, Wu Y, Colbran RJ, Balser JR, Anderson ME. Calmodulin kinase determines calcium-dependent facilitation of L-type calcium channels. *Nat Cell Biol* 2000 March;2(3):173-7.

(31) Wu Y, MacMillan LB, McNeill RB, Colbran RJ, Anderson ME. CaM kinase augments cardiac L-type Ca2+ current: a cellular mechanism for long Q-T arrhythmias. *Am J Physiol* 1999 June;276(6 Pt 2):H2168-H2178.

(32) Brachmann J, Scherlag BJ, Rosenshtraukh LV, Lazzara R. Bradycardia-dependent triggered activity: relevance to drug-induced multiform ventricular tachycardia. *Circulation* 1983 October;68(4):846-56.

(33) Xie LH, Chen F, Karagueuzian HS, Weiss JN. Oxidative-stress-induced afterdepolarizations and calmodulin kinase II signaling. *Circ Res* 2009 January 2;104(1):79-86.

(34) Gerhardstein BL, Puri TS, Chien AJ, Hosey MM. Identification of the sites phosphorylated by cyclic AMP-dependent protein kinase on the beta 2 subunit of L-type voltage-dependent calcium channels. *Biochemistry* 1999 August 10;38(32):10361-70.

(35) Weissgerber P, Held B, Bloch W, Kaestner L, Chien KR, Fleischmann BK, Lipp P, Flockerzi V, Freichel M. Reduced cardiac L-type Ca2+ current in Ca(V)beta2-/- embryos impairs cardiac development and contraction with secondary defects in vascular maturation. *Circ Res* 2006 September 29;99(7):749-57.

(36) Gregg RG, Messing A, Strube C, Beurg M, Moss R, Behan M, Sukhareva M, Haynes S, Powell JA, Coronado R, Powers PA. Absence of the beta subunit (cchb1) of the skeletal muscle dihydropyridine receptor alters expression of the alpha 1 subunit and eliminates excitation-contraction coupling. *Proc Natl Acad Sci U S A* 1996 November 26;93(24):13961-6.

(37) Namkung Y, Smith SM, Lee SB, Skrypnyk NV, Kim HL, Chin H, Scheller RH, Tsien RW, Shin HS. Targeted disruption of the Ca2+ channel beta3 subunit reduces N- and L-type Ca2+ channel activity and alters the voltage-dependent activation of P/Q-type Ca2+ channels in neurons. *Proc Natl Acad Sci U S A* 1998 September 29;95(20):12010-5.

(38) Pragnell M, De WM, Mori Y, Tanabe T, Snutch TP, Campbell KP. Calcium channel beta-subunit binds to a conserved motif in the I-II cytoplasmic linker of the alpha 1-subunit. *Nature* 1994 March 3;368(6466):67-70.

(39) Fan QI, Vanderpool KM, O'Connor J, Marsh JD. Decoy calcium channel beta subunits modulate contractile function in myocytes. *Mol Cell Biochem* 2003 January;242(1-2):3-10.

(40) Telemaque S, Sonkusare S, Grain T, Rhee SW, Stimers JR, Rusch NJ, Marsh JD. Design of mutant beta2 subunits as decoy molecules to reduce the expression of functional Ca2+ channels in cardiac cells. *J Pharmacol Exp Ther* 2008 April;325(1):37-46.

(41) Cingolani E, Ramirez Correa GA, Kizana E, Murata M, Cho HC, Marban E. Gene therapy to inhibit the calcium channel beta subunit: physiological consequences and pathophysiological effects in models of cardiac hypertrophy. *Circ Res* 2007 July 20;101(2):166-75.

(42) Meissner M, Weissgerber P, Londono JE, Prenen J, Link S, Ruppenthal S, Molkentin JD, Lipp P, Nilius B, Freichel M, Flockerzi V. Moderate calcium channel dysfunction in adult mice with inducible cardiomyocyte-specific excision of the cacnb2 gene. *J Biol Chem* 2011 May 6;286(18):15875-82.

Chapter 5:
Conclusions & Future Directions

The goal of this dissertation project was two-fold: i) to understand the molecular and cellular mechanisms for cardiac arrhythmias and ii) to identify therapeutic strategies that can be anti-arrhythmic by targeting the biophysical properties of the L-type Ca^{2+} channel (LTCC). To accomplish these goals I combined cellular electrophysiology, computational modeling and genetic engineering to gain insight on how modifications to biophysical properties of LTCCs influences susceptibility to cellular triggers of cardiac arrhythmias in heart cells. These triggers, called early afterdepolarizations (EADs), have a broad relevance not only to congenital and drug-induced long QT syndromes, but also to heart failure as a consequence of electrical remodeling. I sought to investigate whether EADs and their arrhythmogenic consequences can be prevented by targeting $I_{Ca,L}$ to selectively modify its biophysical properties and consequently alter $I_{Ca,L}$ reactivation without adversely affecting excitation-contraction coupling (in order to maintain the contractile properties of the heart). I used the dynamic clamp technique, which allowed me to patch-clamp cardiomyocytes and record action potentials (APs) while replacing the native L-type Ca^{2+} current ($I_{Ca,L}$) with a virtual conductance where all the biophysical parameters were derived from fittings of experimental $I_{Ca,L}$ recordings in cardiac myocytes. The findings of this study have broad implications for the cellular basis of EAD-related cardiac arrhythmias and for the development of novel therapeutic approaches to treat patients with cardiac arrhythmias.

5.1 Predictive Power of the Dynamic Clamp

The dynamic clamp has proved to be an invaluable instrument for studying the electrical properties of excitable cells such as neurons and myocytes[1-3]. Whether one is interested in studying the effects of a single conductance on electrical impulses or more complex behavior such as synaptic transmission in neuronal networks, dynamic clamp can facilitate our understanding of the interplay between ionic currents and the voltage signals they generate in real-time and in living cells, rather than in computer simulations. Not only does this technique

allow us to manipulate the environment of the cell as we measure the real-time signals, but it also allows us to "bend" reality to gain insight on scenarios that may allow us to alter the behavior of the cell. For example, we can introduce a novel conductance that mimics a given ion channel which is not normally present in a particular cell type, e.g. the BK_{Ca} channel in ventricular cardiomyocytes. From a therapeutic standpoint, this sort of "virtual knockin"[4] gives us an advantage over traditional manipulations of ion channel behavior in biology, such as mutations and pharmaceutical agents, in that we have the flexibility to alter the "virtual" currents or signals in any manner we desire and to any degree. Furthermore, these manipulations are highly specific and therefore off-target effects can be discounted.

For example, as mentioned above, BK_{Ca} channels are not normally found at the sarcolemmal membrane of cardiomyocytes, yet they are otherwise ubiquitous ion channels that set the excitability of many other cell types throughout the body[5, 6]. They open in response to both voltage and intracellular Ca^{2+} and have a very high conductance of potassium ions which serves to restore the resting membrane potential of excitable cells. Since a high concentration of Ca^{2+} is toxic to most cells, by repolarizing the cell, BK_{Ca} channels are protective against Ca^{2+} overload. This regulatory mechanism is evident in the smooth muscle cells of arteries and other blood vessels where BK_{Ca} channels set the vascular tone. First, LTCCs bring Ca^{2+} into the cell to initiate contraction of the muscle fibers which lead to vasoconstriction (Fig. 5.1). The increase in $[Ca^{2+}]$ activates BK_{Ca} channels which repolarize the cell and shut off Ca^{2+} influx through LTCCs, which in turn leads to relaxation of the muscle fibers and vasorelaxation.

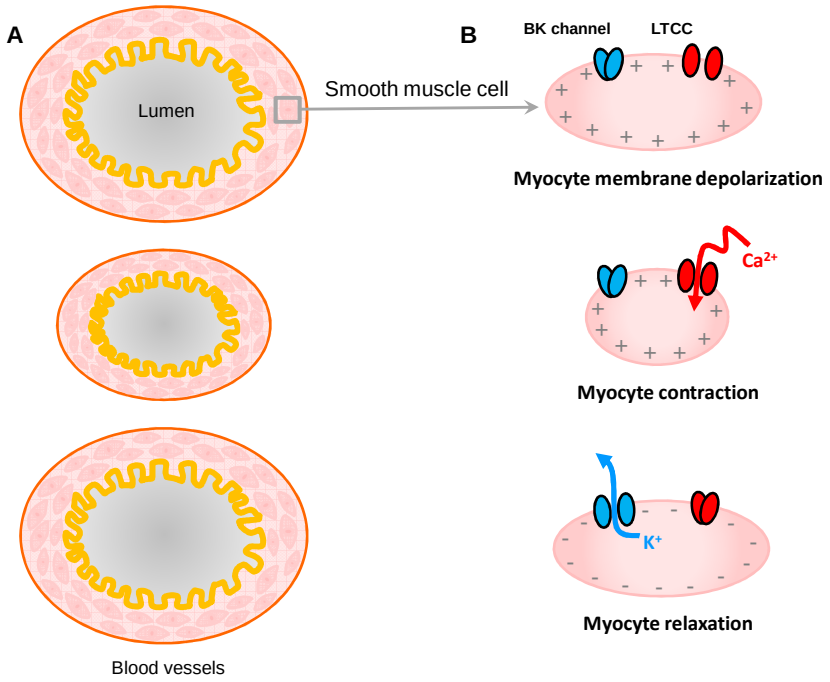

Figure 5.1 The Role of BK_{Ca} channels in Regulation of Smooth Muscle Tone. A) A simplified depiction of a cross-section of blood vessels showing a smooth muscle layer (pink), endothelial layer (orange) and the lumen where blood flows (gray). B) A cartoon schematic of a single smooth muscle myocyte shows both BK_{Ca} and LTCCs on the plasma membrane. Upon membrane depolarization, LTCCs open, allow Ca^{2+} to enter the cell and initiate myocyte contraction, thereby increasing vascular tone which leads to vasoconstriction. The increase in $[Ca^{2+}]$, coupled with the depolarized membrane potential activate BK_{Ca} channels which conduct K^+ ions and repolarize the cell, causing myocyte relaxation and thereby returning the cell to a resting state, and vasodilation. Therefore BK_{Ca} channels play a major role in regulating cellular excitability.

Based on this regulatory mechanism in smooth muscle, we wondered whether BK_{Ca} channels can act similarly in ventricular myocytes in which increased Ca^{2+} influx through LTCCs during pathophysiological conditions leads to an increase in EAD occurrence (for example, the effects of H_2O_2 on $I_{Ca,L}$ demonstrated in chapter 2, Fig. 2.2). Since EADs are transient depolarizations during the action potential, we hypothesized that the combination of an increase in voltage and in Ca^{2+} influx could activate BK_{Ca} during or preceding an EAD and repolarize the membrane potential before any arrhythmogenic consequences can occur. Rather than directly express these channels in cardiomyocytes, due to the following reasons: *i*) the fact BK_{Ca} channels are not expressed at the sarcolemma of ventricular myocytes, *ii*) it may be difficult to selectively target heterologously expressed BK_{Ca} channels to the sarcolemma, *iii*) their Ca^{2+} sensitivity is on

the order of 1-10 μM and *iv*) it is difficult to estimate the [Ca^{2+}] that may be sensed by the heterlogously expressed channels in cardiomyocytes, we opted to instead employ the dynamic clamp to introduce a BK_{Ca} current (I_{BK}) into ventricular myocytes so our hypothesis could be tested promptly without the development of adenoviral constructs, which are time-consuming. In this manner, we could manipulate many of these parameters, such as the K_d at which BK_{Ca} channels activate and the current density (number of channels) required, to design a channel that can protect against EAD occurrence.

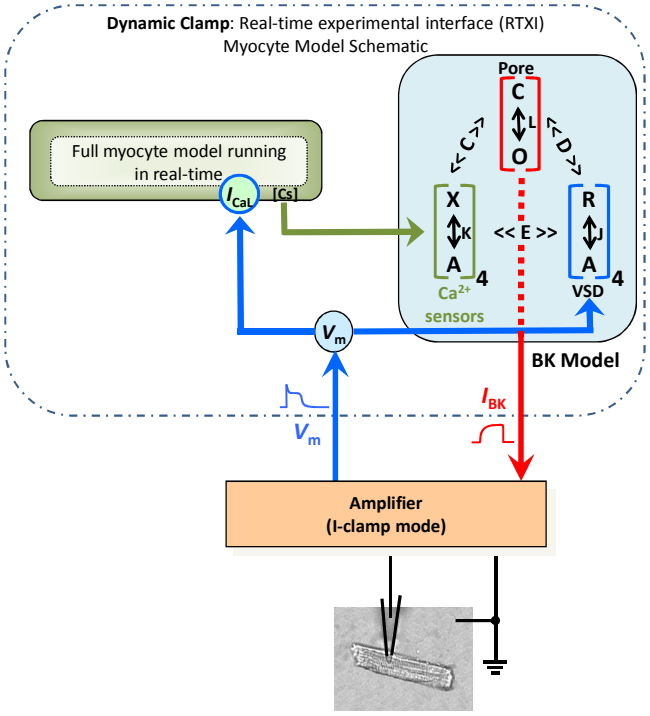

Figure 5.2 Dynamic Clamp Configuration to Explore the Anti-EAD potential of BK_{Ca} Channels. As previously described in Chapter 2, a rabbit ventricular myocyte was in current clamp mode and APs were illicited with a small current pulse. The V_m signal (blue arrow) was acquired by our dynamic clamp set-up, and fed into both the myocyte model and the Horrigan & Aldrich BK model. With each AP, the myocyte model computed the Ca^{2+} dynamics within the virtual compartments yet only the subcellular Ca^{2+} compartment, Cs (green arrow), was fed into the BK model. The resulting BK current (red arrow), from both the Ca^{2+} and voltage inputs, was injected into the cell in real-time.

Thus, we adapted a previous voltage-and-calcium-dependent allosteric model of BK_{Ca} by Horrigan & Aldrich[7] to be implemented in the Real-time experimental interface (RTXI) software[8] We patch-clamped ventricular myocytes that were overexpressing the β_3 subunit. At baseline, these myocytes did not have EADs (Fig. 5.3A), but upon adding H_2O_2 to the bath, we induced a robust EAD regime (Fig. 5.3B). At this time, we turned on the BK model to test our hypothesis. Keeping in mind that BK channels normally sense intracellular Ca^{2+}, we used the subsarcolemmal Ca^{2+}

space (Cs) in the myocyte model used throughout this study as a second input (in addition to membrane voltage) for the BK model. In other words, both the BK and myocyte models were run in parallel in dynamic clamp, and each received the membrane voltage input (APs) from the cell so that the myocyte model could recapitulate the increase in subcellular [Ca^{2+}], while only I_{BK}, generated by the voltage and Ca^{2+} inputs, was injected into the cell (Fig. 5.2). Once I_{BK} was injected into the cell, I could alter the number of channels (the current density), the K_d (Ca^{2+} sensitivity), or the intracellular [K^+] (the K^+ reversal potential). My preliminary results demonstrate that expressing a mutant BK current in which both the voltage and calcium sensitivities are blunted may be effective at suppressing EADs in ventricular myocytes (Fig. 5.3E).

Although considerable tuning of the BK channel parameters is still needed to validate their merit as anti-arrhythmic targets, our finding that I_{BK} can suppress EADs in ventricular myocytes highlights the utility of dynamic clamp to help electrophysiologists shape ionic conductances that are suited towards specific therapeutic goals. Thereby, it can be used predictive tool to guide new discoveries in cellular electrophysiology. One can envision that the results from dynamic clamp studies can be highly valuable to drug discovery studies which aim to identify chemical

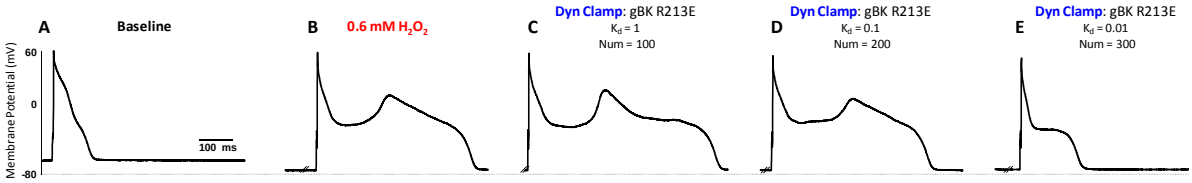

Figure 5.3 BK_{Ca} Current Injection in Ventricular Myocytes has Potential for Suppressing EADs. A) Rabbit ventricular myocytes overexpressing the β_3 subunit were paced at 5 seconds under baseline conditions. B) Addition of H_2O_2 to the extracellular solution promptly induced EADs. C) The dynamic clamp was turned on to inject a virtual BK_{Ca} current based on the R213E BK mutant, which has a reduced voltage sensitivity. With a Ca^{2+} K_d of 1 µM, EADs could not be suppressed. D) Lowering the K_d to 0.1 µM and increasing the number of virtual channels to 200 also could not suppress EADs. E) Only when the K_d was lowered to 0.01 µM and the number of BK channels was increased to 300, were EADs suppressed, although the plateau of the AP was also significantly depressed.

compounds that produce desired effects on ion channel biophysical properties.

Despite these advantages, as with any other techniques, the dynamic clamp poses certain limitations as well. One such limitation is the frequency at which the software can acquire the voltage signal, run the model and inject current into the cell. The frequency must be sufficiently fast that the time course of any voltage oscillations can be detected and that the time-dependent properties of the virtual conductance can be accurately recapitulated. As such, in our dynamic clamp system the calculation frequency was 10 kHz and therefore the voltage signal was acquired, the model computed the output of $I_{Ca,L}$ and injected the resulting current 10,000 times every second, or every 100 microsecond. Meanwhile both the kinetics of $I_{Ca,L}$ and the changes in V_m are on the order of tens to hundreds of milliseconds. Therefore we are confident that the accuracy of the computations performed in real-time did not affect our results appreciably.

Another limitation of the dynamic clamp (and of the patch clamp in general), encountered more frequently by neuroscientists, is the issue of the space clamp. Since neurons often have a large dendritic arbor, current injected at one site may not instantaneously change the membrane potential of the entire cell. This problem is not as relevant in cardiac myocytes, whose cell morphology is more suited towards whole-cell patch clamp studies, particular when low resistance pipettes are used.

Lastly, the current injected by the dynamic clamp consists primarily of the chloride ion, therefore the biochemical effects of Ca^{2+} influx are not a factor in most dynamic clamp studies involving Ca^{2+} channels[2]. Due to this limitation we could not directly measure Ca^{2+}-induced Ca^{2+} release from the SR under dynamic clamp. To overcome this obstacle, the myocyte model includes four different virtual Ca^{2+} compartments with various diffusion properties between them[9], based on measurements found in the literature. However, this may also be advantageous in some

respects because it allows us to differentiate between the electrical and the chemical effect of Ca^{2+} influx. Therefore, my findings highlight the fact that EADs can occur as a result of an electrical imbalance of ions across the membrane and not solely due to excessive Ca^{2+} influx. This is particularly important from a therapeutic standpoint since Ca^{2+} influx is necessary for contraction. Therefore, strategies which maintain the total amount of Ca^{2+} entering the cell, but efficiently alter the voltage dynamics during the AP may represent an ideal way to manage EAD-related arrhythmias.

5.2 Steady-State $I_{Ca,L}$ Biophysical Properties as Therapeutic Targets

Using the dynamic clamp technique, I have found that three steady-state biophysical properties of LTCCs are optimal therapeutic targets for the suppression of EADs: the half-activation potential, the half-inactivation potential and the non-inactivating pedestal current. Small changes in these parameters produced a significant decrease in EAD occurrence in adult ventricular cardiomyocytes without substantially altering excitation-contraction coupling. Therefore approaches in which these biophysical properties are targeted may have promise as an anti-arrhythmic therapy. For example, I found that a reduction in the $I_{Ca,L}$ non-inactivating pedestal current is highly effective at suppressing EADs. This persistent $I_{Ca,L}$ current is analogous to the late sodium current (I_{Na}) produced by sodium channels, which has also been shown to by highly arrhythmogenic and is also augmented by oxidative stress[10]. Recently, a pharmaceutical agent which blocks the late I_{Na}, called Ranolazine, has been identified and approved by the Food and Drug Administration for clinical use and has been shown to have a beneficial effect in chronic angina patients[11-13].

By the same logic, would a drug which selectively blocks the $I_{Ca,L}$ pedestal current be equally effective in a clinical setting? To answer this question, a compound that is specific enough to block only the late component of $I_{Ca,L}$ without blocking the peak current is required. One such

candidate may be an herbal compound which has been extensively studied in the literature for its anti-inflammatory and anti-cancer properties, called Cardamonin[14-19]. Interestingly, a recent study highlighted the effects of Cardamonin on LTCCs in smooth muscle[20]. They demonstrated a sizable reduction in the $I_{Ca,L}$ window current with Cardamonin due to a large hyperpolarizing shift in the steady-state inactivation curve as well as a decrease in the non-inactivating component. Based on this, I have tested cardamonin's ability to reduce the $I_{Ca,L}$ window current in heterogously expressed channels (not shown) as well as its efficacy as an EAD suppressor in ventricular myocytes (Fig. 5.4). Our findings so far demonstrate that Cardamonin suppresses EADs induced by oxidative-stress, however, voltage-clamp studies in cardiomyocytes to study the effects on the $I_{Ca,L}$ window current are, as yet, inconclusive. Therefore, we speculate that there may be other off-target effects which cause some degree of inconsistency and make it challenging to interpret the results. Nonetheless, we believe that with some manipulation of the chemical structure of Cardamonin, one may be able to develop a compound that is more specific for LTCCs and therefore it seems to be a promising agent to suppress oxidative stress-

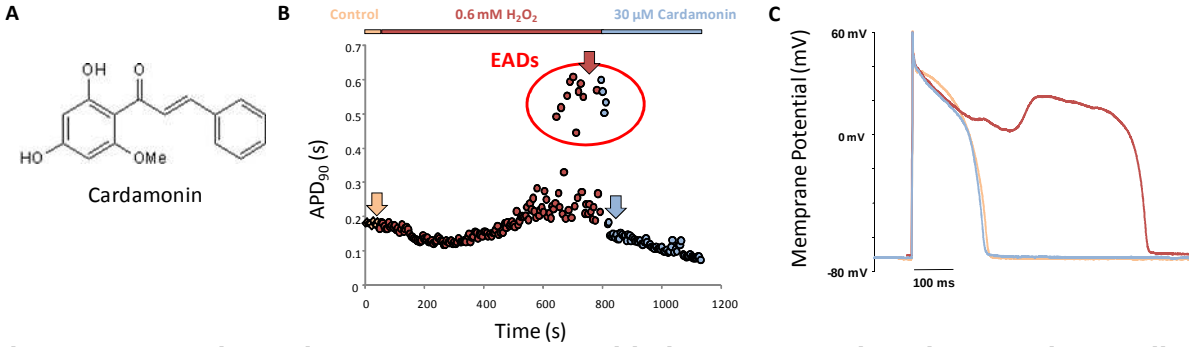

Figure 5.4 Cardamonin Can Suppress Oxidative-stress Induced EADs in Cardiac Myocytes. A) The chemical structure of cardamonin. B) A plot which shows the AP duration as a function of time in a representative experiment with cardamonin. The myocyte was paced at 5 seconds until a steady-state was reached (control conditions, ~200 ms, yellow). Addition of H_2O_2 (red) induced EADs (very long APs, ~ 600 ms, circled) within 10 minutes. Applying 30 µM cardamonin immediately suppressed EADs and restored APD to ~200ms. C) Representative AP traces, indicated by arrows in panel (B), are shown for each condition: control (yellow), H_2O_2 (red), cardamonin (blue).

induced EADs.

5.3 Time-Dependent $I_{Ca,L}$ Biophysical Properties as Therapeutic Targets

In Chapter 3 I demonstrated that changes in the time constants of $I_{Ca,L}$ activation and inactivation had limited potential at suppressing EADs and restoring APD_{90} under a persistent condition of oxidative stress (Figs. 3.3 and 3.4). I found that even large changes in the time constants of activation did not result in a radically different injected virtual $I_{Ca,L}$ during the AP. I interpreted these findings considering that both the biophysical parameters as well as the membrane voltage determine the time course of $I_{Ca,L}$. Thus is seems that while, in voltage clamp, the changes in the activation time constant up to 10-fold are evident (Fig 3.3A), during an AP the relatively slower rise of the AP upstroke, greatly attenuates the relevance of time constant of activation of $I_{Ca,L}$.

On the other hand, the time-dependent decay of $I_{Ca,L}$, which is due to both Ca^{2+} dependent inactivation (CDI) and voltage dependent inactivation (VDI), occurs on a time scale which is highly relevant to the duration of the action potential. However, intriguingly accelerating VDI by up to 10-fold did not significantly alter EAD occurrence and APD, and yet decreasing the rate of VDI by two-fold suppressed EADs in most cells (Fig. 3.4). At first glance, these results seem counterintuitive, however upon further deliberation, I reasoned that the modest increase in inward current generated upon a two-fold slowing of VDI (compared to a ten-fold slowing) conditions may raise the membrane potential (V_m) enough to activate K^+ channels and generate a repolarizing current which would counteract EAD generation, as shown in simulations[21, 22]. Conversely, an excessive slowing of the time course of VDI effectively increases the residual current present at the end of the AP, the non-inactivating pedestal current. Thus, the overall consequence of a large reduction in VDI is similar to an increase in the pedestal current, leading to a higher probability of EAD occurrence. Thus, although EAD occurrence was suppressed by

a modest (two-fold) slowing of VDI, APD_{90} remained longer than the pre-oxidative stress control in all manipulations of τ_{inact}, indicating that this maneuver may not be appealing as a therapeutic intervention. Most telling are the mutations of LTCCs that cause a significant slowing of VDI in Timothy syndrome[23, 24]. Not surprisingly, these patients are predisposed to QT-prolongation, torsade de pointes, ventricular fibrillation and other types of lethal cardiac arrhythmias.

While these results show that the kinetics of voltage-dependent activation and inactivation are not ideal therapeutic targets for suppressing EADs and resulting cardiac arrhythmias, as discussed above the limitations posed by the dynamic clamp did not allow us to specifically alter Ca^{2+}-dependent inactivation (CDI), which is no doubt an important factor in arrhythmogenic mechanisms, as shown by multiple laboratories[25, 26]. I expect that changes in CDI would directly alter SR Ca^{2+} release and hence change entirely the Ca^{2+} autoregulation within the cell[27]. Therefore, a decrease in the rate of CDI may potentiate the Ca_i transient to some degree and lead to a larger inward current driven by the Na^+/Ca^{2+} exchanger(NCX) [28-30]. Furthermore, a long term effect of decreasing CDI and hence Ca^{2+} release, may lead to an increase in the recovery of $I_{Ca,L}$[31]. Therefore, the net result would likely increase EAD occurrence. On the other hand, the effects of the opposite intervention, increasing the rate of CDI, are less obvious. A possible scenario may be that increasing CDI, decreases SR Ca^{2+} release and the inward NCX current leading to a shorter APD. Presumably, this would lead to a greater availability of LTCCs for the next beat causing beat-to-beat alternans[32]. Taken together, these studies suggest that alterations in CDI may be a precarious maneuver to address cellular mechanisms of cardiac arrhythmias since in the heart, Ca^{2+} is a “double-edged sword”.

5.4 Gene Therapy To Treat Cardiac Arrhythmias

In current medical practice, patients with cardiac arrhythmias are primarily prescribed anti-arrhythmic pharmacological agents which are mainly targeted towards blocking ion channels.

While relatively effective at controlling non-fatal arrhythmias such as atrial fibrillation, obvious disadvantages to these pharmacological agents are the systemic side-effects that may raise other health concerns. For example, class IV anti-arrhythmics such as verapamil or diltiazem are Ca^{2+} channel blockers that are frequently used to treat supraventricular tachycardias but may also cause hypotension and bradycardia[33, 34]. Other forms of therapy for arrhythmia patients include ablation, and ICD implantation both of which are invasive procedures with limited efficacy[35-38]. Therefore, there is an immense need for a non-invasive and efficient therapy for patients suffering from or at high-risk of developing cardiac arrhythmias.

In recent years, following a prolific period of advances in genetic engineering techniques, the promise of gene therapy has begun to come to fruition[39, 40]. Clinical trials for wide-ranging disorders such as Parkinson's disease[41], retinal disease[42], and pancreatitis[43] are currently in progress, with the gene therapy recommendation for pancreatitis being the first of its kind in clinical practice in Europe[44]. In the field of cardiology itself, there has been considerable interest in biological therapies from the development of biological pacemakers, treatments for ventricular tachyarrhythmias, regulation of calcium cycling, and improving heart function in heart failure[45-48]. In fact, a recent clinical trial has reported that advanced heart failure patients who received gene delivery of the SERCA pump demonstrated a significant increase in heart function as measured by multiple indicators[49, 50]. Therefore, more confidence can be placed in basic science studies such as ours which bring to light a potential for new therapeutic targets.

One of the most noteworthy findings from this study is that changes in the LTCC subunit composition, which produce substantial changes in the steady-state biophysical properties of $I_{Ca,L}$, may set the susceptibility to EADs in cardiac cells. Therefore it seems that using genetic engineering techniques, we can achieve the anti-arrhythmic outcomes predicted by the dynamic clamp experiments through a biological approach. However, before we can begin to consider

the clinical utility of these findings, the results from this preliminary study need to be thoroughly validated at the cellular, organ and animal levels. As I discussed in Chapter 4, future work aimed at knocking down expression of native auxiliary β subunits, such as the β_2 splice variants, may be more useful at suppressing arrhythmogenic triggers such as EADs while maintaining contractility of the heart. Of course this is merely speculative, as results are highly dependent on a number of practical obstacles inherent to the field of genetic engineering using viral vectors:

i. efficient and targeted delivery of viral particles to specific organs such as the heart.
ii. transient expression of the gene
iii. immunogenicity.

The new generation of adeno-associated viral (AAV) vectors, have addressed many of these issues, making them capable of transfecting both dividing and non-dividing cells, while avoiding an innate host immune response[51]. Additionally, the AAV 9 serotype has been shown to have cardiac specific expression[52], making it ideal for gene therapy studies for cardiac arrhythmias.

5.5 Concluding Remarks

In summary, during the course of this dissertation project I have acquired a wealth of knowledge in a wide range of fields ranging from ion channel biophysics, cellular physiology, mathematical modeling, genetic engineering and cardiovascular medicine. This interdisciplinary approach has allowed me to gain novel insights into the cellular mechanisms for cardiac arrhythmias and has led to the discovery of the central role of L-type Ca^{2+} channels as therapeutic targets for cardiac arrhythmias. In view of the sobering fact that over 300,000 people in the United States alone succumb to sudden cardiac death yearly, I am optimistic that the findings from my studies can be applied towards finding a solution to this lethal heart condition.

5.6 Bibliography

(1) Sharp AA, O'Neil MB, Abbott LF, Marder E. The dynamic clamp: artificial conductances in biological neurons. *Trends Neurosci* 1993 October;16(10):389-94.

(2) Economo MN, Fernandez FR, White JA. Dynamic clamp: alteration of response properties and creation of virtual realities in neurophysiology. *J Neurosci* 2010 February 17;30(7):2407-13.

(3) Wilders R. Dynamic clamp: a powerful tool in cardiac electrophysiology. *J Physiol* 2006 October 15;576(Pt 2):349-59.

(4) Dorval AD, Jr., White JA. Channel noise is essential for perithreshold oscillations in entorhinal stellate neurons. *J Neurosci* 2005 October 26;25(43):10025-8.

(5) Singh H, Stefani E, Toro L. Intracellular BK(Ca) (iBK(Ca)) channels. *J Physiol* 2012 December 1;590(Pt 23):5937-47.

(6) Cui J, Yang H, Lee US. Molecular mechanisms of BK channel activation. *Cell Mol Life Sci* 2009 March;66(5):852-75.

(7) Horrigan FT, Aldrich RW. Coupling between voltage sensor activation, Ca2+ binding and channel opening in large conductance (BK) potassium channels. *J Gen Physiol* 2002 September;120(3):267-305.

(8) Lin RJ, Bettencourt J, Wha IJ, Christini DJ, Butera RJ. Real-time experiment interface for biological control applications. *Conf Proc IEEE Eng Med Biol Soc* 2010;2010:4160-3.

(9) Mahajan A, Shiferaw Y, Sato D, Baher A, Olcese R, Xie LH, Yang MJ, Chen PS, Restrepo JG, Karma A, Garfinkel A, Qu Z, Weiss JN. A rabbit ventricular action potential

model replicating cardiac dynamics at rapid heart rates. *Biophys J* 2008 January 15;94(2):392-410.

(10) Song Y, Shryock JC, Wagner S, Maier LS, Belardinelli L. Blocking late sodium current reduces hydrogen peroxide-induced arrhythmogenic activity and contractile dysfunction. *J Pharmacol Exp Ther* 2006 July;318(1):214-22.

(11) Belardinelli L, Shryock JC, Fraser H. Inhibition of the late sodium current as a potential cardioprotective principle: effects of the late sodium current inhibitor ranolazine. *Heart* 2006 July;92 Suppl 4:iv6-iv14.

(12) Undrovinas AI, Belardinelli L, Undrovinas NA, Sabbah HN. Ranolazine improves abnormal repolarization and contraction in left ventricular myocytes of dogs with heart failure by inhibiting late sodium current. *J Cardiovasc Electrophysiol* 2006 May;17 Suppl 1:S169-S177.

(13) Zerumsky K, McBride BF. Ranolazine in the management of chronic stable angina. *Am J Health Syst Pharm* 2006 December 1;63(23):2331-8.

(14) Chow YL, Lee KH, Vidyadaran S, Lajis NH, Akhtar MN, Israf DA, Syahida A. Cardamonin from Alpinia rafflesiana inhibits inflammatory responses in IFN-gamma/LPS-stimulated BV2 microglia via NF-kappaB signalling pathway. *Int Immunopharmacol* 2012 April;12(4):657-65.

(15) Goncalves LM, Valente IM, Rodrigues JA. An Overview on Cardamonin. *J Med Food* 2014 January 16.

(16) He W, Jiang Y, Zhang X, Zhang Y, Ji H, Zhang N. Anticancer cardamonin analogs suppress the activation of NF-kappaB pathway in lung cancer cells. *Mol Cell Biochem* 2014 January 4.

(17) Park S, Gwak J, Han SJ, Oh S. Cardamonin suppresses the proliferation of colon cancer cells by promoting beta-catenin degradation. *Biol Pharm Bull* 2013;36(6):1040-4.

(18) Pascoal AC, Ehrenfried CA, Lopez BG, de Araujo TM, Pascoal VD, Gilioli R, Anhe GF, Ruiz AL, Carvalho JE, Stefanello ME, Salvador MJ. Antiproliferative Activity and Induction of Apoptosis in PC-3 Cells by the Chalcone Cardamonin from Campomanesia adamantium (Myrtaceae) in a Bioactivity-Guided Study. *Molecules* 2014;19(2):1843-55.

(19) Wei Z, Yang J, Xia YF, Huang WZ, Wang ZT, Dai Y. Cardamonin protects septic mice from acute lung injury by preventing endothelial barrier dysfunction. *J Biochem Mol Toxicol* 2012 July;26(7):282-90.

(20) Fusi F, Cavalli M, Mulholland D, Crouch N, Coombes P, Dawson G, Bova S, Sgaragli G, Saponara S. Cardamonin is a bifunctional vasodilator that inhibits Ca(v)1.2 current and stimulates K(Ca)1.1 current in rat tail artery myocytes. *J Pharmacol Exp Ther* 2010 February;332(2):531-40.

(21) Qu Z, Chung D. Mechanisms and determinants of ultralong action potential duration and slow rate-dependence in cardiac myocytes. *PLoS One* 2012;7(8):e43587.

(22) Corrias A, Giles W, Rodriguez B. Ionic mechanisms of electrophysiological properties and repolarization abnormalities in rabbit Purkinje fibers. *Am J Physiol Heart Circ Physiol* 2011 May;300(5):H1806-H1813.

(23) Splawski I, Timothy KW, Decher N, Kumar P, Sachse FB, Beggs AH, Sanguinetti MC, Keating MT. Severe arrhythmia disorder caused by cardiac L-type calcium channel mutations. *Proc Natl Acad Sci U S A* 2005 June 7;102(23):8089-96.

(24) Barrett CF, Tsien RW. The Timothy syndrome mutation differentially affects voltage- and calcium-dependent inactivation of CaV1.2 L-type calcium channels. *Proc Natl Acad Sci U S A* 2008 February 12;105(6):2157-62.

(25) Alseikhan BA, DeMaria CD, Colecraft HM, Yue DT. Engineered calmodulins reveal the unexpected eminence of Ca2+ channel inactivation in controlling heart excitation. *Proc Natl Acad Sci U S A* 2002 December 24;99(26):17185-90.

(26) Morotti S, Grandi E, Summa A, Ginsburg KS, Bers DM. Theoretical study of L-type Ca(2+) current inactivation kinetics during action potential repolarization and early afterdepolarizations. *J Physiol* 2012 September 15;590(Pt 18):4465-81.

(27) Eisner DA, Choi HS, Diaz ME, O'Neill SC, Trafford AW. Integrative analysis of calcium cycling in cardiac muscle. *Circ Res* 2000 December 8;87(12):1087-94.

(28) chi-Akahane S, Cleemann L, Morad M. Cross-signaling between L-type Ca2+ channels and ryanodine receptors in rat ventricular myocytes. *J Gen Physiol* 1996 November;108(5):435-54.

(29) Grantham CJ, Cannell MB. Ca2+ influx during the cardiac action potential in guinea pig ventricular myocytes. *Circ Res* 1996 August;79(2):194-200.

(30) Bers DM. Calcium fluxes involved in control of cardiac myocyte contraction. *Circ Res* 2000 August 18;87(4):275-81.

(31) Sipido KR, Callewaert G, Carmeliet E. Inhibition and rapid recovery of Ca2+ current during Ca2+ release from sarcoplasmic reticulum in guinea pig ventricular myocytes. *Circ Res* 1995 January;76(1):102-9.

(32) Weiss JN, Nivala M, Garfinkel A, Qu Z. Alternans and arrhythmias: from cell to heart. *Circ Res* 2011 January 7;108(1):98-112.

(33) DeWitt CR, Waksman JC. Pharmacology, pathophysiology and management of calcium channel blocker and beta-blocker toxicity. *Toxicol Rev* 2004;23(4):223-38.

(34) O'Connor SE, Grosset A, Janiak P. The pharmacological basis and pathophysiological significance of the heart rate-lowering property of diltiazem. *Fundam Clin Pharmacol* 1999;13(2):145-53.

(35) Kim YH, Sosa-Suarez G, Trouton TG, O'Nunain SS, Osswald S, McGovern BA, Ruskin JN, Garan H. Treatment of ventricular tachycardia by transcatheter radiofrequency ablation in patients with ischemic heart disease. *Circulation* 1994 March;89(3):1094-102.

(36) Cappato R, Calkins H, Chen SA, Davies W, Iesaka Y, Kalman J, Kim YH, Klein G, Packer D, Skanes A. Worldwide survey on the methods, efficacy, and safety of catheter ablation for human atrial fibrillation. *Circulation* 2005 March 8;111(9):1100-5.

(37) Connolly SJ, Hallstrom AP, Cappato R, Schron EB, Kuck KH, Zipes DP, Greene HL, Boczor S, Domanski M, Follmann D, Gent M, Roberts RS. Meta-analysis of the implantable cardioverter defibrillator secondary prevention trials. AVID, CASH and CIDS studies. Antiarrhythmics vs Implantable Defibrillator study. Cardiac Arrest Study Hamburg . Canadian Implantable Defibrillator Study. *Eur Heart J* 2000 December;21(24):2071-8.

(38) John RM, Tedrow UB, Koplan BA, Albert CM, Epstein LM, Sweeney MO, Miller AL, Michaud GF, Stevenson WG. Ventricular arrhythmias and sudden cardiac death. *Lancet* 2012 October 27;380(9852):1520-9.

(39) Naldini L. Medicine. A comeback for gene therapy. *Science* 2009 November 6;326(5954):805-6.

(40) Bartel MA, Weinstein JR, Schaffer DV. Directed evolution of novel adeno-associated viruses for therapeutic gene delivery. *Gene Ther* 2012 June;19(6):694-700.

(41) LeWitt PA, Rezai AR, Leehey MA, Ojemann SG, Flaherty AW, Eskandar EN, Kostyk SK, Thomas K, Sarkar A, Siddiqui MS, Tatter SB, Schwalb JM, Poston KL, Henderson JM, Kurlan RM, Richard IH, Van ML, Sapan CV, During MJ, Kaplitt MG, Feigin A. AAV2-GAD gene therapy for advanced Parkinson's disease: a double-blind, sham-surgery controlled, randomised trial. *Lancet Neurol* 2011 April;10(4):309-19.

(42) Cideciyan AV, Hauswirth WW, Aleman TS, Kaushal S, Schwartz SB, Boye SL, Windsor EA, Conlon TJ, Sumaroka A, Roman AJ, Byrne BJ, Jacobson SG. Vision 1 year after gene therapy for Leber's congenital amaurosis. *N Engl J Med* 2009 August 13;361(7):725-7.

(43) Kaeppel C, Beattie SG, Fronza R, van LR, Salmon F, Schmidt S, Wolf S, Nowrouzi A, Glimm H, von KC, Petry H, Gaudet D, Schmidt M. A largely random AAV integration profile after LPLD gene therapy. *Nat Med* 2013 July;19(7):889-91.

(44) Gruber K. Europe gives gene therapy the green light. *Lancet* 2012 November 17;380(9855):e10.

(45) Li RA. Gene- and cell-based bio-artificial pacemaker: what basic and translational lessons have we learned? *Gene Ther* 2012 June;19(6):588-95.

(46) Donahue JK. Gene therapy for ventricular tachyarrhythmias. *Gene Ther* 2012 June;19(6):600-5.

(47) Hulot JS, Senyei G, Hajjar RJ. Sarcoplasmic reticulum and calcium cycling targeting by gene therapy. *Gene Ther* 2012 June;19(6):596-9.

(48) Tang T, Gao MH, Hammond HK. Prospects for gene transfer for clinical heart failure. *Gene Ther* 2012 June;19(6):606-12.

(49) Jaski BE, Jessup ML, Mancini DM, Cappola TP, Pauly DF, Greenberg B, Borow K, Dittrich H, Zsebo KM, Hajjar RJ. Calcium upregulation by percutaneous administration of gene therapy in cardiac disease (CUPID Trial), a first-in-human phase 1/2 clinical trial. *J Card Fail* 2009 April;15(3):171-81.

(50) Jessup M, Greenberg B, Mancini D, Cappola T, Pauly DF, Jaski B, Yaroshinsky A, Zsebo KM, Dittrich H, Hajjar RJ. Calcium Upregulation by Percutaneous Administration of Gene Therapy in Cardiac Disease (CUPID): a phase 2 trial of intracoronary gene therapy of sarcoplasmic reticulum Ca2+-ATPase in patients with advanced heart failure. *Circulation* 2011 July 19;124(3):304-13.

(51) Daya S, Berns KI. Gene therapy using adeno-associated virus vectors. *Clin Microbiol Rev* 2008 October;21(4):583-93.

(52) Bish LT, Morine K, Sleeper MM, Sanmiguel J, Wu D, Gao G, Wilson JM, Sweeney HL. Adeno-associated virus (AAV) serotype 9 provides global cardiac gene transfer superior

to AAV1, AAV6, AAV7, and AAV8 in the mouse and rat. *Hum Gene Ther* 2008 December;19(12):1359-68.